MI-0139

List of papers submitted to the 95 PAC

Dallas, TX, May 1-5, 1995.

132Nsec Bunch Spacing In The Tevatron Proton-Antiproton Collider, S.D.Holmes, et al.

The Computer Code BPERM for Wakepotential & Impednace Calculations, T.Barts, SSC Lab; W.Chou, Fermilab.

Review of Beam Instability Studies for the SSC, W. Chou.

Variable Bunch Spacing in Super Collider, W. Chou.

Aluminum Beam Tube for Super Collider: an Option for No-Coating & No-Liner, W. Chou.

The Fermilab Injector Complex, D. Bogert with W.B.Fowler, et al (copy of DB's talk).

The Status of the Fermilab Main Injector Project, D. Bogert, et al.

A 200 kW Power Amplifier & Solid State Driver for the Fermilab Main Injector, J.Reid, H.Miller.

The Main Injector Trim Dipole Magnets, R.Baiod, et al.

Design of the Fermilab Main Injector Lambertson, D.E.Johnson, et al.

The Main Injector Chromaticity Correction Sextupole Magnets: Measurements & Operating Schemes, C.M.Bhat, et al.

Simulations of Transition Crossing in the Main Injector, C.M.Bhat; J.A.MacLachlan.

Radiation Shielding of the Main Injector, C.M.Bhat, P.S.Martin.

Design of the MI40 Beam-Abort Dump, C.M.Bhat, et al.

Magnetic Field Measurements of the Initial Fermilab Main Injector Production Dipoles, D.J.Harding, et al.

Magnetic Field Measurements of the Initial Fermilab Main Injector Production Quadrupoles, D.J.Harding, et al.

The Fermilab Main Injector Dipole & Quadrupole Cooling Design & Bus Connections, J.A.Satti.

132 NSEC BUNCH SPACING IN THE TEVATRON PROTON-ANTIPROTON COLLIDER

S.D. Holmes, J.A. Holt, J. Johnstone, J. Marriner, M. Martens, D. McGinnis
Fermi National Accelerator Laboratory*, P.O. Box 500 Batavia, IL 60510

I. INTRODUCTION

The Tevatron proton-antiproton collider currently operates at a center-of-mass energy of 1.8 TeV, delivering a luminosity greater than $1.5 \times 10^{31} cm^{-2} sec^{-1}$. This is achieved with six proton and six antiproton bunches colliding at two locations, B0 (CDF) and D0. An electrostatic separator system causes the two beams to pass with approximately 5σ separation at the ten other possible collision points around the accelerator. In this configuration each experimental detector, with a sensitivity to about 45 mb of the total p-$\bar{p}$ cross section, witnesses 2.4 interactions per crossing.

The Fermilab Main Injector is projected to support a Tevatron luminosity in excess of $5 \times 10^{31} cm^{-2} sec^{-1}$. Hardware currently under construction will allow operation with 36 proton and 36 antiproton bunches when the Main Injector comes on-line in late 1998. A representative set of collider parameters for the first Main Injector-based collider run (Run II) is given in Table I. Improvements to the antiproton accumulation rate, to low beta systems, and/or reduction of the rms bunch lengths to 15 cm or less hold the promise of raising collider luminosity above 10×10^{31} $cm^{-2} sec^{-1}$. Continued operation with 36 bunches would, however, result in 3-4 interactions per crossing at this higher luminosity. Reducing the number of interactions per crossing below 1 will require circulating more bunches as indicated in the right-most column of the table.

This paper summarizes a preliminary conceptual design for a Tevatron collider configuration in which bunches are spaced at 132 nsec. Increasing the number of bunches is not expected to raise the luminosity--the sole motivation is to reduce the number of interactions per crossing by about a factor of three. Multibunch schemes with 72, 108, 96, and 120 proton and antiproton bunches have been studied.

Implementation of any of these multi-bunch scenarios will require new hardware. The introduction of a crossing angle will result in reduced luminosity and the bunch length must be shortened considerably compared to present operations to minimize this impact. This means that a new rf system, operating at 159 MHz, will be required. Other new hardware probably includes 1)upgraded low beta optics; 2)upgraded abort kicker; 3) new coalescing cavities operating at three times the frequency (7.5 MHz) of those currently operational in the Main Ring and also planned for the Main Injector, and; 4) a new 7.5 MHz rf system in the Antiproton Accumulator.

*Operated by Universities Research Association under contract to the United States Department of Energy

II. DESIGN AND PERFORMANCE ISSUES

The proton-antiproton luminosity in the Tevatron is given by the expression:

$$L = \frac{3\gamma f N_p (B N_{\bar{p}})}{\beta^* (\varepsilon_{Np} + \varepsilon_{N\bar{p}})} H\left(\frac{\beta^*}{\sigma_l}\right)\left(1 + \frac{2\alpha^2 \sigma_l^2}{\sigma_p^2 + \sigma_{\bar{p}}^2}\right)^{-1/2} \quad (1)$$

where γ is the relativistic factor, f is the revolution frequency, B is the number of bunches in each beam, N_p ($N_{\bar{p}}$) is the number of protons (antiprotons) in a bunch, ε_p ($\varepsilon_{\bar{p}}$) is the 95% normalized transverse beam emittance, σ_l is the rms bunch length, β* is the beta function at the interaction point, σ_p ($\sigma_{\bar{p}}$) is the rms transverse beam size at the interaction point, and α is the crossing half-angle. The form factor $H(\beta^*/\sigma_l)$ approaches 1 asymptotically as $\beta^*/\sigma_l \to 0$, clearly indicating that bunch length should be kept as small as is reasonable compared to β* to minimize the luminosity reduction. A 14 cm bunch length is chosen to minimize the impact of the 190 μrad crossing angle.

A major limiting factor in the Tevatron proton-antiproton collider is the beam-beam tune shift. In the present collider mode, with six proton and antiproton bunches, there are twelve potential collision points around the ring. Through the use of electrostatic separators the beams are made to collide with zero crossing angle at the interaction points, but separated by 5σ (center to center) at the other ten (parasitic) crossings. This basic configuration must be continued as the number of number of bunches increases to 36 and beyond.

The separator nearest to the interaction region is beyond the position of the first parasitic crossing for 132 nsec spacing. It does not appear to be possible to avoid these first parasitic collisions unless a crossing angle is introduced to separate the beams within the low β quadrupoles. An interesting alternative technique for avoiding a crossing angle through the use of rf resonant magnets has been envisioned [1], but, at least with existing technology, a substantial crossing angle seems to be inescapable.

The existence of a crossing angle dictates that the orbits be separated within the low β quadrupoles. The necessary aperture in the low β quadrupoles and, conceivably, changes to the low β optics which minimize this separation need to be considered. Also, although long range beam-beam effects are not significant in the current operating mode, once the number of bunches approach 100 such effects can no longer be ignored.

Table I: Collider Parameters for Run II and options for reduced bunch length or bunch spacing

	Collider Run II: 36 bunches 53 MHz 396 nsec	Option I: 36 bunches 159 MHz 396 nsec new low β	Option II: 108 bunches 159 MHz 132 nsec new low β	
Beam Energy	1000	1000	1000	GeV
Circumference	6283.0	6283.0	6283.0	meters
Protons/bunch	3.3×10^{11}	3.3×10^{11}	2.7×10^{11}	
Antiprotons/bunch	3.6×10^{10}	3.6×10^{10}	1.2×10^{10}	
Bunches	36	36	108	
Total Antiprotons	1.3×10^{12}	1.3×10^{12}	1.3×10^{12}	
Proton emittance (95%, norm)	30π	30π	25π	mm-mr
Antiproton emittance (95%, norm)	20π	20π	20π	mm-mr
β*	0.35	0.25	0.25	meters
Longitudinal Emittance (95%)	3	3	2	eV-sec
rf Frequency	53	159	159	MHz
rf Voltage	1	15	15	MV
Bunch length (rms)	0.43	0.17	0.14	meters
Bunch Length Form Factor	0.70	0.86	0.89	
Crossing Half-angle	0	0	0.19	mr
Crossing Angle Form Factor	1.00	1.00	0.77	
Typical Luminosity	8.3×10^{31}	14.2×10^{31}	10.4×10^{31}	$cm^{-2}s^{-1}$
Integrated Luminosity	16.72	28.67	20.99	pb^{-1}/wk
Bunch Spacing	396	396	132	nsec
Interactions/crossing (@45 mb)	2.17	3.73	0.91	
Antiproton tune shift (2 crossings)	0.016	0.016	0.016	
Proton tune shift (2 crossings)	0.003	0.003	0.001	
Average helix separation (d/σ)	5	5	6.5	
Long Range tune spread (antiproton)	0.008	0.008	0.008	

The length of the luminous region is modified appreciably with the introduction of a crossing angle and shorter bunches. Figure 1 shows the distribution dL/dz that will be seen by an experimental detector for various crossing angles and a 14 cm bunch length. The result is a luminous region of ~8cm length (rms)--a factor of four shorter than those currently experienced and a desirable experimental feature.

A. Multibunch Loading

The first collider run of the Main Injector era will operate with 36 bunches of protons and antiprotons. A workable configuration calls for three batches of protons and antiprotons containing twelve bunches each, with the batches spaced symmetrically around the ring. For 132 nsec it would be most natural to continue with a threefold symmetric scheme. There are two possible three-fold symmetric loading schemes, resulting in either 72 or 108 bunches colliding. In 72x72 operation two batches of twelve bunches each would be spaced 396 nsec apart, followed by a 3.7 μsec abort gap. This sequence would be repeated twice more around the ring. The abort gap of 3.7 μsec is larger than that for 36x36 operation, and the abort at A0 could be used. The 108x108 scenario calls for three batches of twelve bunches spaced by 396 nsec followed by a gap of 1.8 μsec.

Single gap configurations are also possible. However, these have the disadvantage of not allowing utilization of existing aborts, and of providing unequal luminosity at B0 and D0.

B. RF System

A 14 cm bunch length is required to minimize luminosity loss due to the 190 μrad crossing angle selected for this study. The total voltage required to produce a 14 cm bunch length, with a beam longitudinal emittance of 2 eV-sec, is 15 MV at 159 MHz or 11 MV at 212 MHz. The 159 MHz system is evaluated here. A total of 12 proton and 12 antiproton cavities would be required. Power requirements are estimated at 935 kW for each system, based on providing 1.25 MV per cavity.

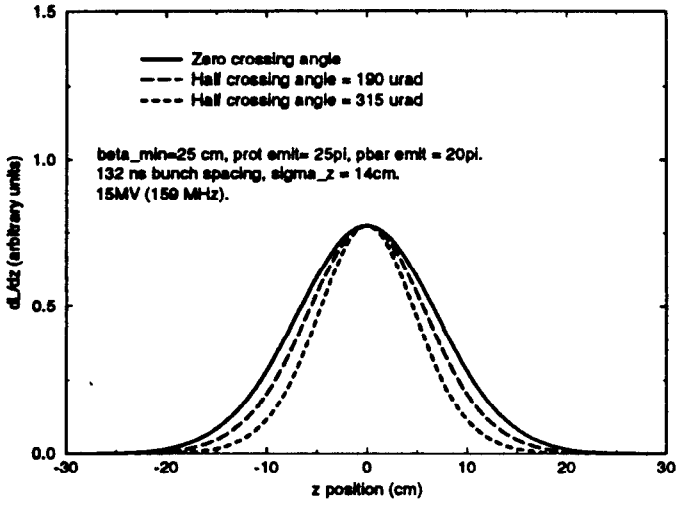

Figure 1: dL/dz for three crossing angles and the Tevatron parameters contained in the rightmost column of Table 1.

C. Interaction Region Optics

Six pairs of high gradient (140 T/m) low β quadrupoles are powered in each Tevatron interaction region. In the present mode of operation dispersion at the IP is zero, but with a non-zero slope, resulting in dispersion reaching its maximum value within the low β triplet - precisely where the beam already reaches its ring-wide maximum from β_{max} ($\geq$1 km). An alternative match to the lattice which gives both η and η'=0 throughout the straight section has been found [2] that uses the current IR physical configuration of magnets and gradients compatible with the existing quadrupoles. Extending to β^*=0.25m requires a maximum gradient in one of the low β quadrupoles of $\approx$185 T/m. This lies beyond the capabilities of the present system and would require an upgrade to quadrupoles similar to those proposed for the CERN LHC [3].

The dispersion-free solution significantly reduces beam-size in the low-beta quads--particularly at injection. This optics configuration is particularly desirable for 132 nsec bunch spacing since the beams must be separated through the IR triplet and the momentum spread in the beam will be large due to the short bunch length.

D. Electrostatic Separators & IP Crossing Angle

A crossing half-angle of 190 μrad, giving 3σ separation at the first parasitic crossing, has been chosen. Assuming the current physical location of electrostatic separators, an average of 6.5σ separation is maintained at all other parasitic crossings. In general the electric fields are comparable to, or less than, those currently in use.

The primary dynamical consequence of a non-zero crossing angle is thought to be the excitation of synchro-betatron resonances. These resonances were a serious problem at the e^+e^- collider DORIS [4]. The excitation of such resonances in the Tevatron has not been studied in detail, but it is expected that they will be less important than in the DORIS experience because of the relatively low synchrotron frequency. Note, however, that the proposed parameters and crossing angle for the Tevatron Collider are rather similar to those proposed for the LHC.

E. Long Range Beam-Beam Effects

The large number of parasitic beam-beam crossings can lead to significant orbit and tune shifts. If the bunches are not uniformly populated and regularly spaced each bunch will have a different orbit and a different tune. In the Tevatron the bunches can not be regularly spaced because of the requirement for an abort gap. A bunch loading scheme that leads to 72 bunches colliding with a 132 nsec spacing has been considered. This configuration was chosen because it was thought to be as irregular as any that might be used. The maximum orbit shift is about 20 μm, 2/3 of the rms transverse beam size at the interaction point. The bunch-to-bunch range of tune shifts is shown in Table II. The range of tune shifts is less than, but comparable to, the maximum working space of 0.025. The range of linear coupling and the range of chromaticities are neither overwhelming nor small.

Table II. Range of tune shifts for the 72 antiproton bunches

Tune plane	Tune shift
Minimum $\Delta\nu_x$	-.0008
Maximum $\Delta\nu_x$	.0026
Minimum $\Delta\nu_y$	-.0118
Maximum $\Delta\nu_y$	-.0017

III. SUMMARY

A number of scenarios for operation of the Tevatron collider with 132 nsec bunch spacing have been analyzed. Collider parameters are summarized for 108 bunch operation in Table I. The 132 nsec spacing, coupled with a 190 μr crossing angle, produces a luminosity approximately 20% low as compared to bunches spaced at 396 nsec colliding head-on. This results primarily from the crossing angle form factor. Other factors, such as reduced proton bunch intensity due to coalescing of fewer bunches, tend to be ameliorated by the resultant lower longitudinal and transverse emittances.

Luminosity in all scenarios will continue to be limited by antiproton availability. Schemes for increasing the antiproton availability, and hence the luminosity, by an additional factor of ten are currently under study at Fermilab.

IV. REFERENCES

1. Gerald P. Jackson, Beam-Beam Collisions of Bunches Separated by 132 nsec without a Crossing Angle, Internal Fermilab Report, Oct. 22, 1994.

2. John A. Johnstone, Report to the Low Beta Study Group I, Internal Fermilab Report, September 29, 1994.

3. The LHC Study Group, LHC, The Large Hadron Collider Accelerator Project, CERN/AC/93-03(LHC).

4. A. Piwinski, DESY 77/18, 1977.

THE COMPUTER CODE BPERM FOR WAKEPOTENTIAL & IMPEDANCE CALCULATIONS

T. Barts, SSC Laboratory,* 2275 Highway 77 North, Waxahachie, TX 75165, USA
W. Chou, Fermilab,† P.O. Box 500, Batavia, IL 60510, USA

Abstract

The program **bperm** is a 2-dimensional code for wakepotential and impedance calculations based on an analytic method of boundary perturbation. It can be employed for periodic structures with rotational symmetry and is useful for structures with small discontinuities such as shielded bellows and valves, tapered transitions, weldments, etc. One principle used in developing the code is portability. It is written in Fortran 77 and is entirely self-contained, with no machine-dependent calls and with simple file input not relying on the namelist extension. The post-processor **gnuplot** has been used for plotting.[1] The code runs on UNIX as well as on VMS computers. It is currently stored on the Common File System (CFS) at the National Energy Research Supercomputer Center (NERSC). A user's guide can be found in Reference [2].

I. INTRODUCTION

The computer code **bperm** is a generalized version of an earlier code using the boundary perturbation method for calculating wakepotentials and impedances for periodic structures.[3] The fundamentals of this method can be found in References [3-6] and are briefly introduced below.

When a rigid Gaussian bunch of rms length σ traverses a periodic structure of period length L and mean radius b_0, the longitudinal and transverse wakepotentials calculated by the boundary perturbation method are, respectively,

$$W_{\parallel}(s)^{m=0}(V/pC) = -1.8\pi \sum_{p=1}^{\infty} p \mid 2c_p \mid^2 \cdot \sum_{n=1}^{\infty} k_{0n}\, Re[\frac{1}{2} e^{-s^2/2\sigma^2} w(\frac{k_{0n}\sigma}{\sqrt{2}} - j\frac{s}{\sqrt{2}\sigma})] \ , \qquad (1)$$

$$W_{\perp}(s)^{m=1}(V/pC \cdot m) = -\frac{360\pi}{b_0^2} \sum_{p=1}^{\infty} p \mid 2c_p \mid^2 \cdot \sum_{n=1}^{\infty} \{\frac{1}{1-{x'_{1n}}^2}\, Im[\frac{1}{2} e^{-s^2/2\sigma^2} w(\frac{k'_{1n}\sigma}{\sqrt{2}} - j\frac{s}{\sqrt{2}\sigma})] - Im[\frac{1}{2} e^{-s^2/2\sigma^2} w(\frac{k_{1n}\sigma}{\sqrt{2}} - j\frac{s}{\sqrt{2}\sigma})]\} \ , \qquad (2)$$

in which s is the distance between the bunch head and the point where the wakepotentials are being calculated, w the complex error function, and

$$k_{mn} = \frac{\pi p}{L} + \frac{L x_{mn}^2}{4\pi p b_0^2} \ , \qquad (3)$$

$$k'_{mn} = \frac{\pi p}{L} + \frac{L {x'_{mn}}^2}{4\pi p b_0^2} \ , \qquad (4)$$

where x_{mn} and x'_{mn} are the n^{th} root of the Bessel functions J_m and J'_m, respectively. All the lengths on the r.h.s. of Eqs. (1)-(4) are in centimeters. The parameter c_p is the Fourier coefficient of the given periodic structure. For a simple geometry it may have an analytic expression. For example, for the structure shown in Figure 1, one has

$$c_p = -j\frac{2\epsilon}{\pi b_0} \frac{\sin(p\frac{\pi g}{L})}{\frac{\pi g}{L}} \frac{1}{p^2} \quad \text{for } p = \pm 1, \pm 3, \ldots \qquad (5)$$
$$= 0 \quad \text{otherwise.}$$

But in general, c_p has to be computed by a Fast Fourier Transform (FFT), as is done in the code **bperm**.

In order to convert the wakepotentials computed by Eqs. (1) and (2) to impedances, one needs to set the time origin correctly. For this purpose, the code shifts the time zero point from the bunch head to the bunch center, and moves the part of the wakepotentials between the bunch head and center to the tail of the wake. The shifted wakepotentials are then Fourier-transformed to impedances.

Since the code is based on analytical formulae, it consumes much less CPU and memory than that by numerical integration codes such as TBCI or ABCI.[7,8] In addition, it can be applied to more general types of geometries (provided that the perturbation is not too big) than some other analytical methods (*e.g.*, the field matching method).

II. CODE DESCRIPTION

The program **bperm** is a 2-dimensional code and can be employed for periodic structures with rotational symmetry. The input is one complete period of the structure described in the **r** (radial) and **z** (axial) plane as an array of points, which are assumed to be connected with straight segments. Input data for **bperm** is in an ASCII file named **bperm.in**. It contains seven keywords: **dataset**, **title**, **pmax**, **smax**, **sigma**, **shape**, and **end**. They are explained in Table 1. The required ones are **shape** and **end**. The former is followed by the **r** and **z** coordinates of the structure, one pair of numerical values per line with the **r** and **z** value separated by either a comma or a space, while the latter ends the geometry description. The other

*Operated by the Universities Research Association, Inc., for the U.S. Department of Energy under Contract No. DE-AC35-89ER40486.

†Operated by the Universities Research Association, Inc., for the U.S. Department of Energy under Contract No. DE-AC02-76CHO3000.

Table 1. Input file keywords

Keyword	Description
shape	Start of shape (structure) data
end	End of shape data
sigma	RMS bunch length in cm (default 1.75)
pmax	Total number of interpolated coordinates used for the structure (default 128)
smax	Region of the wakepotential calculation in units of sigma (min 6, max 140, default 10)
dataset	Name of the output files (default bperm)
title	Plot subtitle
!	Flag for comments

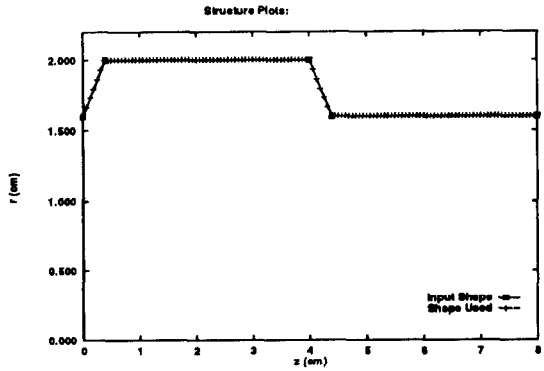

Figure. 1. The structure in the example.

keywords will use the default values if not specified. All keywords can be either upper, lower, or mixed cases. Any number of problem cases can be included in one input file, but each problem case must be separated from the next with the keyword end. Output of bperm is seven ASCII files including five files with plotting data for the structure, wakes and impedances, an information file and a gnuplot command file that will generate 13 plots. Output files are listed in Table 2.

Table 2. Output files

Name	Description
bperm.sh	Structure data
bperm.lw	Longitudinal wake
bperm.tw	Transverse wake
bperm.lz	Longitudinal impedance
bperm.tz	Transverse impedance
bperm.out	Information file
bperm.gp	Input file for gnuplot with commands produced by bperm
bperm.ps	Postscript file with 13 plots of the structure, wakes and impedance generated by gnuplot

Portability was the major principle in the development of bperm. The entire code is written in Fortran 77 and is self-contained, with no machine-dependent calls and with simple file input not relying on the namelist extension.

On a UNIX system, the command for creating the plots (which can be displayed on a X11 color window) and the postscript file bperm.ps is:

```
gnuplot bperm.gp
```

Because the post-processor gnuplot on a VAX/VMS does not execute properly with a load file created with the Fortran 77 compiler, a file named bplot.com is provided by the authors to fix this problem. The command for generating the plots is:

```
@bplot bperm.gp
```

Even though the code is designed to use gnuplot for post processing, any plotting package that uses columns of ordinates and abscissas could be substituted. Also the gnuplot input file can be modified to open a display terminal other than X11.

It needs to be noted that all output files are opened with the status 'unknown.' This increases user-friendliness on UNIX workstations by overwriting existing files with the same names. This overwriting also takes place when running bperm on a VAX/VMS. The VAX/VMS user needs to be very aware of this feature so that files that need to be saved have names changed before bperm makes subsequent runs with identical output dataset names.

III. EXAMPLE

Following is an input file bperm.in for the structure shown in Figure 1.

```
dataset=test
smax=10 sigma=1.75
title=bperm Test Problem
pmax=128 !  pmax stays at the default
shape
1.6 0.0
2.0 0.4
2.0 4.0
1.6 4.4
1.6 8.0
end
```

Figs. 2 and 3 are plots of the wakepotentials calculated with bperm for this input, plotted with gnuplot. As a comparison, the wakes obtained from the MAFIA code, t3210, are also plotted. It is seen that, in the range $[-5\sigma,2\sigma]$, the two codes give similar results. The differences begin to show up beyond that region. This is probably due to the different boundary conditions used in the two codes — bperm assumes a periodic boundary, while MAFIA/t3210 assumes an open boundary.

Figs. 4 and 5 are plots of the real and imaginary longitudinal impedances, and Figs. 6 and 7 the transverse ones.

IV. CODE DISTRIBUTION

Complete packages for bperm are available from the CFS at the NERSC and also via anonymous ftp from gateway.ssc.gov, in the /pub directory. The file bperm.tar.Z is the UNIX compressed tar file and

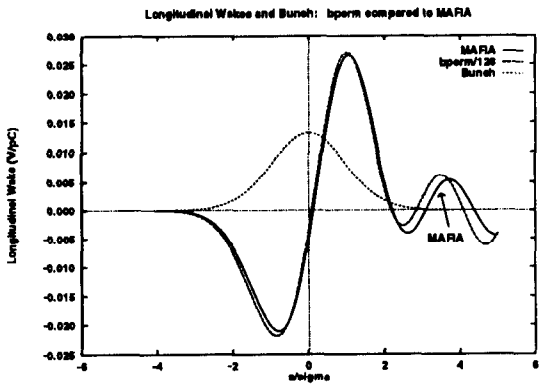

Figure. 2. The longitudinal wakepotential.

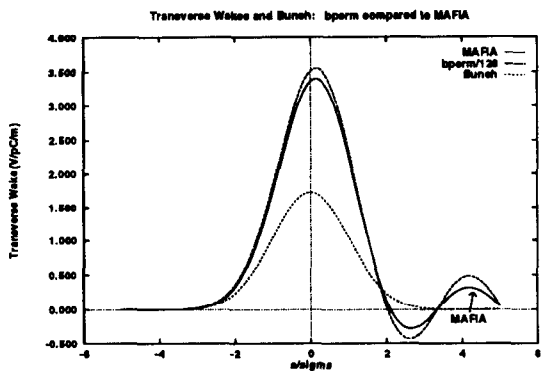

Figure. 3. The transverse wakepotential.

bperm.bck.Z is the VMS save set. Both distributions include the **bperm** source code, either a **makefile** or a command file **make.com**, inputs and outputs for examples and complete documentation including a PostScript file of the User's Guide (*i.e.*, Reference [2]).

References

[1] The **gnuplot** software is available via anonymous ftp from **dartmouth.edu** in the **/pub/gnuplot** directory in the file **gnuplot3.5.tar.Z**.

[2] T. Barts and W. Chou, SSCL-MAN-0035, SSC Laboratory (June 1994).

[3] W. Chou, Light Source Note LS-149, Argonne National Laboratory (1990).

[4] Z. H. Zhang, Acta Physica Sinica, V 28, p 563 (1979).

[5] M. Chatard-Moulin and A. Papiernik, Proc. Particle Accelerator Conference, San Francisco, 1979, IEEE Trans Nucl. Sci. V 26, p 3523 (1979).

[6] R. K. Cooper, S. Krinsky and P. L. Morton, Particle Accelerators, V 12, p 1 (1982).

[7] T. Weiland, "MAFIA Release 3.1," D6100 Darmstadt, Germany (1991).

[8] Y. Chin, "User's Guide for New ABCI Version 6.2," LBL-33091, CERN SL/92-49 (AP).

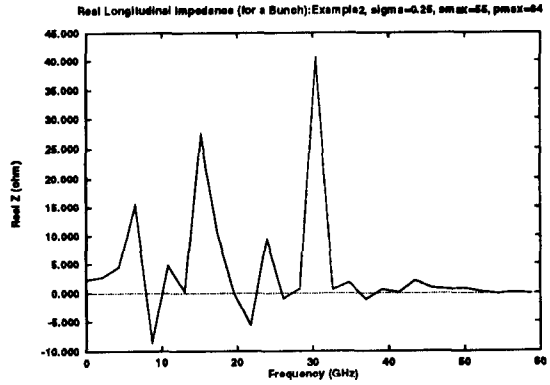

Figure. 4. The real longitudinal impedance.

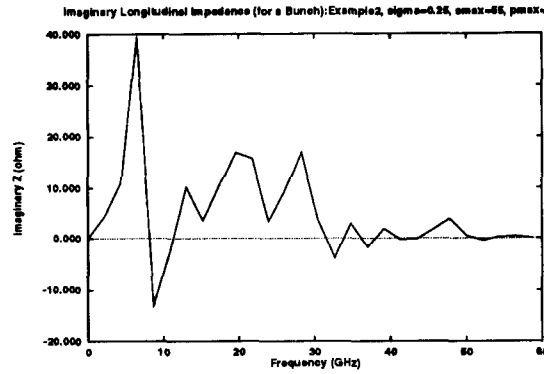

Figure. 5. The imaginary longitudinal impedance.

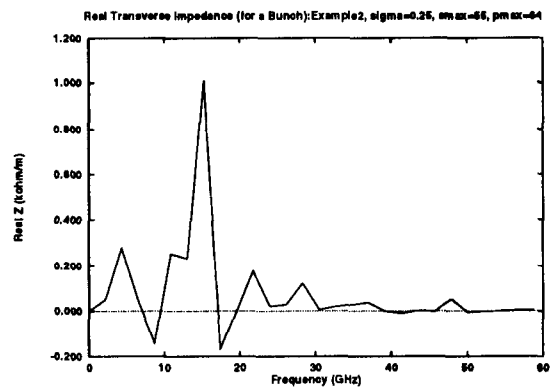

Figure. 6. The real transverse Impedance.

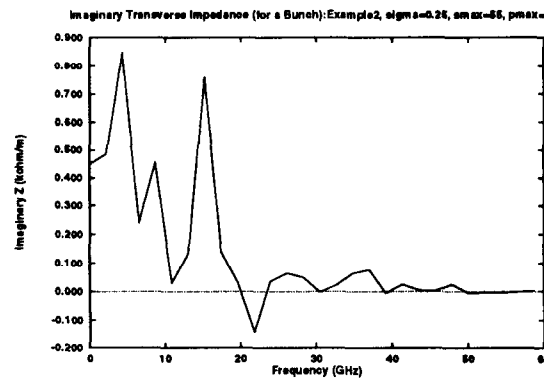

Figure. 7. The imaginary transverse impedance.

REVIEW OF BEAM INSTABILITY STUDIES FOR THE SSC

W. Chou, Fermi National Accelerator Laboratory,* P.O. Box 500, Batavia, IL 60510, USA

Abstract

Beam instability studies for the SSC during the period 1989-1993 are briefly reviewed in this paper. Various topics are covered: single bunch and multi-bunch, single beam and beam-beam, parasitic heating and active feedback, *etc.* Although the SSC will not be built, many of the results obtained from these studies remain as useful references to the accelerator community.

I. INTRODUCTION

Studies on beam instability problems for the SSC started in the early 1980s. A set of preliminary results were included in Reference [1]. Since the establishment of the SSC Laboratory in 1989, these studies have been further pursued and numerous new results have been obtained. In this paper we will briefly review these results. For details the readers are referred to Ref. [2] and the references therein.

The SSC is a low beam current machine. The beam intensity is primarily limited by the cryogenic system for absorbing the synchrotron radiation power. Generally speaking, therefore, collective effects — such as single bunch instability, parasitic heating and beam-beam interactions — do not present a threat to machine operations. However, the coupled-bunch instability may become a real concern, because the number of bunches is enormous (about 17000 per beam) and the transverse emittance is very small (1 π mm-mrad, rms, normalized).

II. IMPEDANCE BUDGET

A. Impedance budget of the baseline design

Each component in the vacuum, rf, diagnostic and injection/extraction systems have been carefully analysed. Computer models for each component have been built. Measurements for some critical components (*e.g.,* the bellows and the liner) have been carried out. Two groups of simulation codes have been put in use. One is numerical, *e.g.,* MAFIA and HFSS.[3] Another is based on a boundary perturbation method and called BPERM, which was developed at the SSC.[4] The results obtained from different codes are in agreement.

The impedance budget is listed in Table 1, where $Z_{\parallel}/n$ is the longitudinal impedance and $Z_{\perp}$ the transverse one. There are several remarks about this budget.

1. Every effort has been made to make the beam pipe as smooth as possible: the bellows are shielded; the valves have rf fingers; the vacuum pump ports are screened; the transitions between two pipes of different sizes are tapered; and the ceramic pipes in the kicker sections are coated with thin metallic layers.
2. Table 2 lists the impedances of two different designs for the bellows rf shield. The reduction comes from a smaller gap and a smoother taper. The specification of the maximum lateral offset is 2.8 mm. Assuming a uniform distribution in misalignment, the resulting increase in impedance is also listed in Table 2.
3. In order to accommodate unforseen sources, the calculated total impedance is multiplied by a factor of two, which is then used in the safety margin estimate.

B. Impedance in the presence of a liner

A perforated liner inside the beam pipe would increase the impedance in two ways:

1. The holes or slots would introduce additional impedance. Below the cutoff, small holes/slots behave like a pure inductance. For a given pumping area, short slots give less impedance than circular holes. Above the cutoff, resonant peaks in the impedance spectrum are observed when the holes or slots are periodically placed. These peaks can be greatly suppressed when the periodicity is destroyed. It is thus concluded that randomly distributed short slots would be the choice for the pattern of the perforation.
2. The installation of a liner would also reduce the inner radius (ID) of the pipe. Consequently, the transverse impedance would increase.

For an area coverage of the holes on the liner surface 4%, the impedance increase is listed in Table 3.

C. Single bunch instability threshold and safety margin

The instability threshold impedances are listed in Table 1. The ratio of the threshold to the impedance budget, called the safety margin, is listed in Table 3. Several measures could be taken to increase this margin, *e.g.,* a larger liner ID, a bigger longitudinal emittance and a higher rf voltage at injection.

III. COUPLED-BUNCH INSTABILITY

In order to suppress the coupled-bunch instability, four types of rf cavities — multiple-cell and single-cell, superconducting (sc) and normal conducting (nc) — have been compared. The rf committee has endorsed the single cell, sc cavity as the choice for the SSC.

The higher order modes (HOM) may also be generated if the beam pipes in the dipole and quadrupole sections have different cross sections, which is called the trapped mode effect. The result could be a continuous beam emittance growth. Therefore, it was decided to use a beam pipe of uniform cross section throughout the entire cold region.

*Operated by Universities Research Association Inc. under Contract No. DE-AC02-76CHO3000 with the U.S. Department of Energy.

Table 1. Impedance Budget (per ring)

Component	Number	Impedance	
		$Z_\parallel/n$ (Ω)	$Z_\perp$ (MΩ/m)
RF cavity (HOM)	8 × 5-cell	0.036	0.016
Transition (tapered)	4	0.004	0.003
Bellows (shielded)	6000	0.12	10
BPM (15 cm, 55°)	968	0.05	4.6
Weldment	12000	0.002	0.2
Valve (shielded)	128	1E-4	0.01
Pump port (screened)	650	0.02	2
Flange gap	12000	TBD	TBD
Resistive wall		0.02	1.7
Scrapers		1.8E-4	0.02
Collimators		2.6E-4	0.08
Injection Lambertson (laminated)		1.5E-3	1.4
Abort Lambertson (solid iron)		–	–
Injection kicker		0.06	2.0
Abort kicker		0.2	4.7
Joint to Lambertson		TBD	TBD
Conical section near IP		–	–
Total		0.51	27
Impedance budget = Total × 2		1.0	54
Instability threshold:			
At 2 TeV		4.0	270
At 20 TeV		16	1200

Table 2. Comparison of Bellows (shielded) Impedance

Case	$Z_\parallel/n$ (Ω)	$Z_\perp$ (MΩ/m)
Baseline design	0.12	10
New design		
No misalignment	0.03	2.5
Max lateral offset 2.8mm	0.06	6.5

Table 3. Transverse Impedance with/without Liner

Case	$Z_\perp^{(liner)}$ (MΩ/m)	$Z_\perp^{(others)}$ (MΩ/m)	$Z_\perp^{(total)}$ (MΩ/m)	Safety Margin
Baseline	–	54	54	5
With liner	37	94	131	2

Table 4. Resistive Wall Impedance Budget

Component	$Z_\perp$ (MΩ/m)	
	2 TeV	20 TeV
Cold beam pipe	4300	4300
Warm beam pipe (stainless steel)	1300	1300
Graphite shadows:		
Upstream to abort Lambertson	7.1	7.1
Upstream to collimator	10	323
Scrapers (copper)	1.4	46
Collimators (stainless steel)	7.7	250
Abort Lambertson (solid iron):		
Symmetric	22	22
Asymmetric	4.6	4.6
Total	5700	6300

IV. RESISTIVE WALL INSTABILITY

The beam tube of the Collider is made of stainless steel, which is coated on its inner surface with a thin copper layer in order to have low electrical resistivity. The resistive wall instability growth time can be approximately written as

$$\tau_w = \left(\frac{2\pi\gamma\,\nu_\beta\,b^3}{N_{\rm tot}\,c\,r_p}\,\frac{\mu\omega}{2}\right)\sigma_e\Delta \qquad (1)$$

where γ is the relativistic energy of the particles, ν_β the betatron tune, b the beam tube radius, μ the vacuum permeability, ω the angular frequency, $N_{\rm tot}$ the total number of particles, c the velocity of light, r_p the classical radius of proton, σ_e the wall conductivity, and Δ the coating layer thickness. The specification is $\sigma_e\Delta \geq 1\times10^5\ \Omega^{-1}$, which corresponds to a wall impedance of 4300 MΩ/m in the cold region. Table 4 is a list of the wall impedance budget, which gives a growth time of 25 ms, or 88 turns, during the about one hour injection period.

An alternative is to use an aluminum beam tube. There are several reasons for considering this option: saving the coating cost, solving the vacuum problem without a liner, and avoiding the adhesion problem in a bi-layer tube. The quantity $\sigma_e\Delta$ remains about the same.

V. FEEDBACK SYSTEMS

The feedback systems serve four different purposes:

1. Correction of the injection errors — The feedback must have enough power to kick the beam back to the orbit before any significant decoherence occurs.
2. Damping of the resistive wall instability — Because this is a fast beam blowup, a feedback system with a large gain is needed.
3. Damping of the coupled-bunch instability — The feedback system needs a wide bandwidth.
4. Control of emittance growth — This feedback system must have very low noise level. The emittance growth rate due to the feedback noise is:

$$\frac{1}{\tau_{\text{noise}}} = 0.64 f_0 \left(\frac{x_{\text{N}}}{\sigma_\beta}\right)^2 \Delta\nu^2 \qquad (2)$$

in which f_0 is the revolution frequency, x_{N} the noise level at the pickup, σ_β the rms beam size and $\Delta\nu$ the total tune spread. The theoretical limit of the pickup resolution due to the thermal and electronic noises, Δx, is also calculable. In designing a feedback system, Δx must be smaller than x_{N}, which is determined by a specified allowable growth rate $1/\tau_{\text{noise}}$.

The specifications of the power, bandwidth, gain and noise level of the feedback systems can be found in [2].

VI. PARASITIC HEATING

The parasitic heating can be calculated by

$$P = k \frac{I_{\text{av}}^2}{M f_0} \qquad (3)$$

where I_{av} is the average beam current, M the number of bunches, and k the loss factor, which is

$$k = \frac{c^2 R}{2\pi b} \int_{-\infty}^{\infty} \tilde{\lambda}^2(\omega)\, R_s(\omega)\, d\omega \qquad (4)$$

in which R is the machine radius, $\tilde{\lambda}(\omega)$ the bunch spectrum. In order not to exceed the heat load budget (which is 1 kW per ring for the parasitic heating), the surface resistance must be kept below a certain level. To estimate R_s correctly, one should consider the co-existence of three extreme conditions:

- Low temperature (4 K).
  The low temperature resistance is described by RRR, the residual resistance ratio. But it is meaningful only at low frequencies and low magnetic field.
- High magnetic field (6.8 T).
  The magnetoresistance can be studied using a Kohler plot. At 6.8 Tesla, the RRR value is about an order of magnitude lower than that at zero field.
- High frequency (1 GHz and above).
  Because of the anomalous skin effect, the surface resistance ratio $R_s(300\text{ K})/R_s(4\text{ K})$ at high frequencies is significantly lower than the dc value.

The measurement of R_s under these conditions was started but not completed.

VII. BEAM-BEAM EFFECTS

A. *Strong beam-beam interactions*

1. Inelastic scattering:
   The particle loss rate is $\mathcal{L}\sigma_{\text{inel}}$, which is $10^8\ \text{s}^{-1}$ per interaction point (IP). The corresponding luminosity lifetime is $180/N_{\text{IP}}$ hours.
2. Elastic scattering:
   This contributes to the emittance growth:

$$\frac{d\epsilon}{dt} = \frac{N_{\text{B}} f_0}{4\pi\epsilon} \sigma_{\text{el}} \sigma_\theta^2 \qquad (5)$$

in which N_{B} is the number of particles per bunch, σ_{el} the elastic cross section, σ_θ the rms values of pp elastic scattering angle in the center of mass system. This gives about 4.6×10^{-17} m-rad/s per IP.

B. *Electromagnetic beam-beam interactions*

1. Incoherent effects:
   (a) Tune shift and tune spread:
   The most significant beam-beam effect is the slow diffusion caused by high order betatron resonances. The budget of the total tune spread (head-on + long-range + nonlinear magnetic field) is 0.02. The calculated tune spread is well below this value.
   (b) Orbit distortion:
   This is induced by long-range interactions. The calculated values are small compared with the beam size at the IP's (less than 10% σ_β).
2. Coherent effects:
   The rigid dipole modes (π- and σ-mode) and high order multipole modes are studied. There are enough stability regions in the (ξ, ν_β) space.
3. Pacman effect:
   There are seven injection gaps (1.7 μs each) and one abort gap (4.1 μs) in the bunch train. Bunches near the edge of the gaps may miss collisions at some IP, thus experiencing an irregular collision sequence. This makes the orbit and tune correction difficult. But simulations show that there is enough working area in the tune space to accommodate this Pacman effect.
4. Synchro-betatron resonance due to crossing angles:
   Computer simulations show that this is not a serious problem. Because the three parameters that determine the strength of the resonance are all small: (a) the beam-beam parameter $\xi = 0.0009$, (b) the synchrotron tune $\nu_s = 0.0012$, and (c) the normalized crossing angle $\alpha\sigma_s/\sigma_\beta = 0.45$.

References

[1] "*SSC Conceptual Design*," SSC-SR-2020, SSC Laboratory (1986).

[2] W. Chou, SSCL-680, SSC Laboratory (1994).

[3] MAFIA is developed by T. Weiland and his associates, HFSS by Hewlett-Packard Company.

[4] T. Barts and W. Chou, SSCL-MAN-0035, SSC Laboratory (1994).

VARIABLE BUNCH SPACING IN SUPER COLLIDER

W. Chou, Fermi National Accelerator Laboratory,* P.O. Box 500, Batavia, IL 60510, USA

Abstract

This paper suggests a variable bunch spacing instead of a fixed value in the SSC. This will give a higher luminosity for a given beam current and provide more flexibility in machine operations. Two possible schemes for varying the bunch spacing, namely, bunch coalescing and beam chopping, are studied and compared. Some of these discussions may be useful to future accelerators.

I. INTRODUCTION

When the beam-beam tune shift limit is not reached, the luminosity $\mathcal{L}$ is proportional to the bunch spacing S_b:

$$\mathcal{L} = \left(\frac{\gamma}{4\pi c \cdot e^2}\right) \frac{I^2}{\beta^* \cdot \epsilon_N} \cdot S_b \qquad \mathrm{cm}^{-2}\mathrm{s}^{-1} \qquad (1)$$

in which γ is the relativistic factor, c the velocity of light, e the electron charge, β^* the β-function at the interaction point, I the average bunch current, and ϵ_N the normalized rms transverse emittance. The average number of events per crossing is:

$$n = \frac{\mathcal{L} \cdot \sigma_{\mathrm{inel}}}{c} \cdot S_b \qquad (2)$$

in which σ_{inel} is the inelastic pp cross section. The baseline parameters are: $\gamma = 21316$, $I = 71$ mA, $\beta^* = 0.5$ m, $\epsilon_N = 1$ mm-mrad, and $S_b = 5$ m. They correspond to $\mathcal{L} = 1 \times 10^{33}$ and $n = 1.7$.

The parameters I, β^* and ϵ_N were chosen based on the limitations of accelerator technology and the costs, whereas the choice of S_b was made by the detector requirement that n should be close to 1. In the following sections, we investigate the merits and penalties of a larger bunch spacing — a multiple of 5 meters — and the means to implement it.

II. MERITS AND PENALTIES

It is seen from Eq. (1) that, when all the other parameters are fixed, a larger bunch spacing will directly translate to a higher luminosity. This fact can be exploited in two different ways: (a) In the first few years during the commissioning stage, we will be on a learning curve. A larger bunch spacing can speed up the pace to reach the design luminosity. (b) When the machine operation is matured, a larger bunch spacing provides one of the easiest ways for a luminosity upgrade.

On the detector side, a larger bunch spacing would be beneficial to the electronics and instrumentation. This is because a lower collision frequency implies simpler electronics, easier synchronization of subsystems and easier bunch crossing identification. Moreover, a larger S_b is preferred by the detectors should the luminosity be below the design value, because it will bring n close to 1. Even when the luminosity reaches the design value, a larger S_b may still be preferred in order to get a higher luminosity in the n-for-$\mathcal{L}$ trade off.

A larger bunch spacing will also have certain negative impact on the pattern recognition of detector subsystems if it results in multiple events per crossing. The main concern is the tracking detector, which is most sensitive to an increase in pile-up per crossing, while the performance of the muon system, the electromagnetic calorimeter and hadron calorimeters will remain unchanged.

It is interesting to note that all the three LHC detectors — ATLAS, CMS, and L3P — claim they can deal with a n much larger than unity.[1-3]

III. IMPLEMENTATION

Assume $\mathcal{L}$ is fixed and S_b increased by a factor of 6. Then n will also be increased by the same factor. Below are two possible scenarios to achieve this bunch spacing.

A. Bunch coalescing

Assuming the coalescing be carried out in the MEB at the flat top (200 GeV), a new 10 MHz rf system (in addition to the main 60 MHz rf) is required. The longitudinal emittance ϵ_L will be increased by a factor of about 6. Because the baseline design includes an intentional ϵ_L blowup by a factor of about 50 when the beam is accelerated from 200 GeV to 20 TeV, the coalescing blowup factor can be absorbed in this process so that the final ϵ_L at 20 TeV will remain unchanged.

The reasons to choose the flat top in the MEB for coalescing are the following:

- The two cold machines, HEB and Collider, are excluded because of the possible quenching that could be caused by the lost particles during coalescing.
- The LEB is a fast cycling machine (10 Hz). It is thus difficult to incorporate the coalescing scheme.
- At the flat bottom (12 GeV), the beam lifetime due to gas scattering is poor, and the rf voltage required to generate the necessary size of the buckets to capture the coalesced bunches is high. In addition, a coalesced bunch with large longitudinal emittance represents a concern during the transition crossing.

The bunch coalescing has been a routine operation at Fermilab (Main Ring) and CERN (PS) for many years. The new features of the MEB coalescing are: (a) Unlike the Main Ring, all the buckets are filled in the MEB; (b) Unlike the PS, more bunches (six) need to be merged.

The procedure is: (a) reduction of the bunch momentum spread by either adiabatic debunching, or rf phase jump, or rf amplitude jump; (b) adiabatic capture and compression by the subharmonic rf system; (c) bunch rotation; (d)

*Operated by Universities Research Association Inc. under Contract No. DE-AC02-76CHO3000 with the U.S. Department of Energy.

recapture of the coalesced bunches by the main rf system; (e) extraction. The simulations show that when coalescing 6 bunches using this scheme, the particles leaking into adjacent buckets are less than 0.5%.

B. Beam chopping

This is to chop a gap in a sequence of micro-pulses of particles, i.e., to create a macro-structure. This has to be done when the beam energy is low, namely, in the linac, in order to avoid the radiation problem.

The injection from the linac to the LEB is a 4-turn process. In each turn, there are 9 micro-pulses injected into each LEB bucket. All the buckets are full. To change the bunch spacing from 5 m to 30 m, one has to chop out a gap of 25 m in the linac pulse sequence and fill up only every 6th bucket in the LEB. Meanwhile, each filled bucket has to contain more particles (a factor of 4, see Table 1) in order to maintain the luminosity. The number of injection turns has to be increased accordingly. The transverse emittance will also have to be blown up (by a factor of 3) due to the space charge. Four schemes have been studied:

1. The transverse deflector:
   This is a pulsed electrostatic deflector consisting of a number of pairs of plates. The voltage is applied to the plates sequentially at a rate that matches the beam velocity as a slow wave structure. In the AGS Booster, it is placed after the RFQ where the beam energy is 750 keV. Its length is about 1 m.[4] In the SSC linac, the beam exit energy from the RFQ is 2.5 MeV. Therefore, the deflector would have to be longer. The main concern of this scheme is that the no-focusing long drift space occupied by the deflector will cause a significant transverse emittance growth.
2. The energy chopper:
   This is a new idea proposed by D. Swenson. It is based on the fact that the Low Energy Beam Transport (LEBT) and RFQ are energy-selective. When the beam energy is 35 keV, the transmission in the RFQ is about 90%. When the energy error is ± 6 keV, the transmission is reduced to almost zero. Therefore, if one lowers the ion source energy down to 30 keV and installs a small acceleration device between the ion source and RFQ to provide alternatively $+5$ keV and -1 keV to the beam, then one can chop the beam by switching this device on and off. The device suggested by Swenson is a Betatron using a high permeability ferrite ring. It needs to provide the rise and fall times of 2-3 ns and the peak pulse length 21 ns. The difficulty is that the ferrite must have both high permeability and high frequency response. In the preliminary measurements using the commercial products CMD5005 and CN20, the rise and fall times of the primary are 200 ps, and that of the secondary are 25 ns (CMD5005) and 5 ns (CN20), respectively. The difference comes mainly from the geometry rather than the material. But the voltage of the pulse generator is too low (several volts) to draw any conclusions from the measurements.
3. The rf switch in the ion source:
   To meet the requirement of the neutron spallation source, V. Smith at LANL proposes to pulse the electrically-isolated collar in the Penning source to chop the H^- beam. The goal of the rise and fall times are on the order of 10 ns, which is still too slow compared with 2-3 ns required by the SSC linac.
4. The laser stripper:
   This is based on the observation that the binding energy of the second electron on the H^- is 0.75 eV and can be stripped by a laser beam of wavelength 1.06 μm (corresponding to a photon energy of 1.18 eV). The photoneutralization cross section is large (35 megabarns). A pair of parallel mirrors of 5 cm length that reflects the laser beam 40 times can give rise to neutralization over 99%. However, if one wants to use this technology to chop 45 out of every 54 micro-pulses, the costs seem prohibitively high.

C. Comparisons

The advantages of the bunch coalescing method are:

1. For the same beam current, it gives more luminosity than that by the chopping method, because it does not have to sacrifice the transverse emittance.
2. For the same luminosity, it can ease the space charge problem in the LEB, because the number of protons per bunch is smaller.
3. It is a proved technology.

The advantages of the beam chopping method are:

1. It is flexible. In principle, it can create any macro-structure in the beam as needed. This is in contrast to the coalescing method, which requires a specific subharmonic rf system for a specific coalescing scenario.
2. It can decrease the current per bunch. This feature will be particularly useful during commissioning.
3. It can reduce the radiation at the LEB extraction.

IV. ACCELERATOR ISSUES

Table 1 lists the changes of the beam parameters when the bunch spacing is increased from 5 m to 30 m by the two different methods. The luminosity is fixed at 1×10^{33} $cm^{-2}s^{-1}$ in these calculations.

1. Space charge in the LEB:
   When the chopping method is used, one has to put about 4 times more particles into a bunch. But this should be okay when one allows ϵ_N to be increased by a factor of 3. The simulation results are supported by the Fermilab Booster measurement data.
2. Injection efficiency in the LEB:
   When the chopping method is used, only a portion of the LEB buckets are to receive particles from the linac. The particles may leak into the neighboring empty buckets and create satellites or cause particle loss. Therefore, one needs to modify the rf voltage profile and inject 7 micro-pulses in each turn instead of 9. Simulation shows the particle loss will be less than 3%.

Table 1. Beam Parameter Dependence on Bunch Spacing

Parameter	$S_b = 5$ m $\epsilon_N = 1 \times 10^{-6}$	$S_b = 30$ m $\epsilon_N = 1 \times 10^{-6}$ Coalescing	$S_b = 30$ m $\epsilon_N = 3 \times 10^{-6}$ Chopping
Events per crossing n	1.7	10	10
Time interval between crossings Δt (ns)	17	100	100
Events per second (s^{-1})	10^8	10^8	10^8
Average current I (mA)	71	29	48
Protons per bunch N_b ($\times 10^{10}$)	0.81	2.0	3.3
Number of bunches M	17424	2904	2904
Head-on tune shift $\Delta\nu_{HO}$	0.0038	0.0094	0.0053
Long range tune shift $\Delta\nu_{LR}$	0.0067	0.0027	0.0046
Long range tune spread $\delta\nu_{LR}$	0.0020	0.0008	0.0041
LEB space charge tune shift $\Delta\nu_{SC}$	0.38	0.16	0.53
Synchrotron radiation P_s (kW/beam)	9.0	3.7	6.1
Parasitic heating P_{loss} (kW/beam)	1.3	1.3	3.6
Instability threshold $Z_\parallel/n$ (Ω)	3.7	1.5	0.9
$Z_\perp$ (MΩ/m)	250	100	60
Resistive wall instability τ_{wall} (turns)	106	260	155
Dynamic aperture during injection (σ)	13	13	8.0
Dynamic aperture at IR (σ)	11	11	6.2
Beam-beam luminosity lifetime $\tau_{\mathcal{L}}$ (h)	78	32	54
Intrabeam scattering lifetime τ_x (h)	211	86	516
τ_z (h)	120	49	109
Luminosity reduction factor R_r	0.91	0.91	0.97

3. Dynamic aperture in the Collider:
   When ϵ_N is 3 times larger, the dynamic aperture, expressed in terms of the beam size σ, will be reduced. The values listed in Table 1 are obtained by a scaling formula. More accurate data by long term tracking (10^5 turns) gives 9σ.
4. Single bunch instability threshold:
   This should not be a serious problem because there is a relatively large safety margin (about 6) in the design. Furthermore, this margin can be improved by redesigning the longitudinal emittance budget.
5. Beam-beam interaction:
   The head-on tune shift is increased because there are more particles in a bunch, whereas the long range tune shift is decreased because of a larger S_b. The total change is small and the sum is well below the tune shift budget of 0.02.
6. Synchronization during beam transfer:
   When the chopping method is used, the linac and LEB need to be phase locked. In addition, the beam transfer must be bucket-to-bucket. The SSC synchronization scheme assures that these can be done.
7. Instrumentation:
   The specifications (dynamic range, bandwidth and accuracy) of the orbit and phase measurements need to be revised in order to serve variable bunch spacing.
8. Other issues:
   (a) The average beam current becomes smaller, whereas the peak current becomes larger.
   (b) The synchrotron radiation is proportional to the average beam current. Therefore, it is also decreased.
   (c) The parasitic heating is proportional to the product of the average and peak beam current. It remains the same (in the case of coalescing) or is increased (in the case of chopping). This term may become a dominant loss term if more and more charges are put in a bunch for luminosity upgrades.
   (d) The beam-beam luminosity lifetime becomes shorter because the number of protons is smaller.
   (e) The total number of bunches is reduced by a factor of 6. This will make the machines more stable.

V. ACKNOWLEDGEMENT

This paper represents a collaborated work that involves many people's contributions, in particular, J. Griffin, D. Swenson, R. Shafer, D. Raparia, D. Anderson, S. Machida, N.K. Mahale and F. Pilat.

References

[1] ATLAS Collaboration Internal Note GEN-NO-001, CERN (January 25, 1993).
[2] CMS Collaboration Internal Note CMS-M/93-05, CERN (January 25, 1993).
[3] L3P Collaboration, "L3P Physics Performance and Increased LHC Bunch Spacing," memorandum to the LHC Committee, CERN (1993).
[4] J. M. Brennan *et al.*, Proc. 1989 IEEE Particle Accelerator Conference, March 1989, Chicago, p. 1154.

ALUMINUM BEAM TUBE FOR SUPER COLLIDER: AN OPTION FOR NO-COATING & NO-LINER

W. Chou, Fermi National Accelerator Laboratory,* P.O. Box 500, Batavia, IL 60510, USA

Abstract

This paper proposes to use a single-layer beam tube made of high strength, high resistivity aluminum alloy (such as 7039-T61 or A7N01) to replace the double-layer copper coated stainless steel tube in Super Collider. The merits, technical issues and possible implementation are briefly discussed. For details the readers are referred to Reference [1]. This work was originally done for the SSC. But it may also be useful to future colliders.

I. INTRODUCTION

The baseline design of the SSC Collider beam tube calls for a stainless steel (SST) pipe of about 2-mm thickness with a thin copper (Cu) layer (about 0.1-mm thick) coated on its inner surface. The purpose of the copper coating is to reduce the surface resistance, thus suppressing the possible beam instability caused by the resistive wall and reducing the beam-induced wall heating. This paper suggests a drastic change in the choice of the beam tube, namely, a single-layer aluminum (Al) alloy pipe without coating. The merits are as follows:

- There will be a potential saving of about $2300 per tube, as shown in Table 1, or $23M for a total of 10000 tubes.
- An extruded aluminum tube with a specially designed cross section (with antechambers or plate insertions) will more easily accommodate a distributed cryopump and, therefore, will eliminate the need for a separated liner addition to the tube.
- There is a concern about adhesion in the bi-layer Cu+SST tube over a 25-year lifetime. This will not be a problem for a single-layer aluminum tube.

Aluminum beam tubes have been used in many lepton storage rings. They were ruled out in the early SSC design mainly because of the concerns about eddy currents and mechanical stability during quench, and the technical difficulty of making leak-free joints between aluminum and stainless steel . However, we will show that the recent industrial development of some high strength, high resistivity aluminum alloys (e.g., 7039-T61 or A7N01) can meet performance requirements in a quench, and that the Al-SST joints have been successfully tested and employed in a cryogenic environment at DESY, KEK and LANL.

*Operated by Universities Research Association Inc. under Contract No. DE-AC02-76CHO3000 with the U.S. Department of Energy.

II. TECHNICAL ISSUES

A. Surface resistance

A.1 Low frequencies — Resistive wall instability problem:

In order to control the beam instability, the requirement on the surface resistance of the beam tube is:

$$\sigma_e \Delta \geq 1 \times 10^5 \quad \Omega^{-1} \tag{1}$$

in which σ_e is the electrical conductivity and Δ the thickness (which is assumed to be smaller than the skin depth δ) of the wall material. Table 2 shows that the product $\sigma_e \Delta$ of a 2.5-mm thick aluminum tube is comparable to that of a 0.1-mm thick copper layer (RRR = 30).

A.2 High frequencies — RF heating problem:

In calculating the parasitic heating due to the beam and wall resistance, the anomalous skin effect (which was overlooked in the early SSC design) plays an important role.[1] The surface resistance ratio $R_s(300\ \mathrm{K})/R_s(4\ \mathrm{K})$ of copper at high frequencies is significantly lower than the dc value.[2,3] The data measured by LANL using a copper coated stainless steel tube is listed in Table 3.[4] In order to have a realistic comparison between Cu and Al, more measurements are needed in the presence of cold temperature (4 K), high frequency ($\geq$ 1 GHz) and strong magnetic field (6.8 T).

B. Quench problem

B.1 Eddy current:

The eddy current during quench is proportional to the product $\sigma_e \Delta$:

$$I = 2\dot{B}b^2 \cdot \sigma_e \Delta \tag{2}$$

in which $\dot{B}$ is the rate of decrease of the magnetic field B, and b is the beam tube radius. It is seen from Table 2 that the eddy current is comparable for the two tubes.

B.2 Quench stress and tube thickness requirement:

To analyze the stress during quench, three effects need to be taken into account: thermal contraction during the cool down from room temperature to 4 K, the vaporized helium pressure P_{He} (which is isotropic in the radial direction pointed inward) and the Lorentz pressure P_{max} (which is in the horizontal direction pointed outward, has a cos-θ distribution and peaks at the equator). For $P_{\mathrm{He}} = 488$ psi and $P_{\mathrm{max}} = 100$ psi, a stress analysis using the 3D code

[1] When the frequency is high enough such that the mean free path of electrons becomes larger than the skin depth, the normal conduction theory based on electron collisions breaks down and the surface resistance becomes independent of the conductivity σ_e of the material. This is called the anomalous skin effect.

Table 1. Cost Comparison

Cu Coated SST Tube		*Al Tube*	
15-m 304LN tube	\$930	15-m A7N01 tube, extruded	\$240
Copper coating	\$2000	Two Al-SST welding joints	\$200
		Two Al-SST demountable joints	\$156
TOTAL	\$2930	TOTAL	\$596

Table 2. Surface Resistance Comparison

Material	σ_e $(\Omega^{-1}\mathrm{m}^{-1})$	δ (mm)	Δ (mm)	$\sigma_e\Delta$ (Ω^{-1})
Cu	1.8×10^9	0.6	0.1	1.8×10^5
Al	5.6×10^7	3.6	2.5	1.4×10^5

Table 3. Surface Resistance of a Copper Plated Tube

Frequency	Ratio $R_s(300\ \mathrm{K})/R_s(4\ \mathrm{K})$
dc	107
0.959 GHz	4
1.865 GHz	3.2
7 GHz	3.7

ANSYS for a 2.5-mm thick aluminum tube gives a maximum stress $\sigma_{\max} = 16.9$ ksi.[5] The critical buckling pressure P_c is 4.57 ksi. According to the American Society of Mechanical Engineers, the allowable stress for membrane loading is:

$$\sigma_{\text{allow}} = 1.5 \times \min\{0.25\sigma_t^u,\ 0.67\sigma_t^y\} \tag{3}$$

in which σ_t^u is the ultimate tensile strength of the tube material, and σ_t^y is the yield tensile strength. For the aluminum alloy 7039-T61 at 4 K, one has $\sigma_{\text{allow}} = 36.75$ ksi. The allowable buckling pressure is:

$$P_{c\ \text{allow}} = \frac{P_c}{4} = 1.14 \quad \text{ksi} \tag{4}$$

To estimate the needed tube thickness, the stress ratio method is employed. The requirement is:

$$\frac{\sigma_{\max}}{\sigma_{\text{allow}}} + \frac{P_{\text{He}}}{P_{c\ \text{allow}}} < 1 \tag{5}$$

For a 2.5-mm thick aluminum tube, this ratio is 0.89. Therefore, it should be safe during quench.

B.3 Quench test:

A convincing evidence of the quench survivability of an aluminum tube comes from a preliminary quench test.[6] The sample is a 2-m A7N01 pipe (1.7-mm thick), which is co-extruded with an A1100 pipe (0.2-mm thick). The eddy current and Lorentz pressure of this clad pipe in a quench are comparable to what is calculated above. The test results showed that the elastic deformation was < 0.1 mm, and the plastic deformation < 0.01 mm.

C. Gas desorption problem

C.1 Photon induced gas desorption:

The main concern of the vacuum problem in the Collider is the photodesorption due to the synchrotron radiation of the protons. Previous measurements at NSLS and CERN showed that the initial photodesorption rate η of aluminum is higher than that of copper and stainless steel. But the rate of decrease is also greater. At sufficiently high photon dose, η for all the three metals tend to similar low values.[7]

C.2 Ion induced gas desorption:

The ionized molecules of the residual gas, which are accelerated by the potential field of the proton beam (about 400 V in the Collider), can desorb gas molecules from the accumulated layer on the tube surface. This effect is usually described by the quantity $\eta_i I$, the product of the ion desorption coefficient and the beam current. Thanks to the low beam current (0.07 A) in the Collider, this effect is small no matter what material (Al, Cu or SST) is used for the beam tube.

C.3 Electron multipactoring:

Because aluminum has a high secondary electron emission coefficient, the electron multipactoring could become a problem as has been observed in the ISR. However, the calculations using Gröbner's model show that this should not be a concern due to the low beam current and short bunch length in the SSC.[8]

D. Al-SST joint problem

The Al-SST joint presents a technical challenge in a cryogenic storage ring because of the possible leak of helium at the joint near the end of the coldmass. In recent years, however, it has been successfully used in a helium environment.

- The demountable joint:[9]
  It uses bolted aluminum and stainless steel flanges manufactured by Hakudo/SMC and is employed in a superconducting RFQ at LANL. The pipe contains helium gas at 450 psi. After 100 thermal cycles between room temperature and 22 K, there was no detectable helium leak. The cost is about \$78 per joint.
- The explosion bonded Al-SST transition piece:
  This has been used in cryogenic and vacuum environments at KEK for years and proved reliable and leak-free.
- The friction welding method:
  In the dipoles of the HERA proton ring, the helium cooling tube of the 40 K shield is made of aluminum. It

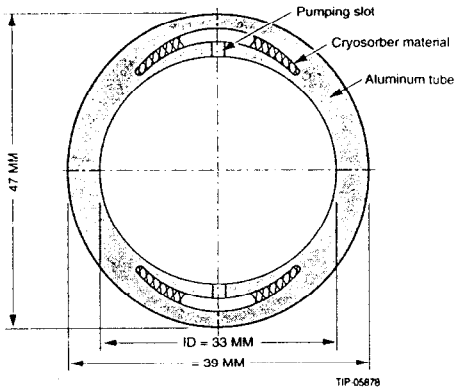

Figure. 1. An aluminum tube with antechambers.

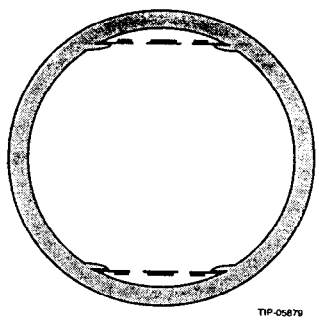

Figure. 2. An aluminum tube with two plate insertions.

is connected to the stainless steel flanges and bellows by friction welding. The helium pressure is 300 psi. During the past several years of operation, no helium leak from these welds has been found.[10] These joints are manufactured by Thevenet Clerjounie Co. The price is about $100 apiece for a mass order.

III. IMPLEMENTATION

There are three possible ways to employ the aluminum beam tube in the Collider.

A. A beam chamber with antechambers

Because aluminum is easy to extrude, one may design a complex cross section to accommodate a cryosorber while eliminating the liner, such as the shape shown in Figure 1. It consists of a beam chamber and two "ears". The "ears" are the antechambers housing the cryosorber material such as coconut charcoal. The chamber and antechambers are connected by a series of pumping slots. The top-bottom symmetry is desirable for reducing the coupling impedance and the multipole magnetic field errors. The extrusion of a 15-m aluminum tube with such a cross section is feasible. There are, however, two potential problems: (1) Machining of the slots is not easy. (2) The two "ears" consume certain radial space that are precious to the magnet measurements.

B. A beam chamber with plate insertions

An alternative is to use a circular tube with two plate insertions as shown in Figure 2. The beam tube is extruded such that there is small bump on the inner surface that can support the plates. During magnet field measurements, the plates are not in place and, thus, a larger aperture is available. After the measurements, the two plates, which are perforated and have cryosorber material on one side, will be inserted into the beam tube for pumping purpose.

C. A beam chamber with an anodized layer

This is proposed in Ref. [11] and is illustrated in Figure 3. The anodized layer serves as a cryosorber. Therefore, no need for a liner. However, there are concerns about the impedance presented by this insulating layer and about the direct exposure of the layer to synchrotron radiation.

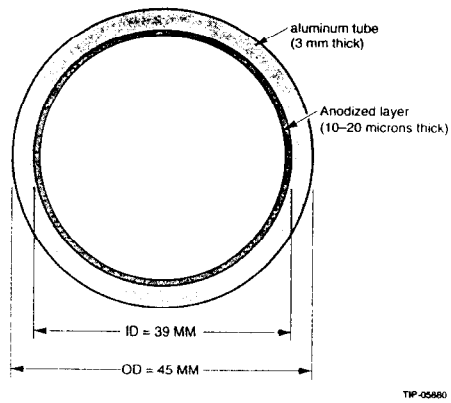

Figure. 3. An aluminum tube with an anodized layer.

References

[1] W. Chou, SSCL-649, SSC Laboratory (1994).
[2] Y. Suetsugu and H. Ishimaru, Japanese Journal of Appl. Phys., Vol. 27, p. 1077 (1988).
[3] J. T. Rogers *et al.*, Appl. Phys. Lett., Vol. 52, p. 2266 (1988).
[4] E. Gray, LANL, private communication.
[5] K. Leung, SSCL, private communication.
[6] H. Ishimaru and M. Nilno, "*Result of Quench Test For Aluminum Alloy Clad Pipe,*" unpublished.
[7] A. G. Mathewson *et al.*, American Vacuum Society Series 12, Conference Proceedings No. 236, p. 323 (1991).
[8] W. Chou, "*Bunch Induced Multipactoring at the SSC,*" Internal Technical Note PMTN-0081C, SSC Laboratory (1993).
[9] N. G. Wilson *et al.*, Conference Record of 1991 IEEE Particle Accelerator Conference, Vol. 4, p. 2459.
[10] H. Kaiser, DESY, private communication.
[11] W. Nexsen, internal technical memo to W. Turner, SSC Laboratory, Sept. 27, 1991.

THE FERMILAB INJECTOR COMPLEX
(The Status of the Fermilab Main Injector Project)

Dixon Bogert
With
W. Fowler, S. Holmes, P. Martin & T. Pawlak
May 1, 1995

The Main Injector is a part of Fermilab III.

A program to increase Collider luminosity by at least a factor of 30 compared to the 1988-89 baseline of $1.6 \times 10^{30} cm^{-2} sec^{-1}$.

Several projects already completed; Main Injector designed to produce the final factor of five increase in luminosity.

Completed projects include:

1) New low-β focusing systems at both Collider experiments.
2) 22 electrostatic separators - helical orbits.
3) Antiproton source improvements.
4) Linac Upgrade Project.

These have combined to produce initial luminosities in excess of $2 \times 10^{31} cm^{-2} sec^{-1}$.

Can hope for Collider luminosity above $1 \times 10^{32} cm^{-2} sec^{-1}$ with Main Injector.

Fermilab is a cascade of four accelerators:

1) 400 MeV Linac
2) 8 GeV Booster
3) 150 GeV Main Ring
4) Tevatron

The Main Ring and Tevatron share a common enclosure. Main Injector will functionally replace the Main Ring in a new accelerator enclosure. Ancillary benefit will be the removal of antiproton production acceleration from the vicinity of Collider experiments.

Main Injector has two-fold symmetry - a sheared oval - siting considerations.

Circumference is 3319 meters.

7 times the Booster
28/53 of the Main Ring

90° FODO cell lattice.

Zero dispersion straight sections created with short dipoles.

Transverse admittance is 40π mm.mrad.
Longitudinal admittance is 0.5 eV-sec.
βmax is 58 meters - stronger focusing than Main Ring.

In addition to the 3319 meter accelerator there are five beam lines:

- 8 GeV Injection from Booster
- 150 GeV protons to Tevatron
- 150 GeV antiprotons to Tevatron
- 120 GeV protons to antiproton source
- 120 GeV protons to existing switchyard

New technical components include:

- 344 dipoles - 128 4 meter - 216 6 meter
- 12 dipole power supplies - 9500 Amp
- 80 long quadrupoles
- 108 sextupoles
- 208 dipole correctors
- 18 rf power amplifiers

"Recycled" technical components now in Main Ring include:

- 18 rf cavities
- 128 quadrupoles and 6 power supplies
- 102 correction magnets
- 589 assorted magnets for the beam lines
- assorted power supplies, controls, and instrumentation

Transfers to Tevatron for acceleration are made at 150 GeV. Tevatron requires 12 Booster batches to fill for Tevatron fixed target physics. This will require two Main Injector cycles.

Antiproton production and Main Injector dedicated fixed target physics will operate at 120 GeV. Main Injector can be filled with 6 Booster batches and send one to antiproton production and use the other five for fixed target physics.

Main Ring admittance at 8 GeV injection has been degraded to only 12π mm.mrad, much worse than original 400 GeV accelerator. The causes are vertical dispersion from overpasses and many more injection/extraction points. Main Injector is designed to have at least 40π mm.mrad transverse admittance at 8 GeV.

This requires large aperture magnets with good field quality and careful location of injection/extraction points.

Fast cycle time (1.5 sec for antiproton production; 1.8 sec including neutrino production) also puts demand on magnets.

The cost estimate reported in the March, 1995 monthly report (dated 4/27/95) was:

WBS	Area	Estimate
1.1	Technical Components	$101.1M
1.2	Civil Construction	$88.7M
1.3	Project Management	$ 8.2M
	Sub Total	$198.0M
	G&A	$ 1.4M
	Contingency	$30.2M
	TOTAL	$229.6M

It is necessary to consider the actual appropriations profile of the FMI to understand some aspects of the construction status at this time. The funding profile has severely constrained the actual obligations.

The Appropriations Profile (History and Projections based on the President's Budget) is:

Fiscal Year	Appropriation Incremental	Cumulative
1992	$11.650M	$11.650M
1993	$15.000M	$26.650M
1994	$25.000M	$51.650M
1995	$43.000M	$94.650M
(History above, projection below)		
1996	$52.000M	$146.65M
1997	$52.000M	$198.65M
1998	$30.950M	$229.60M

It was decided at an early point in the project that the work would be accomplished with approximately the following priorities until funding was not an almost absolute restriction:

1) Technical R&D
2) Technical EDIA
3) Civil EDIA
4) Start Civil Construction
5) Start Dipole Magnets
6) Start Other Technical Components

The result of this prioritization has been that with the exception of the Wetlands Mitigation which was begun in late FY92, the actual civil construction began in FY93, the Dipole Magnet construction in FY94, and the rest of the Technical components in FY95.

Even with this slow start, both the civil and dipole magnet obligations have been subdivided into small amounts with extensive use of 'phased funding'. In addition, the rate at which work has been scheduled has been generally determined by fiscal constraints rather than a consideration of attempting to maximize parallel endeavors.

In spite of the constraints, it is now possible to report that very considerable progress has been made and that the rate of production of those technical components being built and the accomplishment of civil construction has now reached approximately the rates projected when the project schedules were baselined, although in both instances with a several month 'start-up delay' offset. In other words the amount of costs accrued in recent months has reached a steady state supported by the appropriations profile.

The Civil EDIA is being accomplished by the joint efforts of the Fermilab Facilities Engineering Services Section (FESS) and an outside architectural/engineering (AE) firm, Fluor Daniel. Fluor Daniel was selected by an AE selection board following DOE procedures when a State of Illinois Challenge Grant was made available to start environmental assessment and to extend conceptual design. This grant of $2.5M enabled the FMI project to get an early start while awaiting DOE approvals.

Working with a conceptual design prepared by FESS, Fluor Daniel first re-estimated the civil cost of the project, and then after the appropriate DOE approvals prepared the Title I design. The wetlands mitigation package, including work required by the US Army Corps of Engineers permit granted as part of the environmental assessment work, was prepared under the Challenge Grant. The actual wetlands mitigation work was the first package approved for bidding and construction by DOE, and the work was completed in FY93.

After the DOE approved the Title I package Fluor Daniel began work on the rest of the Title II design, divided into packages as best as FMI project management could judge that funding and scheduling would permit. It should be noted that over the course of the FMI project to date, the funding profile has undergone several changes to date. The effect has been to stretch out the project by reducing the obligation authority in the early years of the project. Thus, some of the structure of the work packages initially specified to Fluor Daniel has been modified either in scope at design or by dividing into phases at bidding.

Fluor Daniel has completed the Title II design work and bid specification documents with the single exception of the 8 GeV beam line at the Booster Connection where Fermilab has suggested a change in the radiation shielding specification (from passive shielding to interlocked detectors) to reduce the impact on the SW Booster tower.

Roughly speaking, the current list of bid packages (civil contracts) is now:

1) Wetlands Mitigation
2) Accelerator Enclosure @ MI-60
3) MI-60 Service Building
4) Site Prep, roads, utilities (3 phases)
5) Substation Hardstand
6) Enclosure Precast Units (3 phases)
7) 8 GeV Line Precast Units
8) FMI Ring Enclosure (2 phases)
9) 8 GeV Line (3 phases)
10) FMI Service Buildings (8 structures)
11) Cable Trays in enclosures
12) 13.8kV Distribution
13) 345kV Transmission Line
14) Kautz Road Substation
15) Commonwealth Edison 345kV connection
16) Addition @ MR-F0 Service Bldg.; new F17
17) Cooling Ponds & Cooling system
18) Connection of FMI at MR/TeV F0
19) Connection of 8 GeV Line at Booster
20) Landscaping, Road Paving, etc.

additional acquisitions/construction projects include:
A) Various Transformers
B) Shielding Steel
C) Survey Monuments
D) Reconstruction of the E4R facility

At this moment, the following work on the above list has been completed:

1) Wetlands Mitigation
2) Accelerator Enclosure @ MI-60
3) MI-60 Service Building
4) Site Prep, roads, utilities (3 phases)
5) Substation Hardstand
C) Survey Monuments

Work is in progress on the following:

6) Enclosure Precast Units (3 phases)
   (approximately 1140 of 1181 built)
   (production rate 4/day)
   (should complete 5/15/95)
7) 8 GeV Line Precast Units
   (221 units under contract)
   (will follow #6 above)
   (should complete 7/31/95)
8) FMI Ring Enclosure (2 phases)
   (approximately 50% complete)
   (approximately $8.5M of $17M costed)
   (approximately 794 of 1181 units set)
9) 8 GeV Line (3 phases)
   (Started 4/10/95)
   (Phases 1 & 2 FY95 money)
   (Phase 3 FY96 money)
   (Phase 2 requires accelerator shutdown)
B) Shielding Steel

Bidding and/or contractual negotiations will soon be in (or are in) progress on:

15) Commonwealth Edison 345kV connection
(DOE negotiates this work)
(EDIA will be obligated FY95)
(Construction, etc., in FY96)
A) Various Transformers
D) Reconstruction of the E4R facility

The following work will be obligated in FY96; in some instances phased funding will extend into FY97 and even FY98:

10) FMI Service Buildings (8 structures)
11) Cable Trays in enclosures
12) 13.8kV Distribution
13) 345kV Transmission Line
14) Kautz Road Substation
17) Cooling Ponds & Cooling system

The following work will be obligated in FY97:

16) Addition @ MR-F0 Service Bldg.; new F17

The following work will be obligated in FY98:

18) Connection of FMI at MR/TeV F0
19) Connection of 8 GeV Line at Booster
20) Landscaping, Road Paving, etc.

To date, the actual civil construction work has been bid below estimates, and work completed, including changes to work in progress has not exceeded the baseline estimates. Civil EDIA has, however, exceeded initial estimates.

The FMI civil designs have included a number of capabilities for future utilizations including several possible extraction points, room for Siberian Snakes, and room for possible additional ring in the enclosure. Fermilab has requested Fluor Daniel to design and estimate a stub at the extraction point for a possible neutrino beam to Soudan, Minnesota. This work was added to the scope of the Main Injector and negotiations to add the stub to the ring enclosure contract are complete.

Various slides illustrating civil construction progress to date will be shown to illustrate what has been accomplished.

The Technical Components of the FMI are divided at WBS Level 3 into the following areas:

1) Magnets
2) Vacuum
3) Power Supplies
4) RF Systems
5) Kickers and Slow Extraction
6) Instrumentation
7) Controls
8) Safety Systems
9) Utilities and Abort
10) Installation

Three of these areas were the subject of the now essentially completed R&D program. These were the dipole magnets, the dipole power supply, and a redesign of the RF power system. The dipole magnet R&D program was designed to flow smoothly into the production of the guide field dipoles, and indeed when the R&D program was finished approximately the end of 1QFY94 the production of dipole magnets was initiated. Since Fermilab acts as the 'general contractor' for the dipole magnets and only performs the final assembly (about 6% value added) there was a long 'start up' period while all the queues were filled.

Now production has reached a steady state of approximately one dipole completed every two working days. There are essentially two streams of material that have to meet just prior to final assembly for this to work correctly. The magnets each consist of two insulated copper coils and two steel half cores fabricated from stacked steel laminations. One stream has to provide the insulated coils at the rate of a pair every two days, and the other stream needs to provide a pair of stacked half cores every two days.

The copper coils are wound at Everson Electric in Pennsylvania. The bare copper coils are shipped (via Fermilab) to Tesla Engineering in England (via rail and sea) to be insulated, and returned (via sea and rail) to Fermilab. The steel is fabricated in the form of coils at LTV steel, shipped to a coil 'slitter', and then shipped to a lamination stamper. The steel production is not a 'continuous process', but rather a series of supposedly reproducible runs. To avoid systematic variations as much as possible, the steel laminations are shipped to the 'stacker' (SVF in Rock Falls, IL) according to a 'recipe' selection which the stacker then follows.

SVF is also responsible for the manufacture of 'end packs', special small stacks of laminations using non-standard laminations to produce the desired end fields. The completed half cores are then delivered to Fermilab. The accompanying slide shows the plan and performance since all these queues began producing in the second half of FY94, leading to a completed set of 60 production dipoles as of 5/1/95, and producing now at the rate of one every two working days.

Dipole issues: Delivery of insulated coils.
Variation in high field performance of the magnets

Not damaging to timely completion of an acceptable accelerator. Source of field variation understood - variations in magnetic permeability in regions of magnet far from saturation. Discussions with LTV to ensure greater variations do not occur.

The FMI will utilize 'recycled' quadrupoles from the Main Ring for most of the quad requirements. Those quads which are to be 'recycled' (which will require a change of the mounting system and a change of beam tube) must be left in the Main Ring until the accelerator shutdown when the enclosure connections are built at MR-F0 and the Booster. Some additional quads are required however to make up a sufficient inventory for the FMI ring and the 8 GeV transfer line. These quads are being fabricated to a larger extent than the ring dipoles at Fermilab. This fabrication, which includes at Fermilab the steps of coil winding, coil insulation, half core stacking, and final assembly, also began in FY94 and is continuing.

All 35 '100-inch' quads have been completed, and coil winding for an eventual complement of 52 '116-inch' quads has begun. 10 '116-inch' half cores have been stacked, and one has been assembled.

113 sextupole magnets are also required. Construction has begun on these which are also built at Fermilab in a fashion similar to the quadrupoles. 10 have been completed, and the present construction rate is 2/month.

As of 5/1/95, all of the completed dipoles, most of the completed quadrupoles, and 2 of the completed sextupoles have been magnetically measured at the Magnet Test Facility.

Procurement of material for Lambertson magnets has begun, and EDIA for the Lambertsons, horizontal trim dipoles, "C" magnets, and "3Q120" quads is in varying degrees of completion.

A dipole power supply was designed and assembled at the 'E4R test facility' as part of the FMI R&D program. A six month test program was operated successfully, using conventional oil filled transformers. This facility is now being converted to operate with relatively newer design dry transformers for evaluation. A second power supply was procured as part of the R&D effort and assembled in the MI-60 building. During FY95 parts for the additional dipole supplies will begin to be ordered as evaluation of the R&D supplies is completed.

Other power supplies are being engineered.

The final piece of the R&D program was a redesign of the RF supply using more modern components than utilized for the Main Ring RF system 25 years ago. Some commercial parts have been acquired in this work, The R&D units have been successfully operating to drive a MRRF cavity for some months now, and the design is regarded as complete and demonstrated. Using FY95 funds approximately $1.25M in requisition activity was initiated in January 1995, and construction of the last R&D equipment is being completed in the MI-60 building.

All the Technical Component Level 3 projects have now been allocated funding to complete design and start construction/acquisition activity to some extent. The utilities installation needed at the MI-60 building has begun, and several $100K-plus tasks representing the first parts of LCW piping are complete. Heat exchangers and associated tanks are in various stages of acquisition for the MI-60 system. Design work for vacuum systems, some kicker supplies, some instrumentation (especially beam position monitors), controls, safety systems, and magnet installation equipment is well advanced. Initial acquisitions in all these areas are funded in FY95.

Reference Information:

The following pages are included and their source acknowledged:

1) S. D. Holmes, November 1994 DOE Review, page 6. "SCOPE"

2) T. Pawlak, November 1994 DOE Review, page 2. "CIVIL SCOPE"

3) T. Pawlak, November 1994 DOE Review, page 3. "CIVIL CONSTRUCTION COST ESTIMATE"

4) T. Pawlak, November 1994 DOE Review, page 24. "CIVIL CONSTRUCTION COST SUMMARY"

5) T. Pawlak, November 1994 DOE Review, page 25. "FLUOR DANIEL FEE SUMMARY"

6) E. G. Pewitt, 1/24/95, "FMI Magnet Systems/Dipole Production Schedule"
   a) Plan
   b) Annotated current status

7) A. L. Read and T. L. Williams, 1/27/95, "Top Level Gantt Chart for FMI Project" (four pages)

THE STATUS OF THE FERMILAB MAIN INJECTOR PROJECT

D. Bogert, W. Fowler, S. Holmes, P. Martin, and T. Pawlak
Fermi National Accelerator Laboratory*, P.O. Box 500 Batavia, IL 60510

The Fermilab Main Injector is a new 150 GeV synchrotron now in the fourth year of a scheduled seven year funding profile. An R&D program has been completed, and both civil construction and the production of technical components are well underway. The Main Injector Project is part of a larger upgrade program at the Fermi National Accelerator Laboratory called Fermilab III which is designed to ensure a Collider luminosity in excess of $5x10^{31}$ $cm^{-2}sec^{-1}$ while simultaneously providing a 2 microAmp resonantly extracted 120 GeV beam. The 120 GeV beam will provide unique capabilities in the realm of rare neutral K decays and long baseline neutrino oscillation experiments. The expected performance characteristics of the Main Injector will be discussed, and the status of the construction and the schedule for completion will be reviewed.

I. OVERVIEW

Fermilab III, a program to produce at least a factor of 30 increase in the Tevatron Collider luminosity as compared with a 1988-89 baseline of $1.6x10^{30}$ $cm^{-2}sec^{-1}$ has included several projects at Fermilab of which the Main Injector is designed to produce the final factor of five increase in luminosity. The other projects: new low-Beta focusing systems at both colliding experiments, 22 electrostatic separators to eliminate collisions other than at the experiments, improvements to the antiproton source, and the Linac Upgrade Project have already produced initial luminosities in excess of $2x10^{31}$ $cm^{-2}sec^{-1}$, leading to the hope of achieving a luminosity above $1x10^{32}$ $cm^{-2}sec^{-1}$ with the Main Injector. The present Fermilab accelerator complex is a cascade of four accelerators (400 MeV Linac, 8 GeV Booster, 150 GeV Main Ring, Tevatron) The Main Ring and Tevatron share a single tunnel enclosure. The Main Injector will functionally replace the Main Ring in a separate tunnel enclosure. An ancillary benefit is to remove the 150 GeV accelerator from the vicinity of the Collider experiments where the operation of the Main Ring introduces an undesirable background which can only be avoided by a combination of shielding and gating. The gating reduces the D-Zero experiment live time significantly.

The Main Injector is an accelerator with the two fold symmetry of a sheared oval, the exact shape being dictated by siting considerations. The circumference is 3319 meters, seven times the Booster, or 28/53 of that of the present Main Ring. The lattice is based upon a 90^0 FODO cell, with zero dispersion straight sections created with short dipoles. The transverse admittance is 40π mm.mrad and the longitudinal admittance is 0.5 eV-sec. β_{max} is 58 meters representing stronger focusing than the Main Ring.

In addition to the 3319 meter Main Injector accelerator, there are five beam lines to provide for: injection from the Booster at 8 GeV, two lines for proton and antiproton transfers from the Main Injector to the Tevatron at 150 GeV, and two lines at 120 GeV for extraction of protons for antiproton production and to the existing fixed target switchyard.

New technical components including 344 dipoles and 12 dipole power supplies, 80 long quadrupoles, 108 sextupoles, 208 dipole correctors, and 18 rf power amplifiers are included in the project. "Recycled" technical components to be relocated from the existing Main Ring include 18 rf cavities, 128 quadrupoles and 6 power supplies, 102 correction magnets, 589 beam line magnets, and assorted power supplies, controls, and instrumentation. A second 345 kVolt substation will be built on the Fermilab site with some back feed capability between the existing substation and the new one.

Transfers to the Tevatron for fixed target physics acceleration cycles, or for Collider operation, are made at 150 GeV. Twelve Booster batches are presently required to fill the Main Ring. The Main Injector will be filled with six Booster batches, requiring two Main Injector acceleration cycles to 150 GeV to fill the Tevatron for fixed target physics at Tevatron energies. Antiproton production at 120 GeV, on the other hand, only requires a single Booster batch. The Main Injector has been designed with a faster cycle time than the Main Ring to increase the rate of antiproton production. If loaded with six Booster batches, one batch is sufficient for antiproton production while simultaneously permitting the direct extraction at 120 GeV of the other five Booster batches for a dedicated fixed target research program at 120 GeV.

When built and operated as a 400 GeV accelerator in the early 1970's the Main Ring had a transverse admittance much higher than the approximately 12π mm.mrad measured today at 8 GeV injection from the Booster. The reduction in admittance is the result of many changes made to the Main Ring since its inception. The most significant of these changes are the introduction of the vertical overpasses at the CDF and D-Zero colliding detectors, a source of vertical dispersion which the original planar machine did not have, and the introduction of more extraction and injection points, especially for antiproton production and Tevatron injection, which has further reduced the aperture of the Main Ring. The reduced admittance of the Main Ring at the 8 GeV transfer from the Booster is the greatest single limitation on luminosity increases left in the acceleration cycle. The Main Injector has been designed to have a minimum of a 40π mm.mrad admittance at 8 GeV. This has been achieved by the design of large aperture magnets and with great care to place injection and extraction devices at advantageous places in the lattice. These considerations, coupled with the requirement

*Operated by Universities Research Association, Inc., under contract with the U.S. Department of Energy

for a 1.5 second cycle time to 120 GeV for antiproton production, or a 1.8 second cycle time for neutrino production, have implied the necessity of designing new conventional copper and iron magnets with a good field quality over a large aperture with a cost effective high ramp rate. Power supplies and rf capabilities matching these requirements have also been developed. The design and prototype production of the dipole magnets, the dipole power supplies, and rf power amplifiers were the subject of the completed R&D Program.

II. DESIGN; R&D PROGRAM; FUNDING

The actual construction of the Main Injector was proceeded by two pieces of the project program, both of which were also necessary in the process of obtaining funding and approval to begin construction. The first was the completion of a design report, which evolved into the Title I design report and later into the Main Injector Technical Design Handbook. The design report was an iterative process that specified the accelerator lattice, the beam transfer lines, injection and extraction techniques, and the necessary equipment: magnets, power supplies, rf, vacuum, instrumentation, controls, utilities, etc. Using the design report, it was then possible for both civil and technical designers to begin detailed designs in each area. Also, the lattice could be checked by tracking programs and then the actual measured values of magnetic fields, with harmonics, could be inserted into the tracking programs used during the initial designs, and the whole process iterated.

On the basis of the design report, it was possible to count the necessary new technical components, as well as to identify those items which could be reused from the Main Ring, such as the main quadrupoles. A complete cost estimate leading to the definition of the project financial baseline was thus generated.

In the course of the design studies, three areas were identified which were the focus of a large R&D effort. These were the main guide field dipole magnets, the dipole power supplies, and an improved rf power amplifier. The R&D program began in FY90 and was completed in early FY95. The first major emphasis was placed upon the demonstration that a reliable large aperture conventional dipole magnet with rapid excitation could be designed and then mass produced at a reasonable cost. The second project was the design, construction, and operation of the necessary 9500 Amp power supply for the dipole guide field, and finally the development of a solid state rf power amplifier using commercially available technology, and a demonstration that it was reliable using the existing Main Ring.

The dipole R&D program consisted of the following activities. First, two dipoles were constructed and completed during FY91. These dipoles were used to first study the body field in the magnet and to assure that the field was adequate at both injection and at 120 GeV and 150 GeV extraction energies. Next, the details of the 'end pack' design were worked out by a combination of design calculations and physical construction, both carried out in iteration. Finally, after consultation with business and procurement personnel from the Department of Energy, a business strategy for the procurement of the dipoles in production quantities was defined, and ten more R&D dipoles were constructed using commercial vendors for all tasks that were not to be done at Fermilab. Additional quadrupoles and sextupoles are also required, and were designed at this time.

A first prototype dipole power supply was constructed and operated with R&D magnets as a test load at site E4R, originally constructed for the 4 cm SSC magnet test string. The prototype design suggested several modifications, and a second dipole power supply was also constructed under the R&D program. Both oil filled and dry type 13.8 kVolt transformers are undergoing evaluation as part of the ongoing testing of the R&D dipole power supply.

A new solid state rf power amplifier using commercial components was constructed and has been operated without failure throughout the most recent Collider run in the Main Ring.

It is not possible to conclude a discussion of the design of the Main Injector without reference to the project funding profile, since this also has a significant iterative impact on the details of the planning for project construction. It was originally conceived that an aggressive funding profile should be assumed since, among other advantages, a rapid funding profile can be easily demonstrated to minimize overall project costs. It was assumed at first that an approximately flat four year profile was both sensible and achievable. In fact, the actual appropriations and the funding profile that has been incorporated in the last three fiscal year's appropriation is not aggressive at all. The project is now shown as a seven year project with a total, then year cost, estimated at $229.6M on the plant line with a total project cost of $259.3M. Now in the fourth year of plant line appropriations, the total appropriated to date (FY92 through FY95) is $94.65M. The actual appropriations have been: FY92 $11.65M, FY93 $15M, FY94 $25M, FY95 $43M, and budgeted amounts for future years are FY96 $52M, FY97 $52M, FY98 $30.60M, with commissioning extending into FY99. It should be noted that in order to start both the technical and civil construction it has been necessary to make extensive use of both phased funding and bids with options to extend, and to divide work which could easily be accommodated into larger contractual obligations into relatively small pieces. This has had an impact on the civil design and on the methodology of technical component construction.

As of April 1, 1995, the cost estimate included $101.1M for technical components, $88.7M for civil construction, $8.2M for project management, $1.4M for G&A, and the remainder ($30.2M) unassigned contingency.

III. CIVIL CONSTRUCTION

The first conceptual civil design for the Main Injector was made by the Fermilab civil engineering group prior to FY91. It was then decided that the detailed Title I design package, the individual Title II bid packages, and a substantial part of the Title III effort would be done by an outside A&E firm in support of the Main Injector Project Office and a small group from Fermilab. Thus in early 1991 an A&E selection board was constituted and as a result Fluor Daniel, a national A&E firm with a substantial Chicago office, was selected as the Main Injector A&E firm. An important early assist to this endeavor was a State of Illinois Challenge grant totaling $2.2M which permitted Fluor Daniel to prepare some advanced Title I designs prior to the formal release of federal funding. The Illinois Challenge grant was also used to help prepare the Environmental Assessment. Details of the approval stages prior to the unrestricted release of funding for construction have been reported previously. [1,2] Fluor Daniel carried out the Title I and Title II design effort on the basis of a negotiated fixed price contract.

The basic civil requirements of the Main Injector are: 1) a Ring Enclosure for the accelerator consisting of 1181 precast units in an inverted "U" shape and cast-in-place tunnel segments at 'non-standard' locations, 2) Tunnel connections for transport of 8 GeV Protons from the Booster to the Main Injector (211 more precast units), and for transfer of 150 GeV Protons and Antiprotons from the Main Injector to the Tevatron, 3) Connections to existing enclosures at the Booster and at MR/Tev F0, 4) Service buildings at appropriate locations around the Main Injector, on the 8 GeV transfer Line, and as necessary for connection to the Tevatron, 5) Site Utilities - water, electrical, new 345 kVolt service, etc., and 6) various other installations.

By the standards of many large civil projects, the Main Injector is not a particularly large construction project. It is possible to consider such a project as either one or a very few construction contracts. The funding profile discussed above, however, led management and the A&E firm to adopt a very different approach. The civil work has been divided into approximately 24 packages for construction and/or procurement. It need hardly be observed that this rather fine subdivision of the work does create a significantly larger number of bid drawings and specifications sets, and even then there is a considerable connection to an assumed obligations profile which, if altered, causes some disruption of assumptions designed and drawn into the many individual bid packages. This all translates into increased EDIA (Engineering, design, inspection, administration) costs as compared with the minimum conceptually possible.

A list of the bid packages (civil construction contracts) and civil procurement items is found in the following table. Projects for which the civil construction is completed are indicated "complete". Details about the scope and bidding of 'completed' projects have been previously reported. [2] Projects in progress are so indicated. Projects to be funded in this or future fiscal years are indicated by the notation of the fiscal year when the obligation is expected.

1) Wetlands Mitigation (complete)
2) Accelerator Enclosure at MI-60 (complete)
3) MI-60 Service Building (complete)
4) Site Preparation, roads, utilities (3 phases)(complete)
5) Substation Hardstand (complete)
6) Ring Enclosure Precast Units (3 phases)(in progress)
7) 8 GeV Line Precast Units (in progress)
8) Main Injector Ring Enclosure (2 phases)(in progress)
9) 8 GeV Line (3 phases)(in progress)
10) Main Injector Service Buildings (8 structures)(FY96)
11) Cable Trays in Enclosures (FY96)
12) 13.8kV Distribution (FY96)
13) 345kV transmission Line (FY96)
14) Kautz Road Substation (FY96)
15) Commonwealth Edison 345kV connection (FY95)
16) Add to MR-F0 Service Building, new F17 (FY97)
17) Cooling Ponds and Cooling System (FY96)
18) Connection of Main Injector at MR/TeV F0 (FY98)
19) Connection of 8 GeV line at Booster (FY98)
20) Landscaping, Road Paving, etc.(FY98)
21) Various Transformer Procurements (FY95)
22) Shielding Steel Procurements (in progress)
23) Survey Monuments (complete)
24) Reconstruction of E4R facility (FY95)

The ring enclosure inverted "U" precast units have been built at the rate of four units per day since early February 1994. The contractor is PBM Concrete of Rochelle, Illinois. Approximately 1140 of 1181 have been completed, and the contract should be finished approximately May 15, 1995. PBM Concrete is also building the 211 precast units for the 8 GeV line. Production will follow immediately upon completion of the ring enclosure precast units and should be completed by July 31, 1995.

The Main Injector ring enclosure was started in April 1994 by the contractor, Wil-Freds of Aurora, Illinois. Approximately 50% of this work is complete and costed. The work consists of excavation following by tunnel construction using precast units set on a cast-in-place base slab, as well as sections of cast-in-place tunnel where non-standard cross sections are required. The work also includes exit stairs and the stairs and backwalls at the locations of future service buildings. The enclosure contract should be completed in early 1996.

The 8 GeV line contract was awarded to Martam Construction of Glen Ellyn, Illinois. Work has just begun on phases 1 and 2 using FY95 funding, the third phase will be funded in FY96. Phase 2 requires an accelerator shutdown which is scheduled to begin July 24, 1995.

Shielding steel procurements subcontracted to Wil-Freds are underway. The use of 'continuous cast salvage slab' steel delivered by rail car to Fermilab has been found to be quite advantageous.

Fluor Daniel has completed the Title II packages for all of the civil construction work with the single exception of some details on the 8 GeV Connection at the Booster. To date, the actual civil construction work has been bid below the Title II estimates, and work completed, including changes to work in progress, has not exceeded the Title I baseline estimates. Civil EDIA has, however, exceeded initial estimates.

The Main Injector civil designs have included a number of capabilities for future utilizations including several possible extraction points, room for Siberian Snakes for polarized protons, and a 'keep away' region for a possible additional ring of magnets in the enclosure. A recently approved addition to the scope of the Main Injector Ring Enclosure added an extraction stub enclosure for a northwesterly extracted beam. This stub was designed at Fluor Daniel and is being added by negotiation to the enclosure contract.

IV. TECHNICAL COMPONENTS

The technical components for the Main Injector Project have been divided into ten "WBS Level 3" areas, each with a "Level 3 Manager" responsible for the cost estimate, scheduling, and overall design and production. These ten areas are: 1) Magnets, 2) Vacuum, 3) Power Supplies, 4) rf Systems, 5) Kickers and Slow Extraction, 6) Instrumentation, 7) Controls, 8) Safety Systems, 9) Utilities and Abort, and 10) Installation.

It was decided at an early point in the project that the work would be accomplished with approximately the following priorities until funding was not an almost absolute restriction: 1) Technical R&D, 2) Technical EDIA, 3) Civil EDIA, 4) Start Civil Construction, 5) Start Dipole Magnets, and 6) Start other technical components. The result of this prioritization coupled with the actual funding appropriations outlined above has been that with the exception of the Wetlands Mitigation which was begun in late FY92, the actual civil construction began in FY93, the dipole magnet production began in FY94, and the rest of the technical components were only funded to start construction in FY95. Even with this slow start, both civil and dipole magnet obligations have been subdivided into small amounts with extensive use of 'phased funding.' In addition, the rate at which work has been scheduled has been generally determined by fiscal constraints rather than a consideration of attempting to maximize parallel endeavors.

In spite of the funding constraints, very considerable progress has been made and the rate of production of technical components being built and the accomplishment of civil construction has now reached approximately the rates projected when the project schedules were baselined, although in both instances with a several month 'start-up delay' offset. In other words, the amount of costs accrued in recent months has reached a steady state supported by the appropriations profile.

The dipole magnet R&D program was designed to flow smoothly into the production of the guide field dipoles, and when the R&D program was finished approximately at the end of the first quarter of FY94 the production of dipole magnets was initiated. Since Fermilab acts as the 'general contractor' for the dipole magnets and only performs the final assembly (about 6% value added) there was a long 'start up' period while all the queues were filled.

Now production has reached a steady state of approximately one dipole completed every two working days. There are two streams of material which meet just prior to final assembly for this to work correctly. The magnets each consist of two insulated copper coils and two steel half cores fabricated from stacked steel laminations. One stream has to provide the insulated coils at the rate of a pair every two days, and the other stream has to provide a pair of stacked half cores every two days.

The copper coils are wound at Everson Electric in Pennsylvania. The bare copper coils are shipped, via Fermilab, to Tesla Engineering in England (via rail and sea) to be insulated, and returned, (via sea and rail) to Fermilab. The steel is fabricated in the form of coils at LTV Steel, shipped to a coil 'slitter', and then shipped to a lamination stamper. The steel production is not a 'continuous process' but rather a series of supposedly reproducible runs. To avoid systematic variations as much as possible, the steel laminations are shipped to the 'stacker' (SVF in Rock Falls, Illinois) according to a 'recipe' selection which the stacker then follows. SVF is also responsible for the manufacture of 'end packs', special small stacks of laminations using non-standard laminations to produce the desired end fields. The completed half cores are then delivered to Fermilab. As of the end of April, 1995, approximately 60 production dipoles have been completed and measured, with sustained production over several months at the rate of one every two working days.

Two issues, neither damaging to the timely completion of an acceptable accelerator lattice, have arisen during the last half year of dipole production. An interruption of the delivery of the insulated coils due to transportation labor difficulties in Canada led to a suspension of production while a larger inventory was accumulated. Without some buffer in the inventory a large exposure to small upsets in the delivery transportation system could too easily again interrupt production. A review of delivery experience led to the decision to create a four week inventory to draw against for the insulated coils. Measurement of the finished magnets revealed a larger than expected, although still acceptable, variation in the higher field (only) performance of the magnets which correlated with steel from different production runs at LTV. When the source of this variation was understood, (variations in magnetic permeability in regions of the magnet far from saturation when the gap was at high field) discussions to insure that greater variations did not occur were conducted with LTV and attention to any source of steel variation is constant.[3]

The Main Injector will utilize 'recycled' quadrupoles from the Main Ring for most of the quadrupole requirements. The recycled quadrupoles will require a change of the mounting system and a change of beam tube. These quadrupoles must be left in the Main Ring until the accelerator shutdown when

the enclosure connections are built at MR/Tev-F0. Eighty additional quadrupoles are required for the Main Injector Ring lattice. These quadrupoles are being fabricated at Fermilab to a larger extent than the ring dipoles. The work at Fermilab for these quadrupoles includes the steps of coil winding, coil insulation, half core stacking, and final assembly. This work also began in FY94 and is continuing. To date the complete complement of 35 254 cm (100") quadrupoles has been assembled, and work on an eventual complement of 52 295 cm (116") quadrupoles is underway with over half of the necessary coils wound and 20% of the half cores stacked. One 295 cm quadrupole is fully assembled. 113 sextupole magnets are required and are also being built at Fermilab. Ten have been completed at the rate of two per month. Essentially all of the completed magnets have been powered and measured at the Magnet Test Facility.[3,4]

Procurement of materials for Lambertson magnets and "C" magnets for the transfer lines has begun, and studies of the Lambertson end field configuration have been completed. Other quadrupoles and trim magnets are in various stages of design.

When the evaluation of the dipole power supply built under the R&D program at E4R is complete later in FY95, parts for the full complement of power supplies will be ordered. Parts are being ordered for the kicker supplies as engineering is completed.

Following the completion of the rf R&D program, approximately $1.25M of parts for the production complement of the rf power amplifiers have been ordered since January 1995. This equipment will be assembled in the MI-60 service building as it is delivered.

Design work for a beam position monitor based upon the cross section of the Main Injector beam tube is in progress, and successful prototyping has been completed.

All of the Technical Component Level 3 project areas have now been allocated funding in FY95 to complete design work and to start acquisition and construction activities to some extent. The utilities installation needed at the MI-60 building has begun, and several tasks each in excess of $100K were started in FY95 and some of the low conductivity water (LCW) piping tasks have been completed. Heat exchangers are being acquired and will be installed also. Design work for vacuum systems, controls, safety systems, and magnet installation equipment is well advanced. An installation test in an approximately 30 meter section of standard tunnel cross section in the completed MI-60 enclosure region is underway.

V. SCHEDULE

The present seven year funding profile is much slower than was originally expected or hoped. When the Main Injector was in the conceptual design stage, a four year schedule was believed to be quite realistic, and considering the original schedule for the construction of Fermilab over twenty-five years ago, such a schedule was considered demonstrated. The actual project schedule has been funding limited since the first appropriation and continues to be funding limited.

It will be necessary to turn off the Fermilab physics program for a period of approximately nine months to connect the Main Injector to the existing complex at the Booster and the Tevatron rf straight section (called MR/Tev F0) involving demolition work at both locations. To minimize the down time of Fermilab all the rest of the civil and technical construction, and the installation of new components, must be completed prior to the final civil interconnections at MR/Tev F0 and the Booster. The connection at the Booster could be accomplished at an earlier shutdown of sufficient length if the funding is available. Technical staff cannot be 'double counted' during the shutdown, so all possible prior work must be completed so staff is available to dismantle, remove, and recondition items such as the Main Ring quadrupoles being recycled into the Main Injector. According to the present funding profiles which require $52M in each of FY96 and FY97 it will be just possible to complete the pre-shutdown work in time to permit the 9 month shutdown to begin in February 1998 so that commissioning should be completed in early 1999. It is absolutely necessary that the present funding profile that has existed in the last three of the President's budget proposals to Congress be maintained if this schedule is to be met.

The Main Injector project management team is very encouraged by the progress of the project to date. Progress on all civil and technical design and construction has been rapid given the available funding, and both obligations and costing of completed work are tracking the original project baseline with a less than three month delay, almost all of which represented a slightly slow startup, some large fraction of which was delays in administrative approvals for the first expenditures. Actual contracts have been placed at favorable pricing. The project is essential for the national physics program, a point repeatedly endorsed even prior to the elimination of the SSC project. Project management is anxious to complete the job and to make this research facility available to the research community.

VI. REFERENCES

[1] D. Bogert, W. Fowler, S. Holmes, and P. Martin, "The Status of the Fermilab Main Injector," XVth International Conference on High Energy Accelerators, Hamburg, Germany, Vol.1, p.492, (July 20-24,1992).

[2] D. Bogert, W. Fowler, S. Holmes, P. Martin, and T. Pawlak, "The Status of the Fermilab Main Injector Project," Proceedings of the 1993 Particle Accelerator Conference, Washington, D.C., Vol.5, p. 3793, (May 17-20, 1993).

[3] D. J. Harding et. al., "Magnetic Field Measurements of the Initial Fermilab Main Injector Production Dipoles", Proceedings of this Conference.

[4] D. J. Harding et. al., "Magnetic Field Measurements of the Initial Fermilab Main Injector Production Quadrupoles", Proceedings of this Conference.

A 200 KW POWER AMPLIFIER AND SOLID STATE DRIVER FOR THE FERMILAB MAIN INJECTOR

J. Reid and H. Miller, Fermi National Accelerator Laboratory*, P.O. Box 500 MS-306, Batavia, IL 60510 USA

Abstract

A limitation of the existing Main Ring rf system is the power that it can deliver. The Fermilab Main Injector will require 112 KW for accelerating the full intensity at 240 GeV per second, which is pushing the upper limits for the present rf power amplifiers used in the Main Ring. New 200 KW power amplifiers will be placed on the cavities in the tunnel with 4 KW solid state drivers and 30 KV series tube modulators in the equipment gallery. Design, reliability, and solid state driver operating in a Main Ring rf station will be presented.

I. INTRODUCTION

Reliability testing of the newly designed equipment built under an R&D program by the rf department was made by installing it in the present Fermilab Main Ring accelerator. This gave real time operating experience under beam loading conditions before the equipment went into full production for the Main Injector. The 200 KW power amplifier and a 4 KW solid state driver were installed in May of 1994 on RF-RF station 7. For over 11 months they have operated flawlessly.

II. 200 KW POWER AMPLIFIER

The new amplifier design is based on the following:

1. Reliability. Since this component is located in the tunnel and mounted on top the MR cavities, a failure requires downtime. Only the power module housing the Y-567B tetrode and the cathode resonator would now be in the tunnel. Previous designs have a 14 tube cascode and a 6 tube distributed amplifier attached to the power module in the tunnel.
2. Geometry of the mounting flange and anode circuit had to be compatible with the present MR-RF cavity.
3. We will use the Y-567B power tetrode along with Fermilab's existing tube socket parts (fingers and collets). We have used the Y-567B in our existing amplifiers for many years and the power stage has proven to have excellent reliability.
4. Provide improved water cooling on and around the tube socket and bypass capacitors to remove heat.
5. Provide peak rf current of approximately 21 amps.

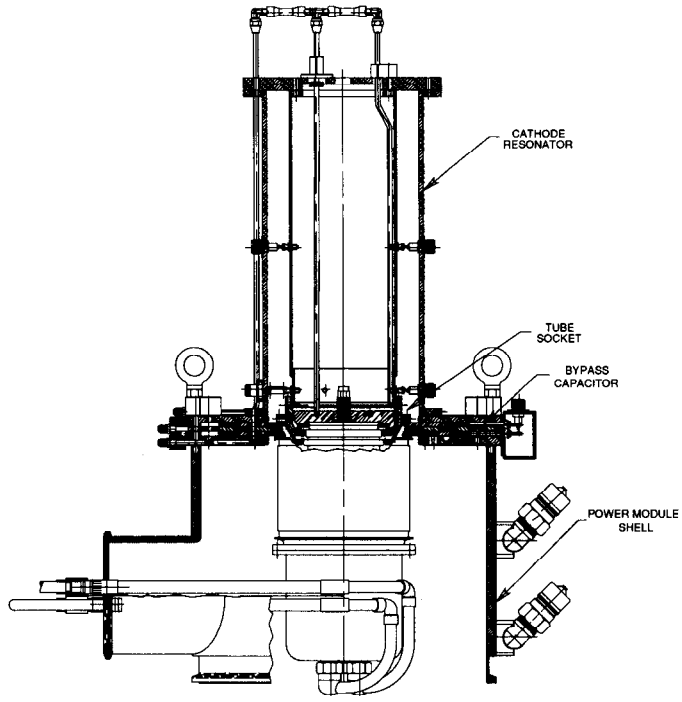

Figure 1. Cross section of the 200 KW power amplifier.

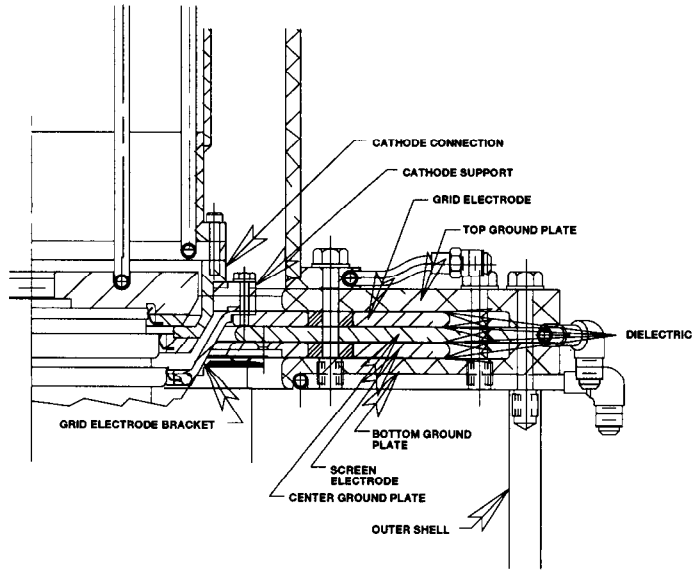

Figure 2. Detailed cross section of tube socket.

* Operated by Universities Research Association, Inc. under contract with U.S. Department of Energy.

Figure 1 is a detailed cross section of the complete amplifier. The grid and screen electrodes, grid bracket, cathode collet, filament block, center ground plane, and cooling rings are made of OFHC copper. The top and bottom ground plates are fabricated using aluminum tooling plate. Most of the other major parts are made from aluminum alloy 6061 T6.

Figure 2 shows the tube socket assembly with bypass capacitors. The screen and grid bypass capacitors are made of copper clad Kapton that is photo etched for the desired copper outline. The use of copper clad Kapton is preferred over plain Kapton. Copper clad provides a more uniform surface area for the electrodes, thus eliminating localized heating due to imperfections in electrodes or ground plates. It also provides consistent capacitance from unit to unit. The grid bypass capacitance is 12.9 nF and the screen bypass capacitance is 12.4 nF.

A filament lead bypass capacitor is located at the top of the cathode resonator. It is constructed using a copper electrode connected to the filament lead. Plain .005" Kapton sheet is sandwiched on either side of the electrode. Capacitance is 14.9 nF. The filament is powered by a commercial DC high efficiency switching supply (15.5 volts at 225 amps) located in the series to modulator.

The cathode resonator is tuned to 53.1 MHz. and has a Q of 10. The low Q and hence wide bandwidth is accomplished by tapping the cathode resonant structure with two 50 ohm terminations tapped for a 4:1 impedance transformation at the cathode (100 ohms). The terminations are physically located upstairs in the equipment gallery and connected to the amplifier's cathode circuit by two 1/2 inch Heliax cables. Over the full dynamic swing of cathode impedance the rf power loss in the cathode circuit is minimal and the impedance range is limited for the solid state amplifier load.

The cathode is driven directly at the base of the tube socket with four phase matched 50 ohm 1/2 inch Heliax cables in parallel (for 12.5 ohms) from the output combiner of the solid state amplifier. The combiner's output impedance is 12.5 ohms, but due to the dynamic impedance swing of the cathode, we only approach a matched 12.5 ohm cathode impedance at full output. Therefore, these cables are not always run as a flat line so lengths are kept near 1/2 λ multiples of 53.1 MHz. This provides tight coupling between driver and cathode.

The grid bias supply is a fast 100 KHz (bandwidth) programmable type with compliance of -500 volts to 0 volts for 0 to 10 volt program. The screen supply is a 3 phase bridge type rated at 1050 volts at 2 amps. Both of these supplies are identical to the ones used in the Tevatron rf system (Fermilab design).

A cathode monitor is installed at the same point as the rf drive. This serves as a voltage monitor and phase reference for system tuning. A second monitor (anode monitor) is placed in the outer shell's side wall in the anode circuit and is used for voltage monitoring. The cathode and anode signals are monitored by a phase detector which controls cavity tuning.

III. 4 KW SOLID STATE DRIVER AMPLIFIER

When we first started our R&D program for the new power amplifier, we made the decision it would be driven by a solid state amplifier located in the equipment gallery. With 20 years' experience maintaining our existing power amplifiers which have tube drivers built on top of the power module we learned that a lot of our failures, while acceptable, were related to the driver components. Our existing 2 KW drivers are made up of 14 parallel 4CW-800F tetrodes (cascode amplifiers) driven by a 6 tube 100 watt distributed amplifier mounted on top of the 2 KW driver. The complexity of small tubes in the tunnel along with their associated power supplies in the equipment gallery led to a higher mean time to failure than we liked.

Initially we could find no commercial solid state amplifier that met our specification (insisting on water cooled units). This led to an in-house design using the MRF-151G Mosfet for the output stage mounted to a copper water cooled heatsink which provided 250 watts of rf power per device. We assembled 16 of these devices (mounted two devices per copper heatsink) and combined them for 4 Kwatts to drive the cathode of the power amplifier. All our initial testing of the 200 KW amplifier was done using this solid state driver.

Later a commercial solid state amplifier was uncovered which, with the exception of narrower bandwidth, could nearly meet our requirements. This amplifier with a few modifications was adapted to meet our water cooling specification and bandwidth requirements.

Past experience with air cooled heatsinks in solid state drivers have led to poor long term reliability because of excessive junction temperatures. It has been our experience that water cooling has proven to increase mean time to failure by more than an order of magnitude. Requiring copper tubing for water paths rather than organic hose greatly reduces the chances of water leaks.

Two of the commercial 1 KW amplifier chassis were modified to give the desired results:

1. Wider bandwidth.
2. Faster gated pulse response without ringing.
3. Improved chassis shielding.
4. Added 37.5 degree flare fittings for water connections.
5. Eliminated all rubber hose inside the 1 KW chassis and replaced them with copper refrigeration tubing.

One of the modified chassis was sent back to the vendor to see if they would modify their design to incorporate our changes. Since they agreed to do this, we ordered 12 additional amplifier chassis for the completion of the three R&D amplifiers.

Table 1 is an abbreviated list of specifications for the 1 KW solid state amplifier chassis.

Frequency:	30 MHz - 80 MHz
Gain:	50 dB
Gain Flatness:	+/- 1.0 dB
Phase Delay:	Less than 24 nSec
Phase:	All amps matched to +/-5 degree
Rf Power Out:	1000 watts
Cooling:	Demineralized LCW

Table 1. Abbreviated Solid State Amplifier Specification.

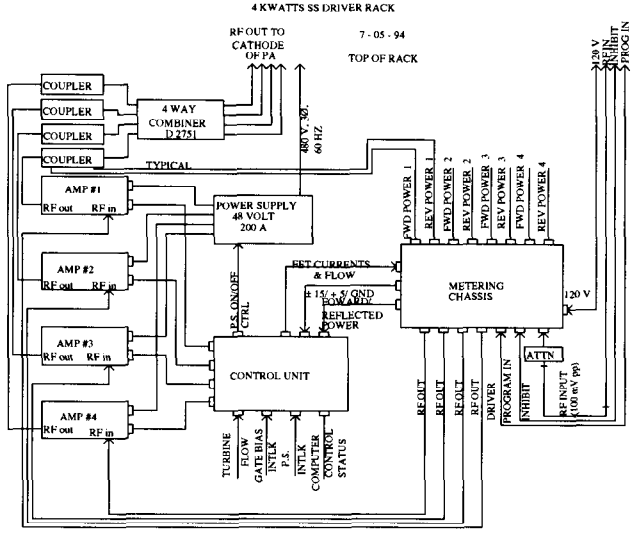

Figure 3. Diagram of the 4 KW solid state amplifier rack.

The control unit and metering chassis are Fermilab designed and fabricated. The final output combiner, dual directional couplers, and 48 volt 200 amp power supply were purchased commercially.

The metering chassis performs the following functions:

1. Measures and displays Mosfet current in each output stage.
2. Diode detectors for processing forward and reflected power of each amplifier for local and remote readout along with protection circuitry for each.
3. Variable gain rf amplifier for programming rf level to 1 KW amplifier modules in response to an input program of 0 to 10 volts (constant phase).
4. Program inhibit (TTL line).
5. Four - way rf splitter.

The control unit provides the protection, local control, and remote interface for the solid state amplifier. It utilizes a Europac HF 3U chassis with 9 plug-in modules. The modules include a water flow processor for the turbine flow meter, forward power, reflected power, amplifier monitor module for each 1 KW amplifier (4 total), power supply controller, and on/off master controller with remote status and control.

IV. INSTALLATION AT MR-RF STATION 7

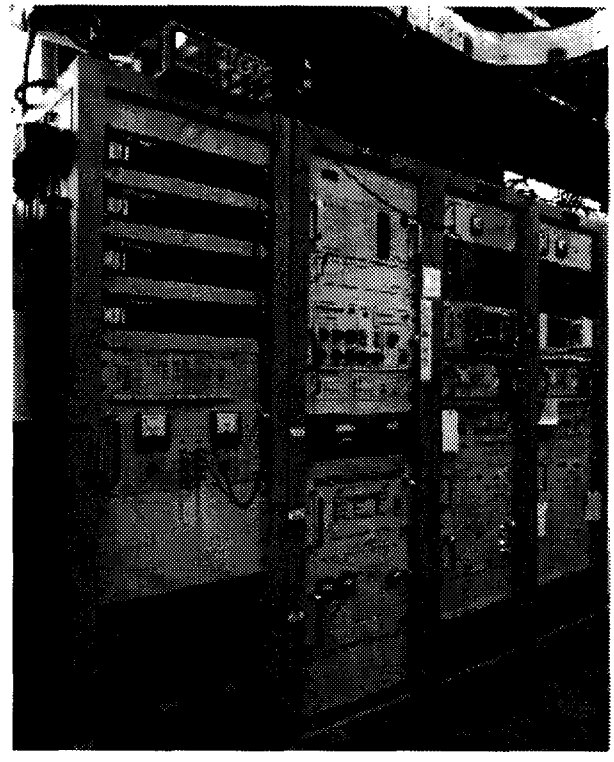

Figure 4. Installed Solid State Driver at MR-RF St. # 7.

In the foreground of Figure 4, is the 4 KW solid state driver rack positioned next to the station 7's control racks. From top to bottom are the four - 1 KW solid state rf amplifier modules, control unit, metering chassis, four - way output combiner, and power supply.

A condition for installing and running a long term test was the station had to be controlled in the normal fashion from the control room by the operations' group. The solid state driver's control unit was interfaced to the station's existing control system. With minor software programming modifications, new parameters for the solid state driver could be displayed on the usual parameter pages. This provided the operations' group full remote control, read-backs, and alarms to the control room as with a normal station.

In May of 1994 the station was made operational with the new 200 KW power amplifier and solid state driver. The 200 KW power amplifier typically runs with a peak anode voltage of 18 KV from the series tube modulator, a peak negative grid bias of -300 volts, and a peak forward power of 1700 watts from the solid state driver with beam intensities of 3.1 E12 on pbar production cycles (beam loading compensation active).

To date we have had no failures or downtime associated with the new 200 KW amplifier and solid state driver. Even though this is the only station operating this way, it is a good indication that the designs are sound.

THE MAIN INJECTOR TRIM DIPOLE MAGNETS

R. Baiod, D.J. Harding, D. E. Johnson, P.S. Martin, S. Mishra, Fermi National Accelerator Laboratory*,
P.O. Box 500, Batavia, IL 60510 USA

Abstract

To correct field and alignment errors, provide full aperture steering at injection, and control the horizontal orbit in the straight section, a 0.060 T-m and a 0.090 T-m correctors were designed. The two magnets were chosen to have identical lamination cross section and identical coil packages, however the normal low field corrector has no cooling while a water cooled plate is incorporated to the high field one. Diffusion of the heat through the copper conductor, insulations, and magnet steel, with and without plate cooling, was analyzed, and temperatures were estimated. We report in this presentation the calculations of the various magnet parameters, and in particular, the procedure to optimize the temperature of the steel and the temperature of the inner copper coil.

I. Design requirements and constraints

Tracking studies at 8.9 and 120 GeV/c [1] have established that correctors with rms value of $\pm$ 35 μr in strength, will provide adequate correction at all energies. With a strength of 0.060 T-m, our normal corrector will provide 120 μr of steering at 150 GeV, a factor of 3.4 standard deviation at the highest energy. This should allow for correction for unexpected field/alignment errors and/or future orbit control requirements at high field. To reduce unexpected dipole field variations, we will consider shuffling the main ring dipoles during installation, and realigning the quadrupoles during commissioning.

Stronger correctors around the straight sections are required to provide position and angle control around the electrostatic septa and Lambertsons during injection and extraction. To minimize corrector strengths at these locations, the high field orbit is first determined by quadrupole alignment. Then a corrector strength of only 0.090 T-m will provide 180 μr at 150 GeV/c and still provides a safety factor of about 2 above the required strength.

In addition to the beam requirements, the design of the trim dipole correctors was strongly restricted by first, the available space, and second, the necessity to accomodate existing power supplies. The horizontal trim dipoles are to be located upstream in the proton direction of each quadrupole, occupying a space of no more than 17 inches. For the normal trim dipoles, the maximum current allowed is 10 amperes with a duty factor of 0.7. To provide the stronger dipoles for injection and extraction manipulations, we investigated the possibility of having an optional water cooled plate added to the coil to be able to reach higher currents.

These specifications and constraints were used as a basis of a top-down optimization procedure that is described below. The allowed currents, given the desired ampere turns, precluded us from using copper tubing, but rather required low gauge solid copper wire. We therefore concentrated our efforts in modeling and evaluating the various mechanisms of heat transfer within the magnet components and convection at the outside surface. The main challenge in this optimization was to minimize the temperature of the inner copper to reduce the risk of insulation failure and the temperature of the steel surface for personnel safety consideration. We decided to limit the copper temperature to 95° C (epoxy rating). We also plan in using Dupont Pyre-ML wire coating which can withstand 220° C. The steel temperature is limited to 50° C. Based on failure data of past dipole correctors and other small magnets, we do not believe that extra cooling is necessary for the normal corrector.

We assume an H type of magnet, with pancake coils around the poles. The magnet aperture to accomodate the Main Injector beam pipe is 2 inches for the gap and 5 inches for the pole width, and these define the pole gap and pole width in our magnet. The magnet cross-section is shown in Figure 1

II. Thermal model

The heat starting from the copper wire, flows through the wire coating, the epoxy potting and G10 around the coil, the steel core, and finally is dissipated by convection in the ambiant atmosphere at a 30° C temperature. Each one of this processes generates a temperature differential that will be estimated. A simple series configuration is assumed, and alternate paths with higher resistance to thermal flow have been neglected. We should mention that a more elaborate thermal model of existing Fermilab corrector magnets has been attempted. In this circuit-like model thermal resistances and capacitances (heat capacities) are fitted to measurements.[2]

To start with, we may assume that good thermal contact between the coil and the steel can be realized only at the bottom or top coil surfaces. Using an electrical parallel circuit analogy, the thermal impedance between the side of the copper coil to the steel pole is much larger than its counterpart at the top or bottom interface. Alternatively, we also consider the possibility where good thermal contact is easier to accomplish at the two coil sides. It should be added that a small air gap will add a significantly high series resistance to the heat flow. Therefore, we plan to

*Operated by Universities Research Association under contract with the United States Department of Energy

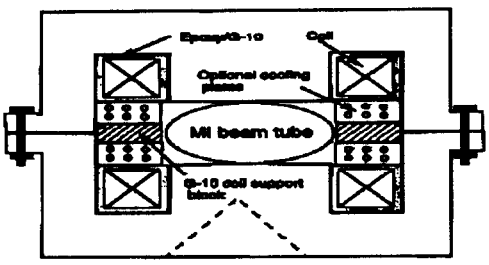

Figure. 1. Horizontal magnet corrector cross-section. The dashed line shows an eventual way to increase the magnet area for better heat transfer.

use thermal grease in all interfaces with the coil, as well as maintaining good contact pressure.

The conductor coil made of copper wire and coating around each wire is modeled as a distributed heat source with an effective thermal conductivity that depends on the coating conductivity, coating thickness, and wire gauge. This effective thermal conductivity can be derived by considering a unidimensional heat flow through a layer of copper, in between two layers of insulation. The accumulated temperature gradient is then:

$$\Delta T = \frac{P}{S}(\frac{2t}{\lambda_i} + \frac{g}{\lambda_c}) \tag{1}$$

where $\frac{P}{S}$ is the heat flow per unit area, t is the coating thickness, and g is the wire thickness (gauge); λ_i and λ_c are the respective conductivities. Since the copper conductivity is much higher than the insulator conductivity, the effective conductivity of this medium is :

$$\lambda_e = \lambda_i \frac{g}{2t} \tag{2}$$

More detailed calculations for the case of cylindrical wires can be found in [3].

We assume a 4 mil thick Dupont Pyre-ML wire coating which can sustain higher temperature (higher glass transition at which mechanical properties change drastically). For this material the thermal conductivity is about 0.16 watt/m.°C. The coil will be dipped in epoxy to reduce air pockets.

The assumption of only one coil-steel contact simplifies the heat transfer within the copper source to an inhomogeneous 1-dimensional Poisson equation that can be solved easily:

$$\frac{d^2T}{dx^2} = -\frac{p}{\lambda_e} \tag{3}$$

p being the heat production rate in a unit volume of copper. In the case of top/bottom contact, the temperature difference between the hottest point ($\frac{dT}{dx} = 0$), on one side of the coil, and the opposite point closest to the steel interface at a distance h (the coil height) is:

$$\Delta T = \frac{p}{2\lambda_e} h^2 \tag{4}$$

In the alternate case of side coil-steel contact, the temperature depends on w (the coil width):

$$\Delta T = \frac{p}{2\lambda_e}(\frac{w}{2})^2 \tag{5}$$

Next, the heat flow through the epoxy and G10, described by an equation similar to Equation 1, assumes a thermal conductivity of 0.65 watt/m.°C. The respective thicknesses are 30 mils and 1/16 inch.

Finally, the convection at the steel surface is described by:

$$\Delta T = \frac{P}{AH} \tag{6}$$

A is the external magnet area, and H is the heat transfer coefficient by natural convection. Vendor painted aluminum plates can reach about 14 watt/m^2.°C. Our magnet will be painted, and we will assume this optimum value.

III. Optimization of the copper and steel

The size of the copper cross-section, and the length of the steel core are dictated by the necessity to simultaneously

- reduce the power needed to energize the normal corrector.

- minimize the temperature of the hottest spot inside the copper,

The total length of the magnet, coil and steel being restricted to 16 inches, we loose steel length as the coil package increases in width. We are left with only the coil width w and coil height h as free parameters.

For a given magnet strength, the power and the inner coil temperature scales like:

$$power \sim \frac{1}{wh}(\frac{1}{L-2w})^2 \tag{7}$$

where $L = 16$ inches, and

$$\Delta T \sim \frac{1}{w^2(L-2w)^2} \tag{8}$$

for a top/bottom contact, or

$$\Delta T \sim \frac{1}{4h^2(L-2w)^2} \tag{9}$$

for a contact from both sides. These relations are plotted in Figure 2.

Figure 2. suggests that a square coil of size 2 inch is a good compromise that does not overdesign the magnet

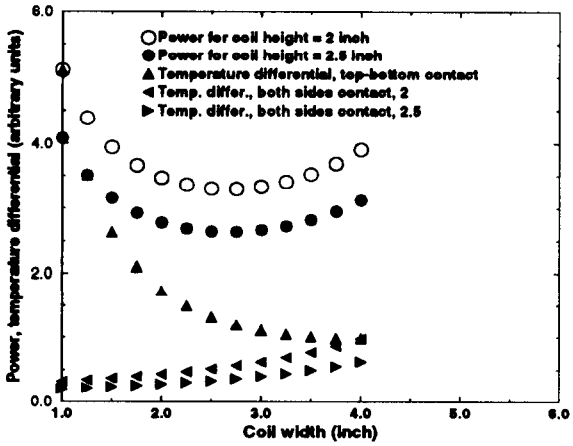

Figure. 2. Effect of coil size on the amount of heat and on hot spot temperature

size. This is the value adopted in the present design. The backleg and yoke are fixed to a thickness of about 1 inch to have enough mechanical strength. No saturation is expected given the low value of the field in the gap.

The magnet core as well as the copper coil are sufficiently defined now to derive other parameters. In particular the amount of heat produced when the magnet is powered to the required strength and duty factor allows us to estimate the temperature of the different components using the above model.

The steel temperature is found to be 58° C. This temperature will be decreased by increasing the magnet area. We are exploring two possibilities. The first one is to have wide endplates while the second one is to have a wedge on the top and bottom of the magnet. The latter reduces the weight of the magnet. The former may create a bottleneck for the heat flow, and increase temperature gradients. In any case, we assume that the temperature of the steel can be maintained below 50° C.

Next, the temperature of the epoxy at the copper coil interface is evaluated. The epoxy is a vulnerable component. If the contact between the steel, G10, and epoxy is tight (thermal grease is utilized), then this interface will be at temperature of about 57° C. An air gap of 5 mils with the same heat flow, will raise this temperature by 12° C.

Last, the inner coil temperature is found to be around 81° C. This is below the limit we specified. At this point we should say that some gradients are short-circuited if we put a water-cooled plate against the bottom or top of the epoxied coil winding. For this option, with a higher current of 15 ampere and the same duty factor we reach a temperature of about 91° C. This is to be compared to 120° C with no plate cooling.

IV. Summary

The modeling of the trim dipole has been dominated by the desire to minimize the temperature of sensitive components. It gave us the following directions in which to orient the engineering efforts:

- There must be as much contact as possible between the coil and the steel.
- The winding impregnation should get rid of the air pockets to maximize the effective thermal conductivity.
- The insulating materials are limiting components, and their thermal conductance and temperature resistance should be as high as possible.
- The lamination design should maximize the external magnet surface.
- The steel should preferably be painted in black.

In addition to the thermal calculations we are in the process of adding bumps in the poletip to maximize field uniformity. This design will have to take into account the sextupole captured at the ends since our magnet steel is rather short, 12 inches.

V. Acknowledgements

We are grateful to J. A. Hoffman, and N. S. Chester for their help with the properties and limitations of insulating materials. We also would like to thank G. E. Krafczyk and P. S. Prieto for communicating to us the results of their thermal modeling and measurements of Fermilab corrector magnets.

References

[1] C.S. Mishra, *Study of the Alignment Tolerance and Corrector Strength in the FMI Lattice*, MI Note-0109 (1994).

[2] G. E. Krafczyk, and P. S. Prieto, private communication.

[3] D. J. Kroon, *Electromagnets*, Boston Technical Publishers, Cambridge (1968).

DESIGN OF THE FERMILAB MAIN INJECTOR LAMBERTSON

D. E. Johnson , R. Baiod, D.J. Harding, P.S. Martin, M. May
*Fermi National Accelerator Laboratory**
P.O. Box 500
Batavia, Illinois 60510

Abstract

A common design has been adopted for a high field (1.1T) Lambertson magnet for use in the four injection/extraction channels of the Main Injector (MI) as well as the Tevatron injection channel[1]. To support the extraction/injection of 150 GeV/c protons and pbars, the field within the "field region" of the Lambertson should reach 1.1 Tesla with less than 0.3% variation in a 2 by 12 inch good field aperture. Utilization for the 8.9 GeV/c pbars and resonant extraction of 120 GeV/c protons place stringent aperture requirements on the magnet design. In addition, this magnet must simultaneously support circulating beam in the energy range of 8.9 GeV/c to 900 GeV/c, through its "field free" region. At maximum excitation, the leakage field in this region must be kept to a minimum to avoid any deleterious effects on the circulating beam. The magnet design parameters which meet the aperture, magnetic, and structural requirements as well as the selection criteria of the steel are discussed.

I. Magnet Requirements

The extraction channels in the Main Injector utilize three vertically bending Lambertsons, with an integrated strength of 9 T-m , and a vertically bending c-magnet with an integrated strength of 3.5 T-m to clear the downstream MI magnets. Four vertically bending Lambertsons, with an integrated strength of 12.1 T-m are required for injection into the Tevatron. Assuming a 1.1 T field for a symmetric Lambertson, imposed by tolerable leakage field, the magnetic length of the Lambetrson was set at 2.8 meters. This, in conjunction with the available free space in the MI lattice, set the flange to flange length at 3.054 m.

The trajectory of 8.9 GeV/c pbars from the Antiproton Source through the de-energized set of Tevatron Lambertsons and into the MI define both the gap width (pole-to-pole dimension) and the minimum physical height of the gap (pole tip width). A minimum of 20% of the aperture is reserved for steering. The field free region must support circulating beam so the aperture defined by the height, width, and opening angle of this region should not be the limiting aperture. The maximum septa thickness is governed by the separation of the injected/extracted beam from the circulating beam. This separation is a function of the kicker or electrostatic septa strength. The physical aperture requirements for usage in both the MI and the Tevatron are listed in Table 1.

The good field height in the bend region, as listed in Table 2, is determined by the maximum excursions of the extracted beam through the Lambertsons in both the MI extraction and the Tevatron injection channels. The field uniformity in this region should not contribute more than 1% to the emittance growth of the extracted beam.

TABLE 1: Aperture Specifications

	MI	Tevatron	
Gap width	2	2	inches
Gap height	± 5	± 7	inches
Field free region height	≥ 2	≈ 3	inches
Field free region width	3.5	3.5	inches
Opening angle	≥ 90	≥ 90	degrees
Septum Thickness	.157	.157	inches
Straightness (both planes)	10	10	mils

Besides the magnitude of the field and field quality in the bending region, the body leakage field into the field free region and the end field contributions, which impact the circulating beam, are specified. The specifications listed here set limits for the sum of the body and end field. Without any compensation, the end field contribution can be an order of magnitude larger than that due to the body leakage field. With careful attention, this can be reduced to the same order of magnitude as the leakage field. The current end field compensation scheme is discussed in a companion paper. [2]

TABLE 2: Magnetic Specifications

	MI	Tevatron	
Nominal field	1.072	1.072	Tesla
Good field height	± 4.6	± 6	inches
Field Uniformity	< 0.28	< 0.28	percent
Leakage Field	< 0.038	< 0.019	T-m
Leakage Gradient	$< .78$	$< .336$	Tesla-m/m

Due to the symmetry of the magnet, the predominant body leakage fields to contend with are the dipole, and skew quad. The magnitude of the allowed dipole field is specified to produce less than a 2 mm closed orbit distortion without downstream orbit compensation. From this the total allowed dipole field in the field free region is estimated and the results are listed in Table 2.

To set the upper limits on the skew quad field allowed in the field free region, the magnitude of the allowed tune shift (assuming a fully coupled ring) for the circulating beam in the field free region at maximum excitation has been specified to be less than 0.005 units. This criteria corresponds

*Operated by the Universities Research Association under contract with the U. S. Department of Energy

to $\int dB_x/dxdl < 4\pi\delta\nu(\beta\rho)/\beta$ in units of Tesla-m/m, again as a sum of the contributions from the body leakage field and the end field.

The project requires 16 Lambertsons plus spares, so a common design will reduce design effort, fabrication costs, and the quantity of required spares. Therefore, the design is based upon the requirements for usage in the Tevatron which automatically satisfies the Main Injector specifications.

II. Physical Design

The requirement for a large aperture (both planes) in the bending region, led to the design of a Lambertson absent of an internal beam pipe. This is accomplished by using two sets of symmetric laminations, one set for the inner cores and one for the outer cores, as shown in Figure 1. The inner cores are assembled with a precision ground matched set of stainless steel space bars near each coil to define the gap width. The left/right symmetry of the inner cores assure an assembly which meets the straightness criteria in bend plane. This assembly is "skinned" with a 30 mil Type 321 stainless steel vacuum skin and terminated at each end by a single vacuum end plate. All vacuum welds are external. A set of 8 distributed 30 liter/sec ion pumps (4 on each side) are utilized to maintain a vacuum of $\approx 5 \times 10^{-9}$ torr for use in the Tevatron.

The coil is a 24-turn split saddle coil with the saddle extending laterally beyond the inner core to allow for the inner core end assembly to extend beyond the coil with out interference. The conductor dimensions and number of turns are determined by the desire to utilize an existing 200 Volt/2500 Amp power supply while maintaining adequate copper volume and cooling.

The coil and inner core assembly are captured by a pair of symmetrical outer cores designed to provide straightness in the non-bend plane. The assembly is held together by a set of tie plates which produce stiff boxed beam structure.

Construction of previous Lambertsons at FNAL have required laborious straightening techniques of welding stripes on the outer core to meet the straightness criteria. This design deviates from the construction of previous Lambertsons at FNAL in that it is designed to meet the straightness criteria without the previously required straightening techniques.

III. Magnetic Design

A 2D magnetic model was constructed to allow adjustment of basic geometrical parameters such as the septum thickness, septum radius, septum angle, and geometries of the field free region, inner core, outer core, gap height and width, pole face contour, and tiebars to aid in magnet design choices. The model additionally included the stainless steel skin around the inner cores and air gaps around the skin and tiebars. These parameters were adjusted to optimize the field uniformity in the gap, minimize the leakage field in the field free region, and trim the back leg.

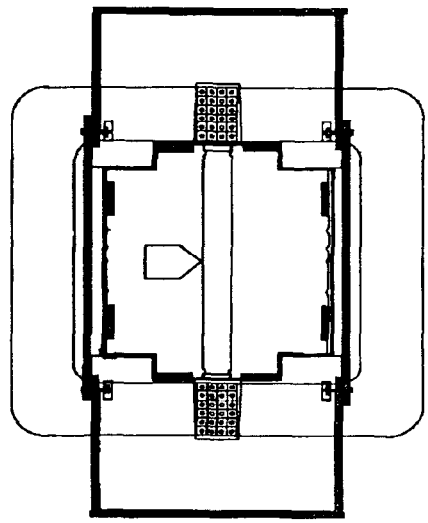

Figure. 1. Cross section of Lambertson core showing inner and outer cores, tiebars, and coil configuration.

A. Field Region Design

The uniformity in the central region of the gap is governed predominately by the location of the field free region. Its symmetric location provides excellent uniformity in this central region. The height of the "good field" region, defined by the uniformity specification, is governed by the coil and stainless steel spacer bar geometry and the shape of the pole tip near the coil. Without any pole tip shaping, the good field region extended to ± 5 inches, about a gap width less than the physical height. Adjusting the width of the stainless spacer bar (i.e. its penetration into the iron of the inner cores) and adding a ± 50 mil thick by 200 mil long pole tip shim increased the height of the good field region to ± 6 inches, meeting the specification, as seen in the lower plot of Figure 2. However, the field falls off rapidly and increasing the the pole tip height from 7 to 8 inches linearly increases the height of the good field from 6 to 7 inches as shown in the upper plot of Figure 2.

B. Field Free Region Design

The leakage field from the iron into the field free region is governed by the continuity condition that H(parallel) must be continous across the iron/air interface. From this boundry condition, the flux density (in Gauss)in the field free region will just be $\mu_0 H_{steel}$. To maintain control over the leakage field, a steel with a high permeability at the expected values of H in the iron near the cavity should be chosen. The choice of steel is discussed in the next section.

The selection of septum thickness, septum radius and opening angle are not only based upon the aperture requirements discussed earlier, but were selected to minimize the saturation in the iron near the septa, the magnitude of skew quad in the cavity, and the magnitude of the leakage flux density, respectively.

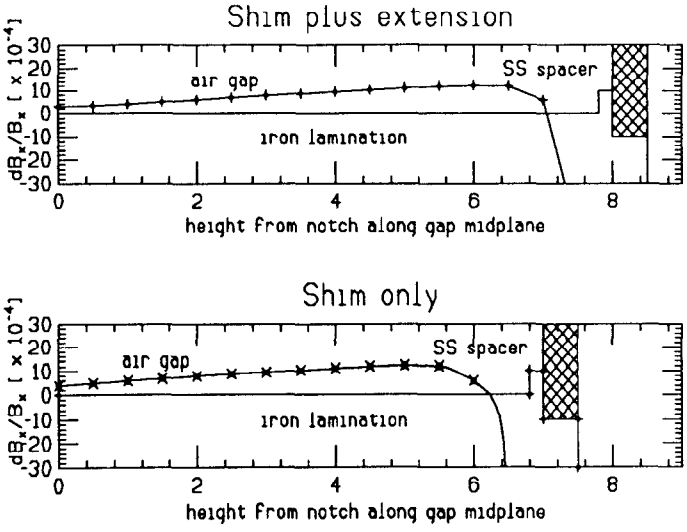

Figure. 2. Calculated field uniformity in the bend region after shimming and extending the field region.

Figure 3 shows the magnitude of the field, in Gauss, on axis in the field free region as predicted by OPERA-2D. The small skew quad component is realized by a combination of reducing the opening angle from the 90 degree specificaion to 78 degrees and increasing the septum radius to 0.2 inches maintaining the vertical aperture near the notch. The magnitude of the field in the gap is 1.1 Tesla.

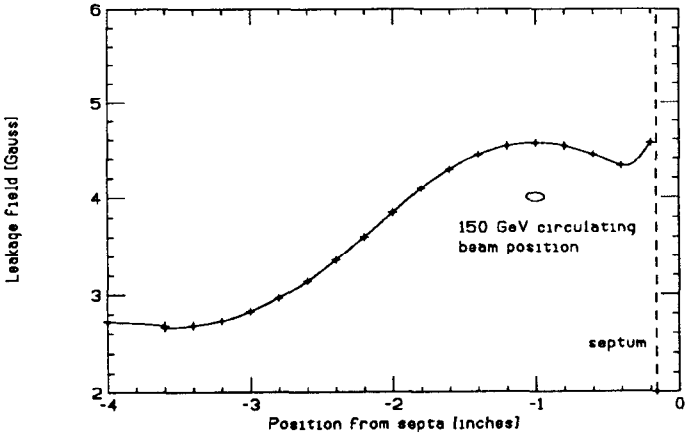

Figure. 3. Leakage Field in the field free region at a bend field of 1.1T.

C. Steel Selection

The selection of steel is not only governed by technical specifications but by more realistic issues like market availability and cost. For example, cobolt/vanadium alloys such as supermendure offer a high permeability at the lower excitations, which would offer better shielding around the cavity or decrease the integrated magnet length. They are, however, cost prohibitive at $\approx$ \$30/lb. as compared to $\approx$\$0.50/lb for Si and low carbon steel. Therefore, we limited our selection of steel for the Lambertson magnet to either a silicon electrical steel or a low carbon steel. Figure 2 shows the measured hysteresis curves for 24 guage Epstein strip samples of a fully processed low carbon (0.006 %) steel and a M-47 grade Si steel. This shows the Si steel clearly having a higher permeability and a lower coercive force than the low carbo[redacted] in the sheared condition (dashed line). Shearing a[redacted]mination punching increase stress within the steel wh[redacted]vers its permeability. Both sets of samples were stress[redacted] annealed at 750 degrees C for two hours. The perme[redacted] of both samples is shown as the solid lines. A mor[redacted]ounced improvement from stress relief annealing is s[redacted] the l[redacted] steel. For this project, the low carb[redacted]el ha[redacted]e parameters.

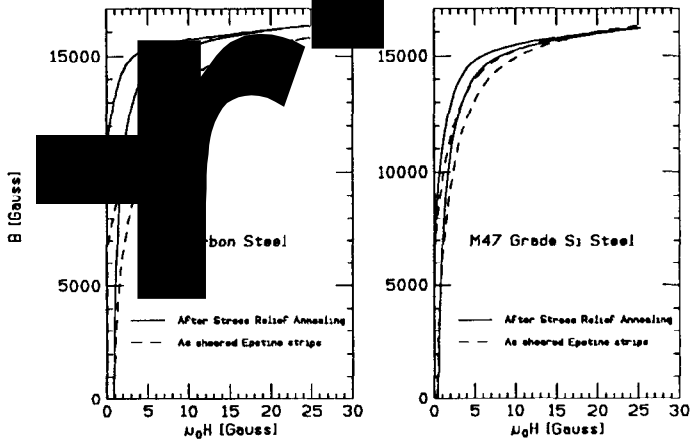

Figure. 4. Hysteresis curves of low carbon and Si steel showing the improvement to each due to stress relief annealing.

D. End Design

A 30" prototype Lambertson has been constructed to aid in the design of the magnet end configuration. The ratio of magnetic length to physical (flange-flange) length must remain $\approx$92% due to space constraints in the Main Injector. The geometry of the prototype includes a 2 by 13 inch gap without any shimming. The field free region geometry used is listed in Table 1.

IV. Acknowledgements

The authors would like to thank Linda Alsip, John Carson, Nelson Chester, Gerry Davis, Fritz Lange, Arie Lipski, Gale Pewitt, Reid Rihel, Bill Robotham, Kay Weber, John Zweibohmer, for their contributions to this design.

References

[1] The Fermilab Main Injector Technical Design Handbook, August 1994.

[2] J.-F. Ostiguy and D.E. Johnson, "3D End Effects in Iron Septum Magnets", these proceedings.

THE MAIN INJECTOR CHROMATICITY CORRECTION SEXTUPOLE MAGNETS: MEASUREMENTS AND OPERATING SCHEMES

C. M. Bhat, A. Bogacz, B. C. Brown, D.J. Harding, Si J. Fang,
P.S. Martin, H. D. Glass and J.Sim
Fermi National Accelerator Laboratory*
P.O. Box 500, Batavia, IL 60510

Abstract

The Fermilab Main Injector (FMI) is a high intensity proton synchrotron which will be used to accelerate protons and antiprotons from 8.9 GeV/c to 150 GeV/c. The natural chromaticities of the machine for the horizontal and the vertical planes are -33.6 and -33.9 respectively. The $\Delta p/p$ of the beam at injection is about 0.002. The chromaticity requirements of the FMI, are primarily decided by the $\Delta p/p = 0.002$ of the beam at injection. This limits the final chromaticity of the FMI to be ± 5 units. To correct the chromaticity in the FMI two families of sextupole magnets will be installed in the lattice, one for each plane. A sextupole magnet suitable for the FMI needs has been designed[1] and a number of them are being built. New chromaticity compensation schemes have been worked out in the light of recently proposed faster acceleration ramps. On an R/D sextupole magnet the low current measurements have been carried out to determine the electrical properties. Also, using a Morgan coil, measurements have been performed to determine the higher ordered multipole components up to 18-poles. An overview of these results are presented here.

I. Chromaticity Compensation Schemes for the FMI

Previously a scheme for chromaticity compensation in the FMI had been worked[2] out taking into account the effect of beam tube eddy current, the dipole saturation, and the end-pack sextupole fields generated by the dipole magnets. The data were taken from measurements on R&D dipole magnets. Since then, several developments have taken place:

1. The measured[3] combined contribution of the saturation and static fields in the dipoles showed a slightly negative sextupole component (i.e., $b_2 = -0.05\ m^2$) at low fields (which is in contrast with the earlier scheme).

2. The material of the FMI beam tube is selected to be 316L stainless steel (resistivity of 74×10^{-8}Ohm m)[4].

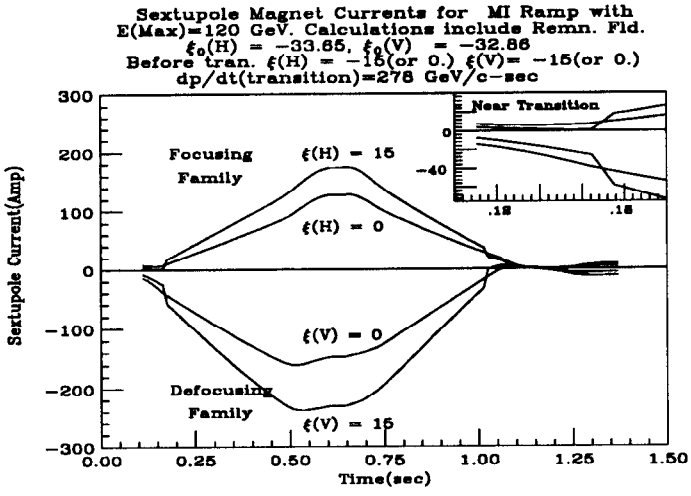

Figure 1: The FMI sextupole magnet operating scheme for 120 GeV/c fast ramp. The 8.9 GeV/c beam is injected at 0.1 sec extracted at 0.64 sec. The total cycle time is 1.4 sec. The chromaticity sign changes at transition from negative to positive.

3. A faster ramp[5] is selected to reduce the emittance dilution at transition. The $\dot{p}$ at transition in the present FMI operating scheme is about 280 GeV/c-sec (fast ramp) which is nearly 70% larger than the previously proposed ramp (viz., $\dot{p}_t = 167$ GeV/c-sec, slow ramp).

Hence, a new chromaticity compensation scheme has been developed. Here we essentially adopt the method outlined in Ref. 2.

Figures 1 and 2 show the examples of operating schemes for two different types of FMI accelerating ramps viz., fast and slow ramps respectively. The Fig. 1 illustrates the fast ramp. Here, a 8.9 GeV/c beam will be injected into the FMI at about 0.10 sec in to the accelerating cycle and the beam will reach its peak momentum of 120 GeV/c at 0.61 sec. The required sextupole magnet currents as a function of the cycle time for two chromaticities, viz., 0 and 15 units, are shown for both focusing and defocusing families of sextupole magnets. The Fig. 2 displays the expected sextupole magnet current for the slow ramp. In this case the maximum momentum reached is 150 GeV/c.

*Operated by the Universities Research Association, under contracts with the U.S. Department of Energy

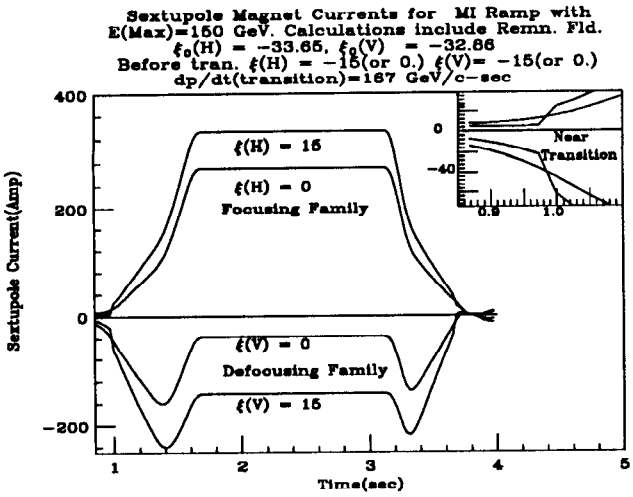

Figure 2: The FMI sextupole magnet operating scheme for 150 GeV/c slow ramp. The 8.9 GeV/c beam is injected at 0.84 sec and extracted at 3.10 sec. Here the total cycle time is 4 sec. The chromaticity sign changes at transition from negative to positive.

The selection of $\dot{p}_t \approx 280$ GeV/c-sec has resulted in a very large amount of eddy current contribution to the sextupole field component at low B fields. For instance, near the transition energy the contribution to the sextupole component b_2 arising from the eddy current reaches a maximum value of 0.8 m^2 for the fast ramp, and about 0.5 m^2 for the slow ramp. The effect of this 60% increase in the sextupole field strength on the operating scenario is quite noticeable near transition energy as shown in the insets of Figs. 1 and 2. This suggests that in order to have enough safety margin for the operation of the FMI below 25 GeV/c we might need a bipolar power supply for the focusing family of sextupoles. However, for the defocusing family of sextupoles a unipolar power supply should be sufficient.

II. Electrical Model

The sextupole magnet is a three-terminal device with two coil terminals and one magnet case ground. The electrical characteristics of the magnet can be described by a 3×3 impedance matrix at non-saturation. The equations for this three-terminal device network can be written as

$$\begin{bmatrix} I_1 \\ I_2 \\ I_3 \end{bmatrix} = \begin{bmatrix} Y11 & Y12 & Y13 \\ Y21 & Y22 & Y23 \\ Y31 & Y32 & Y33 \end{bmatrix} \begin{bmatrix} V_1 \\ V_2 \\ V_3 \end{bmatrix}$$

The elements in the matrix are frequency dependent variables. The magnet equivalent circuit can be determined by measuring the impedance matrix as shown in Fig. 3.

Terminal 1 and 2 are coil bus terminals and terminal 3 is the case ground. Z11, Z22, Z12 and Z22 measure the

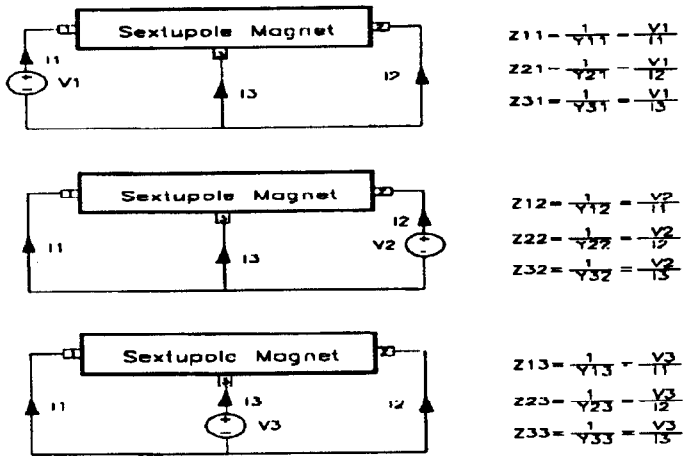

Figure 3: Impedance Matrix Measurement.

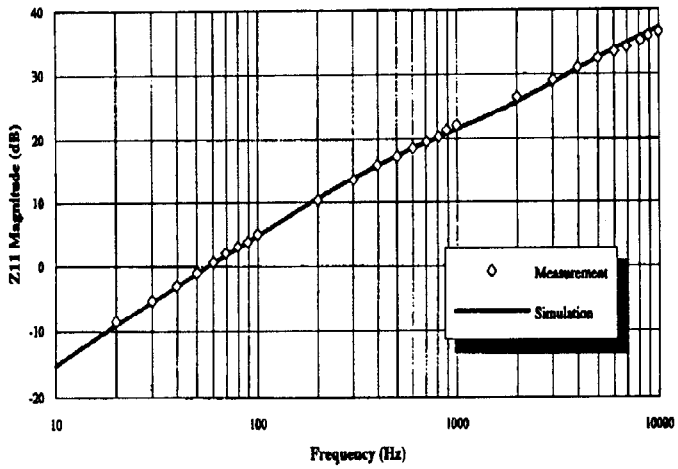

Figure 4: Z11 Magnitude Plot.

coil bus impedance. Total bus to ground capacitance is measured by Z33. Z13 and Z31 measure the capacitance between terminal 1 and ground while terminal 2 is shorted to ground. Similarly, Z23 and Z32 measure the capacitance between terminal 2 and ground while terminal 1 is grounded. The Z13, Z23 and Z33 are capacitance measurements since the slope of the measurements data is -20 dB/decade in Bode plot.

The circuit simulation program Spice is used to curve fit the sextupole magnet electrical model into its impedance matrix as shown in Fig.4 for Z11.

Figure 5 shows the sextupole magnet electrical model. T1 represents the copper loss and R2 is for the core loss. L1 and R3 are the air core inductance and skin depth effects respectively.

III. Magnet Measurements

The magnets are measured at the Fermilab Magnet Test facility (MTF) using a rotating Morgan coil with the data base-controlled MTF software[6]. The coil is rotated at

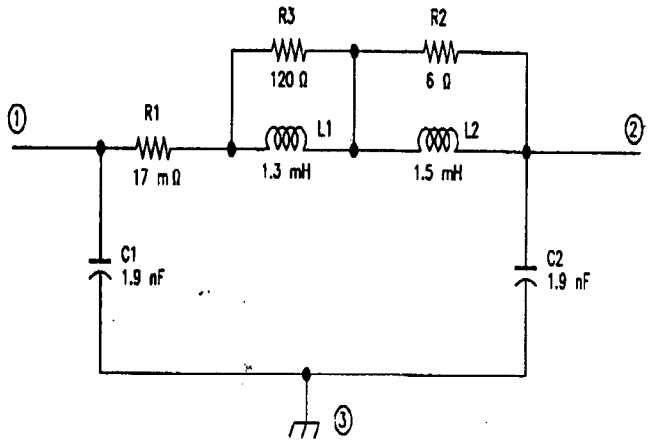

Figure 5: Main Injector Sextupole Electrical Model.

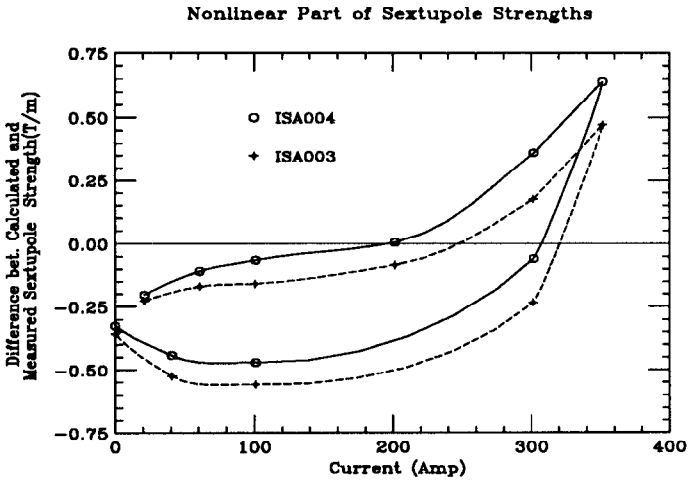

Figure 6: The nonlinear part of the sextupole strengths is obrained by substracting the measured field integral from the value calculated from normal geometry and infinite mu. Results are shown for two R&D sextupole magnets. Extraction of the nonlinear components is carried out by using a method outlined in Ref.6.

the center of the magnet at a constant current. Activating different coil windings on the probe allows the measurements of the sextupole strength and the contributions to the field shape from other harmonic components up to 18 poles. We have made measurements of both normal as well as skew components. We find none of the components are of significant importance for FMI operation scheme except the remanent field. A remanent field of -0.3 (Tm/m^2) is seen for the magnet that is ramped up to 350 Amp. Using the scheme outlined in Ref.6 we have extracted the non-linear part of the sextupole field. The result is shown in Fig. 6. In our chromaticity compensation scheme developed for FMI in section I, we have included this non-linear part of the sextupole field. The sextupole field arising from the eddy current and the remanent field of the sextupole magnet counteract. Hence, the focusing sextupole magnet power supplies need not go much negative.

Authors would like to thank the MTF personnel for their help during the magnet measurements.

REFERENCES

[1] D.J. Harding, N.Chester, and R. Baiod, Proc. of the 1993 IEEE Part. Accel. Conf. (1993) 2826

[2] S.A. Bogacz, Proc. of the 1993 IEEE Part. Accel. Conf. (1993) 77.

[3] D.J. Harding R. Baiod B.C. Brown J.A. Carson N.S. Chester E. Desavouret J. Dimarco J.D. Garvey H.D. Glass P.J. Hall P.S. Martin P.O. Mazur C.S. Mishra A. Mokhtarani J.M. Nogiec D.F. Orris J.E. Pachnik A.D. Russell S.A. Sharonov J.W. Sim J.C. Tompkins K. Trombly-Freytag D.G.C. Walbridge and V.A. Yarba, "Magnetic Field Measurements of the Initial Production Main Injector Dipoles", (Procedings this conference).

[4] D. G. Walbridge and M. E. Bleadon and B. C. Brown and H. D. Glass and D. J. Harding and and P. O. Mazur and J. W. Sim, "Measurements of Beam Pipe Eddy Current Effects in Main Injector Dipole Magnets", "Int. J. Mod. Phys. A (Proc. Suppl.)" Vol. 2B, (1993) 617 and Proceeding of the XVth International Conference on High Energy Accelerators, Hamburg, July 20-24, 1992 also available as FERMILAB-Conf-92/220

[5] The Main Injector Technical Design Handbook 1994.

[6] J.W. Sim et. al., 'Software for a Database-Controlled Measurements System at Fermilab Magnet Test Facility' (these proceedings)

[7] B.C. Brown, Analysis of Magnet Strengths from Steel B-H Curves and Geometry' Fermilab MTF-94-0078,(1994).

SIMULATIONS OF TRANSITION CROSSING IN THE MAIN INJECTOR

C. M. Bhat and J. A. MacLachlan

Fermi National Accelerator Laboratory*
P.O. Box 500, Batavia, IL 60510

Abstract

The design goal for the Fermilab Main Injector (FMI) is to accelerate a minimum of 6×10^{10} protons per bunch through the transition. We present here the results from simulation studies of the transition crossing in the FMI using the particle tracking code ESME[1].

I. Introduction

The Fermilab Main Injector (FMI)[2] that is under construction is intended to be a high intensity 150 GeV proton injector to the Tevatron. The beam in the FMI will be accelerated from 8 GeV to 150 GeV through a transition energy of 20.48 GeV. The longitudinal emittance of the proton beam at injection is about 0.1 eVs, and the intensity will be more than 6×10^{10} protons per bunch. Maintaining the beam intensity as well as its longitudinal emittance through the acceleration cycle is very important for the FMI operation. In the past, preserving the beam emittance and the intensity through transition crossing in a proton synchrotron has been one of the major problems. A number of techniques have been suggested to cure these problems[3,4]. Two of the suggested techniques viz., a) γ_t-jump scheme[3] and a) focus free transition crossing(FFTC) [4] have been investigated in some detail for proton synchrotron along with with the normal transition phase jump (NTPJ) scheme. Here, the particle tracking code ESME[1] has been used study the longitudinal beam dynamics of the transition crossing in the FMI for these three different schemes.

The condition of non- adiabaticity[5] exists in a proton synchrotron when,

$$\frac{|\gamma-\gamma_t|}{\gamma_t} \leq \left[\frac{\gamma_t(eV_{rf}sin\phi_s)^2}{4\pi hE_oeV_{rf}\mid cos\phi_s\mid}\right]^{1/3} \qquad (1)$$

where γ_t is the relativistic quantity γ at transition, V_{rf} is the peak rf voltage at transition, ϕ_s is the synchronous angle of the beam with the rf wave form, h is the harmonic number of the machine and E_o is the rest mass of proton.

*Operated by the Universities Research Association, under contracts with the U.S. Department of Energy

By assuming that the γ is increasing linearly near transition at a rate $\dot{\gamma}$ this expression can be converted to a non-adiabatic time period in the vicinity of the transition time,

$$T_{na} = \pm T_s\left[\frac{f_sE_o{\gamma_t}^4}{4\pi h\dot{\gamma}eV_{rf}\mid cos\phi_s\mid}\right]^{1/3} \qquad (2)$$

where f_s=1/T_s is the revolution frequency of the synchronous particle. Since all the particles in a bunch do not pass through the transition at the same time, there will be a non-linear period during which some particles are above the transition energy while others are below it. The non-linear time is given by,

$$T_{nl} = \pm\frac{\beta^2+\alpha_1/\alpha_o+1/2}{\dot{\gamma}} \qquad (3)$$

where β is the ratio of particle velocity and the velocity of light. α_1 is the second order term in the expansion of path length in Δp/p (= δ). During this time the rf focusing force causes increased momentum spread and a number of different instabilities come into play. Since the non-adiabatic and non-linear time decrease with increased $\dot{\gamma}$, the simulations have been carried out for two different values of $\dot{\gamma}$ for the FMI operating scenarios.

II. ESME Simulations of Transition Crossing

In ESME, the collective behavior of the beam particles is treated using a pair of Hamilton-like difference equations describing synchrotron oscillations in the energy-angle (ΔE, ϕ) phase space, (where ΔE = E-E_o and $0\leq\phi\leq 2\pi$). The particles in a bunch are assumed to have an elliptical distribution which is a good representation of the beam bunches coming from the Fermilab Booster. For a cylindrical beam pipe of radius 'b' and a co-axial beam of radius 'a', the impedance, Z_ω seen by a single Fourier component of the beam current at a frequency $\omega/2\pi$, is,

$$\frac{Z_\omega}{n} = -j\frac{Z_og}{2\beta\gamma^2} + \frac{Z_W}{n} + \frac{Z_\parallel(\omega)}{n} \qquad (4)$$

where Z_o = 377 Ohm (Impedance of free space), Z_W is total wall impedance of the beam pipe and the geometry

factor g = 1+ $2ln(b/a)$. The average values of 'a' and 'b' are listed in Table II. The $Z_{||}$ is given by,

$$Z_{||}(\omega) = \frac{R_s}{1 + jQ(\frac{\omega_c}{\omega} - \frac{\omega}{\omega_c})} \quad (5)$$

For quality factor Q=1, Equation 5 represents the broad-band impedance. R_s is the strength of the effective shunt impedance. For the FMI we have taken design value R_s = 5 Ohm which is almost surely a considerable over estimate. with enough safety margin.

Table I. The parameters used for ESME simulations.

Parameter	Values
Mean radius of FMI	528.3019 m
γ_t (nominal)	21.838
$\dot{\gamma}$ at transition	167(Slow Ramp) sec^{-1} 280 (Fast Ramp) sec^{-1}
α_1	0.002091
Principal rf sys.	53 MHz 4 MV (max)
Init. emittance and Bunch intensity	0.1 and 0.2 eVs 6×10^{10}
Coup. imp. $Z_{||}/n$	5 Ω 2.17 GHz cutoff
Transverse Beam size(a)	0.0022 (m)
Beam pipe Radius (b)	0.03 (m)
FFTC : Shaping rf for FFTC Type of Tran. Crossing	 159 MHz 280 kV (max) Non-symmetric
γ_t- jump : $\Delta\gamma$ Type of Tran. Crossing	 1.0 Non-symmetric

The effect of transverse space charge force producing horizontal betatron tune shift is proportional to the particle density distribution in a bunch at a longitudinal position ϕ. Very close to the transition, η goes to zero. Therefore even a very small correction to γ_t becomes a sensitive parameter to determine the longitudinal beam dynamics. In the present calculations the dispersion of momentum compaction factor was taken into account by expanding,

$$\alpha_p \approx \alpha_o + (\alpha_o + 2\alpha_1 - \alpha_o^2)\delta \quad (5)$$

For the Main Injector we take α_1 to be 0.002091. This corresponds to a Johnsen parameter[3] of 0.8. Thus, each particle has its characteristic γ_t depending on the deviation of its momentum from that of the synchronous particle. Table I lists the parameters used in the present simulation studies. The results of ESME simulations have been displayed in Table II. The FFTC and γ_t-jump scheme

Table II. The results of the longitudinal beam dynamics simulations for transition crossing using ESME. The fractional growth $\Delta\epsilon$ / ϵ for different schemes are listed. .

$\dot{\gamma}_t$/sec	Init. Long. Emittance (eVs)	NTPJ	FFTC	γ_t-jump
167	0.1	3.0	0.6[a]	0.15
	0.2	0.09	0.04[a]	0.02
300	0.1	1.6	-	0.25
	0.2	0.06	-	0.02

[a] In these cases the ESME simulations have been carried out for $\dot{\gamma}_t$ = 169 /sec.

prefer symmetric settings for beam emittance larger than 0.2 eVs. For smaller emittance beam, where the space charge forces play important role in emittance blow up, the non-symmetric transition crossing is essential. Figure 1 shows a comparison of evolution of ϵ_l for NTPJ ,FFTC and γ_t-jump schemes in the Main injector for initial longitudinal emittance of 0.1 eVs. All these calculations have been performed by incorporating both space charge effects and the broad band Z/n. Since the δ increases as a bunch approaches transition energy, it is necessary to take into account of the the momentum acceptance of the FMI. From these simulations we find that the γ_t-jump scheme is preferable compared to FFTC. However, for emittance $\leq$ 0.1 eVs, and with the fast ramps the benefits are limited. With the FFTC scheme the emittance growth will be in between those for NTPJ and the γ_t-jump scheme. For emittance $\geq$ 0.2 eVs we find that the FFTC and γ_t-jump schemes give almost no emittance growth, while, with the NTPJ there is a maximum of about 10% emittance growth. Thus, with $\dot{\gamma}_t$ = 300 /sec and with $\epsilon_l \geq$ 0.2 eVs we may not need any of the schemes like FFTC or the γ_t-jump for transition crossing in the FMI.

In a separate set of calculations we have estimated the negative mass instability using ESME. Our results confirm the calculations of Ng[6], who employed the analysis of Hardt[7]. We find for 6×10^{10} protons/bunch a limit of $\epsilon_l \leq$ 0.16 eVs for $\dot{\gamma}_t$ = 167 /sec and $\epsilon_l \leq$ 0.12 eVs for $\dot{\gamma}_t$ = 300 /sec.

III Summary and Conclusions

We have simulated the transition crossing for the pro-

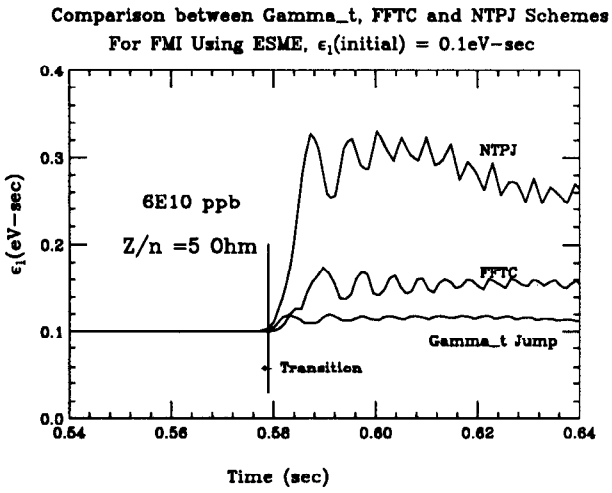

Figure 1: A comparison between γ_t-jump, FFTC and NTPJ schemes for the FMI. The initial emittance is 0.1 eVs, number of protons per bunch = 6×10^{10}. The $\dot{\gamma}_t$ = 167 /sec.

ton beam with 6×10^{10} particle /bunch. Three different schemes of transition crossing in the FMI have been investigated. We find that for an operating scenario of $\dot{\gamma}_t$=300 /sec and $\epsilon_l \geq 0.2$ eVs we do not need any special schemes like γ_t-jump or FFTC.

Authors would like to acknowledge Dr. K.Y. Ng for useful discussions, especially the treatment of negative mass instability.

References

[1] J.A. Maclachlan, User's Guide to ESME v.8.13, Fermilab TM-1856(1994).

[2] D. Bogert, W. Fowler, S. Holmes, P. Martin and T. Pawlak, 'The status of the Fermilab Main Injector Project' (these proceedings).

[3] A. Sorenssen, Part. Accelerators. Vol. 6 (1975) 141.

[4] J. Griffin, Synchrotron Phase Transition Crossing Using an RF Harmonic, Fermilab TM 1734 (1991).

[5] E.D. Courant and H.S. Snyder, Annals of Phys. 3(1958) page 1.

[6] I. Kourbanis and K.Y.Ng, Proc. Part. Accel. Conf. (1993) 3630.

[7] W. Hardt, Proc. 9th Int. Conf. on High Energy Accelerators, Stanford 1974.

RADIATION SHIELDING OF THE MAIN INJECTOR

C. M. Bhat and P.S. Martin

Fermi National Accelerator Laboratory*
P.O. Box 500, Batavia, IL 60510

Abstract

The radiation shielding in the Fermilab Main Injector (FMI) complex has been carried out by adopting a number of prescribed stringent guidelines established by a previous safety analysis[1]. Determination of the required amount of radiation shielding at various locations of the FMI has been done using Monte Carlo computations. A three dimensional ray tracing code as well as a code based upon empirical observations have been employed in certain cases.

I. Introduction

The Fermilab accelerator complex consists of a chain of four proton accelerators with a beam energy up to 800GeV for fixed target experiments and up to 2 TeV (center of mass energy) for collider experiments. The Fermilab Main Injector (FMI) which is being built in a separate enclosure, will replace the 150 GeV Main Ring (MR) accelerator which is currently being used as an injector to the Tevatron. FMI has many added advantages over the MR[2]. Having larger admittance both in the transverse and in the longitudinal phase space, the FMI is capable of providing more than 5E12 protons/batch at 120 GeV for the antiproton production target and over 3E13 protons/batch at 150 GeV for the fixed target operations. When such a high energy and high intensity facility is being built, it is necessary that proper care is taken regarding environmental protection as well.

II. Shielding Guidelines

The radiation safety is an important and mandated requirement for all Fermilab facilities. In order to meet this responsibility a number of guidelines have been provided in the FERMILAB RADIOLOGICAL CONTROL MANUAL and have been followed for designing the FMI. Many of the stated guidelines in this manual are more stringent than the DOE standards. A list of Fermilab standards which are relevant to the aspects of radiation shielding evaluation at the FMI, are given in Table I.

*Operated by the Universities Research Association, under contracts with the U.S. Department of Energy

Table I. Fermilab standards for radiation shielding evaluations.

Description	Maximum Allowed Dosage
Visitors and public: Whole body	0.05 rem/year (i.e., 0.025 mrem/hr) (Unlimited Occupancy)
Non-radiation workers: Whole body	0.05 rem/year (i.e., 0.025 mrem/hr) (Unlimited Occupancy)
Radiation workers: (direct 'prompt' radiation)	1.5 rem/year ($\leq$300 mrem / quarter)
Ground water activation[a]	20 pCi/ml-year (^{3}H) 0.4 pCi/ml-y (^{22}Na)

[a] These nuclides are of major concern to Fermilab. However care has been taken to meet the requirements of DOE order N0. 5400.5 for other radioactive nuclides causing contamination in the ground water.

Using the guide lines in Table I and the results of Monte Carlo calculations with CASIM[3] for some typical cases, the following shielding criteria have been developed[1]:

1. For unlimited occupancy we need soil equivalent shielding of 7.92 m (26 ft) for 150 GeV beam-lines enclosures, and a soil equivalent shielding of 7.46 m (24.5 ft) forthe 8 GeV beam-lines and the FMI enclosures.

2. 0.305 m (1 ft) of steel[4] is a soil equivalent of 0.88 m (2.89 ft) and 0.305 m of heavy concrete (78% concrete with 22 % steel) is a soil equivalent of 0.46 m.

These are used very often in deciding the shielding thickness for radiation protections.

III. FMI Design, Beam Intensities and Beam-losses

FMI is located underground. The tunnel floor of the FMI is at an elevation of 217.47 m (713.5 ft) which is about 1.82 m lower than the Tevatron tunnel floor. It has a total circumference of 3319.41 m. A geometric layout of the

FMI along with some critical area of interest from the radiation shielding point of view are shown in Fig. 1. For the purpose of injection and extraction of the proton beams, a total of seven beam lines will be built. Some beam lines have varying elevations.

Each region of FMI and its beam-lines that poses potential radiation safety problems has a unique structure, so they have to be treated individually. For instance, the RF gallery near the MI60 straight section is one such area. The proton and the antiproton beams from the FMI will be injected in to the Tevatron near(under) this gallery. The two accelerators are at different elevations. A total of five beam lines originate in the vicinity of this region. The walls in the beam enclosure have a number of utility penetrations and alcoves. At the surface level (at an elevation of 226.31 m) there is the MI60 service building. Evaluating the radiation shielding for a region like this is very difficult task. We will briefly discuss the shielding aspects of this region later.

The beam in the FMI will be accelerated to 120 GeV and 150 GeV depending upon the application. The operating scenarios for the FMI are listed in Table II. The FMI is capable of operating in five different modes. The beam intensities shown in Table II are design goals.

Table II. The beam intensities for different operation scenarios of the FMI and beam loss terms.

FMI Mode of Operation	Proton Beam Intensity and Cycle time
pbar Production	5E12p/1.5sec @120GeV
Fast Resonant Extraction	3E13p/1.9sec @120GeV
Slow Resonant Extraction	3E13p/2.9sec @120GeV
Collider Injection	5E12p/5sec @150GeV
Tevatron Fixed Target	3E13p/30sec @150GeV
Beam-loss Scenario	Source Term
Operation Losses (Annual)	1E19 @8GeV 4.1E18 @120GeV
Accidental Losses	5.7E16 @8GeV 8.5E15 @120GeV

Defining the beam-loss term for an accelerator is a difficult task. Generally they are categorized into, a) normal operational beam-losses and, b) accidental beam losses. A

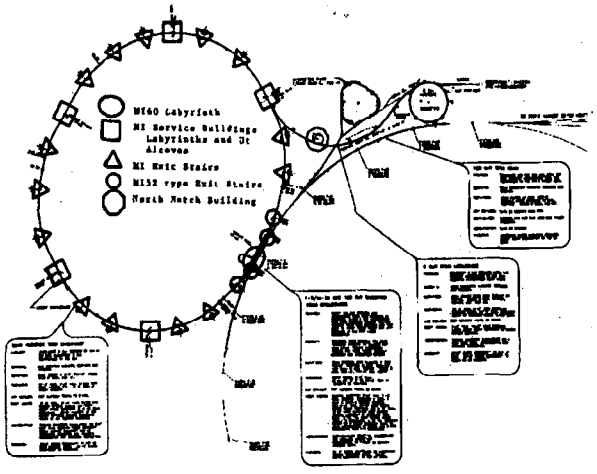

Figure 1: A geometric layout of the FMI. Ellipse : MI60 labyrinth, square:MI Service Buildings, Triangle : MI Exit Stairs, Circle : MI52 type Exit Stairs, Octagon : 8GeV North Hatch Building.

conservative estimate for the FMI has been made based upon our past experience with the Main Ring operation and are listed in Table II. These beam-losses have been used as source terms for shielding evaluations. There is also an estimated annual proton beam abort for the FMI which has been taken into account in designing the FMI beamdump[5].

IV. Shielding Calculations

After establishing the guidelines and beam-loss terms, radiation shielding calculations have been performed. When a high energy particle interacts with a material, a shower of particles mainly consisting of protons, neutrons and pions will be produced. These in turn interact further resulting in cascades of particles with angular distribution peaked in the forward direction. If the beam is lost in an energized magnet, the angular distribution need not be symmetric. The radiation dose at any point will be calculated using the number of stars produced at that location which depends upon the hadron flux, the energy, the angle and the shielding in between. When multi-GeV primary protons are lost in a target, the contributions to the prompt radiation dose in the transverse direction will be dominated by the low energy neutrons, while in the forward direction the muons (which are long-ranged) will dominate. For shielding purposes we have to consider both of them separately.

We have carried out shielding calculations for most of the locations around the FMI using Monte Carlo codes[3] CASIM (for hadrons) and MUSIM (for muons) in cylindrical geometry. The culverts are some of the locations of potential problems around the FMI which do not have cylindrical symmetry. In these cases, we have used a derivative of the code CASIM (called CASPEN [3]) and the required amount of steel under the culverts were determined. There

DESIGN OF THE MI40 BEAM-ABORT DUMP

C. M. Bhat, P.S. Martin and A.D. Russell

Fermi National Accelerator Laboratory*
P.O. Box 500, Batavia, IL 60510

Abstract

A beam-abort dump for the Fermilab Main Injector to handle 3E13 protons per pulse at 150 GeV has been designed. A 120 GeV beam line goes through the beam-dump off-set by 27cm from its center. The design and the environmental safety aspects of the beam-dump are described here.

I. Introduction

A beam-abort dump or beam stop is an important part of a high energy accelerator. In an accidental condition the beam must be automatically deflected on to a dump to avoid any damage to the accelerator components. Even during routine accelerator studies low intensity beam gets frequently aborted. In any of these cases, the beam-dump should be able to handle the aborted beam. Also, the area around it should have enough radiation and environmental protection.

Fermilab Main Injector (FMI) is a 8-150GeV proton synchrotron that is being built as a high intensity injector to the Tevatron. The Main Injector beam-dump is to be built near the MI40 straight section and has the base elevation of 214.27 m (703ft). It is planned to be a water-cooled dump. The maximum number of protons per machine cycle on the beam-dump exceeds 3E13@150 GeV. Since this beam-dump will be much closer to the aquifer than any existing beam-dumps in the Fermilab accelerator complex, it is extremely important that the design minimize the soil activation and reduce the ground water contamination.

To establish As Low As Reasonably Achievable (ALARA) radiation exposure to Fermilab workers and visitors a number of guidelines have been worked out and they are stated in FERMILAB RADIOLOGICAL CONTROL MANUAL. According this, the on-site and off-site radiation level should be less than 0.025 mrem/hr and 10 mrem/year respectively. The allowed ground water radioactive contamination should be less than 20pCi/ml-year. Also, the policy of Fermilab is, not to accelerate beams for which there is not a user. Aborting the maximum number of protons per hour, while not strictly an accident condition, is a violation of that policy.

*Operated by the Universities Research Association, under contracts with the U.S. Department of Energy

II. Design

We started out with the design of the presently existing beam-dump[1] in the Tevatron (near the C0 straight section) and arrived at an optimized design for the MI beam-dump. However, unlike the buried C0 Tevatron beam-dump, the FMI beam-dump will be placed in an accessible enclosure. The optimization has been carried out using the Monte Carlo code CASIM[2]. The total radiation dose above the berm of the beam-dump which is at an elevation of 227.38 m (746 ft) and the total number of stars in the soil is designed to be at least a factor of two below the acceptable limit. To have the ability for easy access, a 1.1 m wide walking space will be allowed around the beam-dump. The design of the beam-dump is shown in Fig.1. Provision has also been made for a 7.62 cm beam pipe through the iron core of the beam-dump for future extracted beam. The core of the beam-dump will be of high melting point graphite embedded in a 2.74 m aluminum box. This box will be cooled by 40°C low conductivity water (LCW). In front of the aluminum box concrete bricks will be hand stacked. The aluminum box is surrounded by layers of 0.84 m thick steel and 1.1 m thick concrete. The total length of the beam-dump will be 10.7 m. The LCW cooling system will be installed behind the beam-dump in the available space.

The transverse emittance of the beam[3] in the Main Injector is expected to be 12π or larger. The horizontal and vertical β-functions at the surface of the graphite core is 225 m. This makes the minimum beam spot size on the beam-dump about 0.15 cm. The instantaneous maximum temperature rise in the core within the area occupied by the beam due to the interaction of 3E13 protons at 150GeV is about 100°C. This beam will deposit about 330 kW of power in the beam-dump. Out of that about 55% of the energy (i.e. 200 kW) will be deposited in the graphite and aluminum core box alone. Hence we have planned to have an LCW cooling system which is capable of extracting at least 300 kW.

III. Estimation of Radiation Level

The radioactivity in and around a beam-dump can be categorized into two classes. The first one is for the beam

on conditions (prompt radiation), i.e., the instantaneous electromagnetic and hadronic showers developed due to interactions of the high energy particles with the beam-dump. The second arises from the residual radioactivity of the dump. Both of these are dependent upon the total number of primary protons aborted and the beam energy. The average number of protons to be aborted on the FMI beam-dump per year under normal operating conditions[4] is about 3.26E18 @150 GeV. The maximum number of protons continuously aborted in any one incident is estimated to be 6.0E16 @150 GeV per hour.

Table I. Dose due to prompt radiation around FMI beam-dump and ground water activity.

Concern	Radiation dose
Neutrons :	
Max. Rad. Dose	1.1E-5(mrem/hr)
(Allowed dose	(For N.O.)
Unlimited Occp.	
Limit.=0.025 mrem/hr	1.2E-3(mrem/acc.)
for N.O. and	(Maximum Beam
1 mrem/accident	Abort)
Muons :	
On-site	5.4E-5(mrem/hr)
(Allowed dose	(For N.O.)
Unlimited Occp.	
Limit=0.025 mrem/hr	6.0E-3(mrem/acc.)
for N.O. and	(Maximum beam
1 mrem/accident	Abort)
Off-site muons	
Annual Limit=	≤3.2E-5(mrem/y)
10 mrem/y	
Ground Water :	
Annual	^{3}H 2.12pCi/ml-y
Activation	^{22}Na 0.07pCi/ml-y (A)
(Annual Limit	
20 pCi/ml-y of ^{3}H	^{3}H 0.01pCi/ml-y
0.4 pCi/ml-y of ^{22}Na)	^{22}Na 0.148pCi/ml-y (B)

(A) Single Resident Well Model (B) Concentration Model

A. Prompt Radiation

The prompt radiation dose is calculated using the number of "stars" (interaction points) produced in a unit volume per incident particle. With a soil equivalent shielding thickness between the FMI beam-dump and the berm of about 9.75 m, the low energy neutrons and muons are the main contributors to the radiation dose at the surface level. Here, these two contributions have been evaluated in separate sets of Monte Carlo calculations. Figure 2 displays isodose contours obtained using CASIM. The results for muons are displayed in Fig. 3 along with a sectional view of earth in the downstream of the beam-dump. Using these results, the expected radiation dose for normal and maximal beam loss conditions have been evaluated. The results are listed in Table I along with the standards adopted at Fermilab.

Radioactive contamination of the ground water is one of the major considerations in designing a beam-dump. The aquifer around FMI is only about 4.88 m below the FMI beam-dump. Of all the radioactive nuclei produced in the spallation reactions the greatest hazards in ground water are from ^{3}H and ^{22}Na. The EPA-allowed limits for these nuclides in ground water are listed in Table I. There are two methods to determine the increase in the concentrations of these nuclides in the aquifer viz., A) the single resident well model and B)the concentration model[5] (which was developed very recently and is more suitable for an accelerator complex like Fermilab). The first one depends upon the total amount of stars in the soil and the second method uses the maximum star density in the soil near the base of the beam-dump. The results obtained from these two models are displayed in Table I. We find that they are at least a factor of two below the allowed limits.

B. Induced Radioactivity in the Beam-dump

As a result of hadronic showers developed in the beam-dump a variety of short and long lived radioactive nuclides will be produced. These give rise to residual radioactivity. Here we use the method suggested by Barbier[6] to estimate it.

Table II. Residual radioactivity for MI Beam-Dump at contact. T_i = irradiation time in days (d). T_c = cooling time.

Description	Dose on Contact (rad/hr)	
	T_i=360d T_c=1d (7d)	T_i=30d T_c=1d (7d)
Carbon		
Front	10 (10)	3.3 (3)
Back	10 (10)	3.3 (3)
Al. Box		
Top Front	26 (4)	0.4 (0.4)
Top Back	26 (4)	0.4 (0.4)
Iron		
Front	0.2(0.1)	0.1 (0.07)
Middle Top	0.02 (0.02)	0.01(0.007)
Back	≤4E-3 (≤1E-3)	≤2E-3 (≤1E-3)
Concrete		
(Max)	≤2E-3 (≤4E-4)	≤2E-3 (≤4E-4)
Concrete Wall		
(Max)	≤8E-4 (≤2E-4)	≤8E-4 (≤2E-4)

The radiation dose $\dot{D}$ is given by,

$$\dot{D}(rad/hr) = \Omega/4\pi \times \Phi \times d$$

where Φ is the hadron flux (which related to the star density and the incident proton flux). For dose measurements at contact, $\Omega/4\pi = 0.5$. d is referred to as the danger

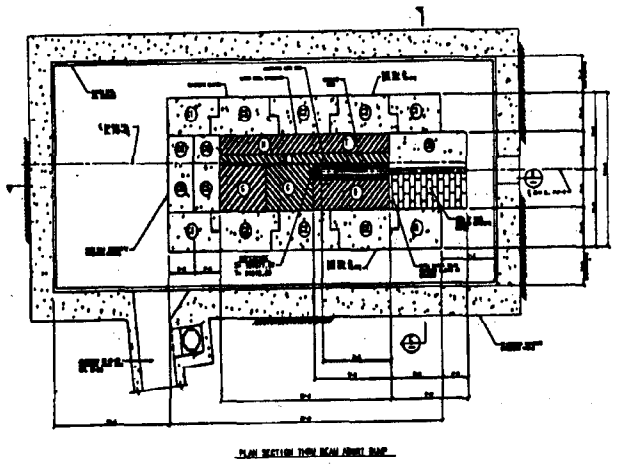

Figure 1: Longitudinal section of FMI beam-dump.

parameter which depends upon the material which is being irradiated, the duration of irradiation, T_i, the production cross section for various radioactive spallation products and the cooling time, T_c, of the target. For FMI beam-dump, the danger parameters are taken from Ref.6. The results of calculations have been listed in Table II.

IV. Summary

A beam-dump suitable for the Fermilab Main Injector that can handle 3E13p/pulse has been designed and is presently under construction. We have allowed for a beam line to go through the iron core without affecting the radiation level at the berm. There is enough clearance around the beam-dump for easy access and maintenance. We estimated that the prompt radiation dose level and the ground water contamination level is at least a factor of two less than the prescribed limits in FERMILAB RADIOLOGICAL CONTROL MANUAL. The residual radioactivity around the beam-dump will be less than 2 mr/hour after one day of cooling.

The authors would like to acknowledge Dr. A. Van Ginneken and Dr. N.V. Mokhov for useful discussions.

REFERENCES

[1] A. Van Ginneken CASIM Fermilab-FN272(1975), MUSIM Fermilab-FN594(1992).
[2] T.C. Murphy et al, Fermilab TM1196 (1983).
[3] Fermilab Main Injector Technical Design Handbook (1994).
[4] Fermilab Main Injector PSAR (1992).
[5] A.J. Malansek et al, Fermilab TM1851 Aug. 1993.
[6] M. Barbier, Induced Radioactivity, North-Holland Pubs. Comp. (1969).

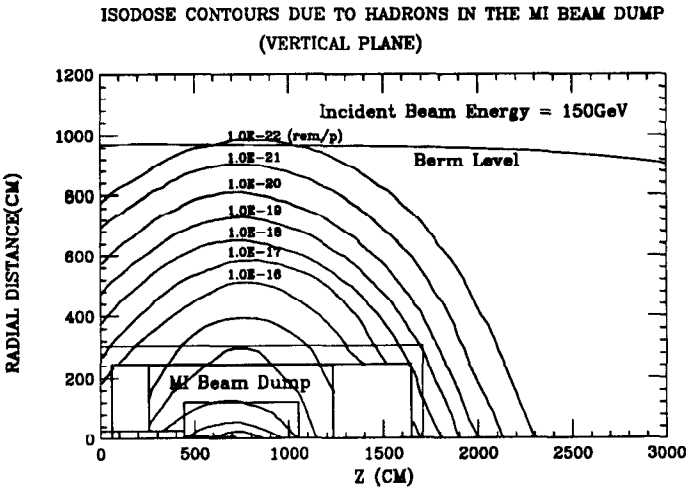

Figure 2: Iso-dose contours for 150GeV proton beam aborted on FMI beam-dump.

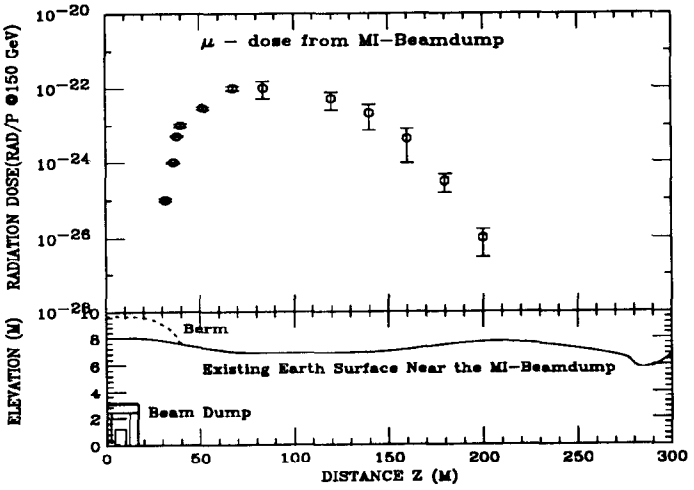

Figure 3: The muon dose in the vicinity of FMI beam-dump for 150GeV proton beam abort.

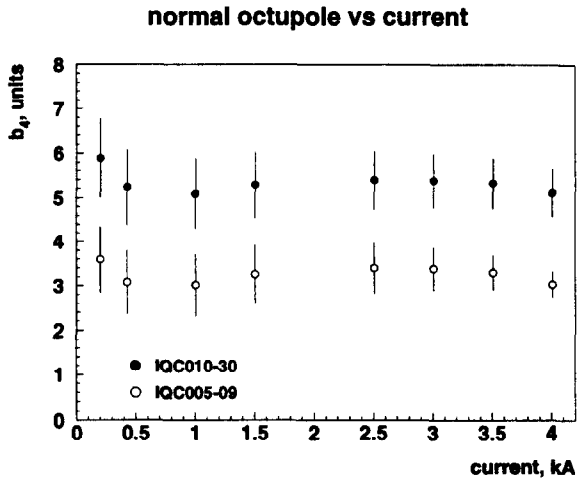

Figure. 4. Average octupole component vs current

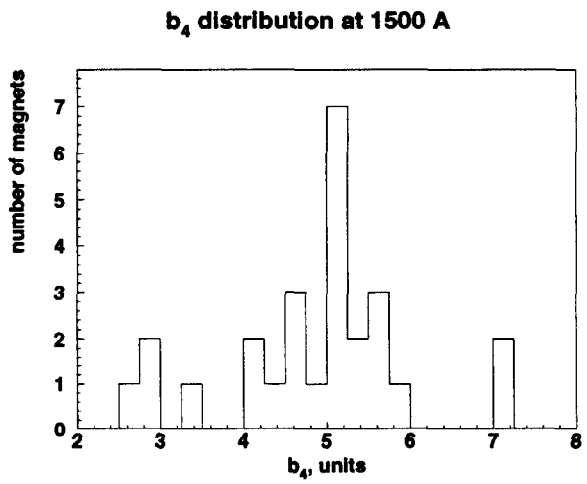

Figure. 5. Distribution of octupole strengths at 1500 A

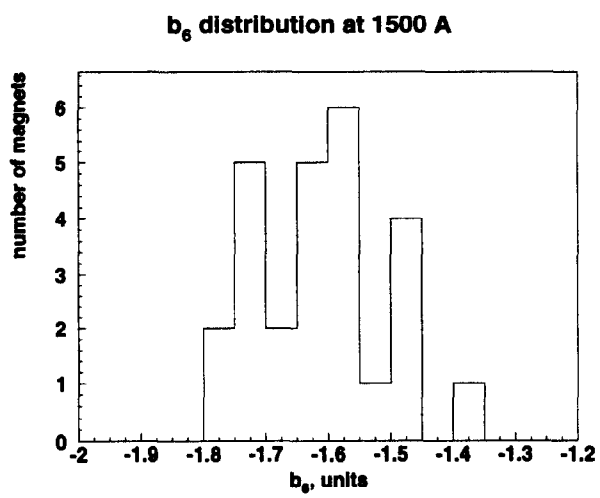

Figure. 6. Distribution of 12-pole strengths at 1500 A

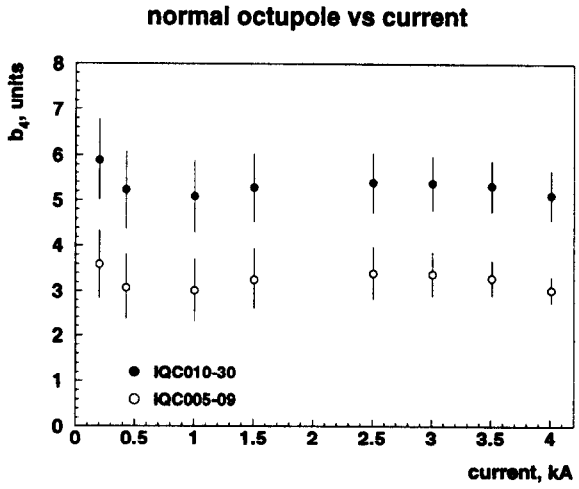

Figure. 4. Average octupole component vs current

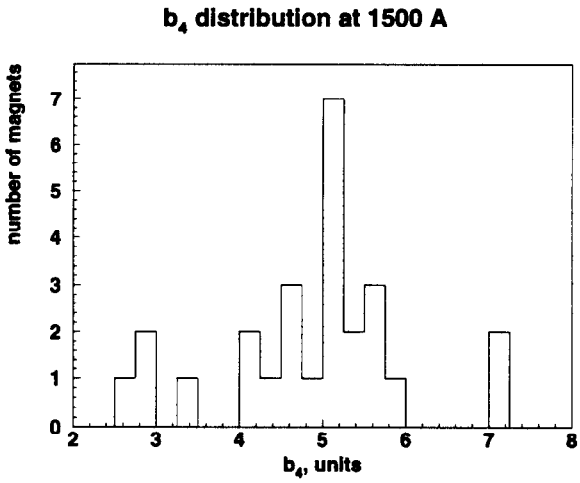

Figure. 5. Distribution of octupole strengths at 1500 A

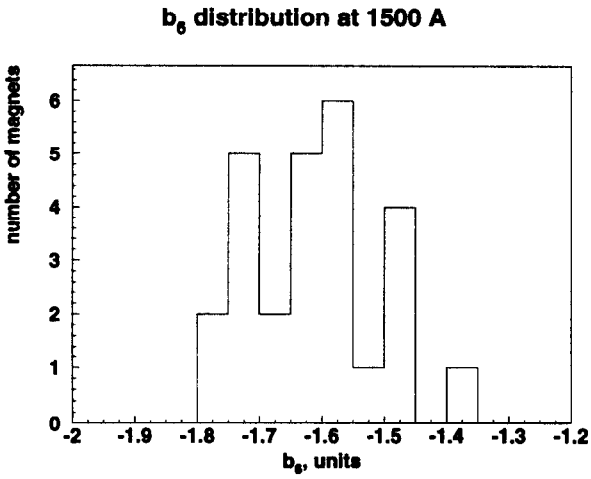

Figure. 6. Distribution of 12-pole strengths at 1500 A

MAGNETIC FIELD MEASUREMENTS OF THE INITIAL FERMILAB MAIN INJECTOR PRODUCTION QUADRUPOLES

D.J. Harding, R. Baiod, B.C. Brown, J.A. Carson, N.S. Chester, E. Desavouret, J. DiMarco, J.D. Garvey, H.D. Glass, P.J. Hall, P.S. Martin, P.O. Mazur, C.S. Mishra, A. Mokhtarani, J.M. Nogiec, D.F. Orris, J.E. Pachnik, A.D. Russell, S.A. Sharonov, J.W. Sim, J.C. Tompkins, K. Trombly-Freytag, D.G.C. Walbridge, and V.A. Yarba, Fermi National Accelerator Laboratory*, P.O. Box 500, Batavia, IL 60510 USA

Abstract

A large sample of the 2.54-meter quadrupoles for lattice matching in the Fermilab Main Injector have been fabricated and measured. The resulting properties are reported and compared to the accelerator requirements.

I. Magnet requirements

The Fermilab Main Injector is a new proton and antiproton accelerator currently under construction at Fermi National Accelerator Laboratory. It will replace the existing Main Ring in all functions. While many of the quadrupoles used in the Main Injector will be reused from the Main Ring, the lattice requires some new quadrupoles of the same design but different lengths (2.54 m and 2.96 m, compared to 2.13 m for the Main Ring quads) to run on the same busses. The performance requirements of the quadrupoles have been studied extensively [1] [2] [3]. The two significant areas of magnetic performance are the magnet-to-magnet variation in the integrated magnetic field ("strength") and the variation of the strength as a function of transverse position ("shape"). These are discussed here separately.

A. Strength

We define the strength to be $\int_{-\infty}^{\infty}(dB_y/dx)dz$. The integral is taken at the center of the aperture. When discussing relative strengths we quote fraction differences in "units" of parts in 10^4.

Based on experience, we expected to be able to hold the variation in strength to 10 units (10×10^{-4}). The majority of our tracking studies have used the more generous assumption of a root mean square deviation of 24 units and have found that with that distribution we only need to select which magnet is placed on which bus (focussing or defocussing).

B. Shape

We define the shape to be the variation in the strength as a function of position. We characterize the field by its harmonic decomposition. The normal component of a quadrupole's field can be reconstructed as

$$B_y(x) = B_1(b_1 + 1(\frac{x}{r_0})^1 + b_3(\frac{x}{r_0})^2 + b_4(\frac{x}{r_0})^3 + \cdots),$$

where B_1 is the quadrupole strength, b_n are the normal harmonic components. We quote the components at $r_0 = 25.4$ mm and in "units" of parts in 10^4. Properly centered, the dipole component b_1 is zero.

From the symmetry of the magnet design we expect the field to have significant quadrupole, octupole, and twelvepole components. For our tracking studies we have assumed distributions of the forbidden components that are consistent with the measured spread in values. While these values are larger than the measurement errors and not yet understood, they have no significant impact on the beam dynamics. We concentrate here on the allowed components.

Given the known octupole component in the existing Main Ring quadrupoles, we could choose the octupole of the new quads to meet the beam dynamics needs. The octupole has two demands placed upon it. One need is that the dynamic aperture be large enough to meet the accelerator requirements. The beam should not fall out of the machine on its own. The other need is that the beam be close enough to the edge of stability so that the existing trim octupoles can bring the beam to the point of slow extraction. The beam should fall out of the machine given a little push in the right direction. Based on simulations, an average of 4 to 8 units appears to satisfy both requirements. Magnet-to-magnet variations are not significant dynamically.

The twelve-pole component is clearly measurable, but not large enough to pose a problem for the dynamic aperture of the accelerator. Reasonable variations in the twelvepole are not significant.

II. Measurement systems

The equipment and software used in measuring the magnets is described with more detail in other papers at this conference and elsewhere [4]. The request from the Main Injector project is that every magnet be measured and that in production the strength and shape be determined by at least two independent methods.

To date only a rotating coil system, using a Morgan coil that extends through the length of the magnet, has been implemented. The probe has two orthogonal dipole coils, two orthogonal quadrupole coils, and one each sextupole, octupole, decapole, 12-pole, and 20-pole coils. One quadrupole coil is used to measure the strength of the magnet. The other coils measure the harmonic components while suppressing the signal from the quadrupole field. The

*Work supported by the United States Department of Energy under contract No. DE-AC02-76CH0300

rotating coil measurements are performed at multiple currents on every magnet.

A single wire stretched wire system is currently being commissioned. This will provide the redundant strength and shape information requested, as well as magnet center data.

III. Measurement Data

A. Strength

We have averaged the strength at each current. Figure 1 shows the deviation of the average strength from a linear excitation calculated assuming infinite steel permeability.

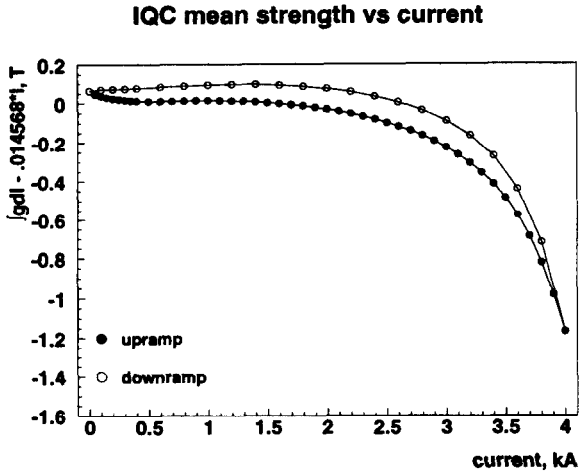

Figure. 1. Deviation of average quadrupole strength from linear vs current

To present the magnet-to-magnet variation, we calculate the fractional deviation of individual magnets from the average. Figure 2 shows the strength at 500 A for all magnets in the sample, relative to the average of all magnets except the first seven. Those seven magnets are significantly different from the later magnets due to experimental modifications of the lamination. In the low current regime the strength is dominated by the geometry, with only a small contribution from the permeabilty of the steel. Note that the strengths are tightly clustered, indicating good control of the geometry. All magnets fall within the expected range. Similarly, even as the steel begins to saturate, the spread in strength is small, as shown in Figure 3.

B. Shape

Figure 4 shows the average octupole b_4 as a function of current. This meets both the need for stability and for slow extraction. The octupole strengths are histogrammed in Figure 5. All magnets fall near the target values, and the average is certainly acceptable. The distribution of the twelve-pole component at 1500 A is shown in Figure 6. It is also within the established limits.

IV. Conclusions

The Fermilab Main Injector project is well into production of the new quadrupoles for the ring. By the end of

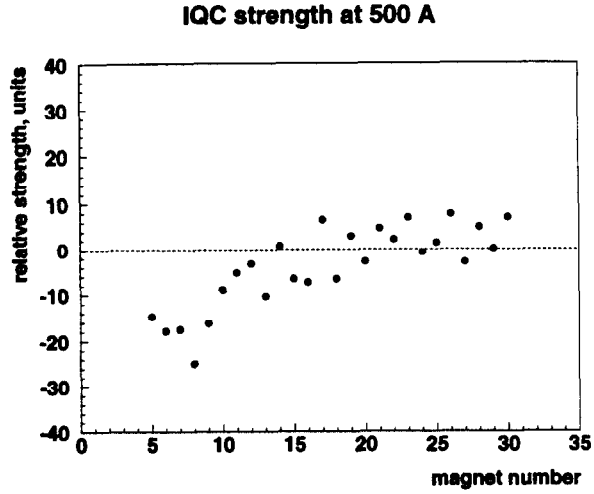

Figure. 2. Relative strength of quadrupoles at 500 A

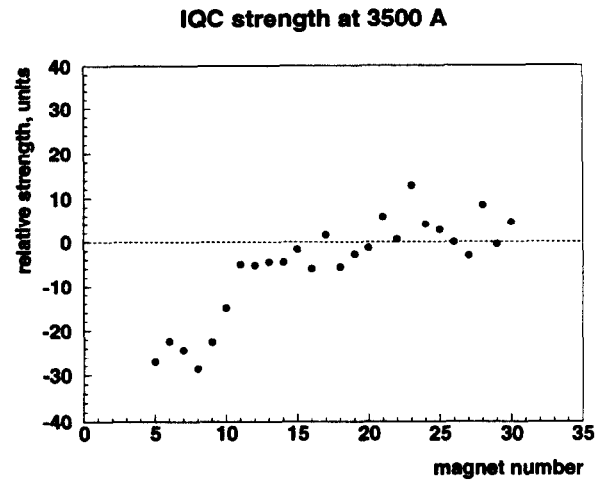

Figure. 3. Relative strength of quadrupoles at 3500 A

March 1995 30 2.54 m quadrupoles, out of 32 required for the ring, had been completed and measured. Magnet performance is within the acceptable range established through tracking studies. Production had just begun on the 48 2.96 m quadrupoles that are required.

References

[1] C.S. Mishra P.S. Martin D.J. Harding H.D. Glass and B.C.Brown. Fermilab Main Injector Magnet Acceptance Criteria. In *Proceedings this conference*, 1995.

[2] C.S. Mishra. Requirement of the Fermilab Main Injector Quadrupole Strength Matching. In *Proceedings this conference*, 1995.

[3] C.S. Mishra. Fermilab Main Injector Quadrupole Placement Scheme. In *Proceedings this conference*, 1995.

[4] J.W. Sim et al. Software for a Database-Controlled Measurement System at the Fermilab Magnet Test Facility. In *Proceedings this conference*, 1995.

The rotating coil system uses a tangential coil that extends through the length of the magnet. The G-10 coil form has a small enough diameter that it easily conforms to the curved central orbit of the magnet and flexes as it is rotated to maintain the curvature. A coil wound on one diameter of the probe provides a measurement of the absolute strength of the magnet. The tangential coil, bucked against the equal-area diameter coil, provides flux measurements on a circle, from which the normal and skew harmonic components are extracted. The rotating coil measurements are performed at multiple currents on every magnet.

The pointscan system uses both a Hall probe and an NMR probe to scan the magnetic field along the magnet's length in 25.4 mm steps. Numerically integrating the field measurements gives the magnet strength. These time-consuming pointscan measurements are performed at two currents on a sample of magnets.

III. Measurement Data

A. Strength

For each measurement system we have averaged the strength at each current. Figure 1 shows the deviation of the average strength from a linear excitation calculated assuming infinite steel permeability.

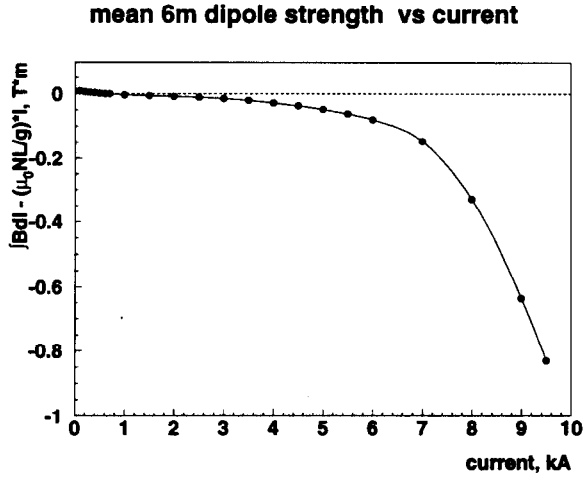

Figure. 1. Deviation of average dipole strength from linear vs current

To present the magnet-to-magnet variation, we calculate the fractional deviation of individual magnets from the average. Figure 2 shows the strength at 1500 A for all magnets in the sample, relative to the average of all magnets except the first eight, whose measurements are significantly noisier than the later measurements. At this current the strength is dominated by the geometry, with only a small contribution from the permeability of the steel. Note that the strengths are tightly clustered, indicating good control of the geometry. All magnets fall within the expected range.

Figure 3 shows the strength at 9500 A (a little over full excitation) for all magnets in the sample relative to the average of all magnets except the first eight. Note that the local average of the strengths started to increase about half way into this group of magnets. Although no magnet falls outside the acceptable range, it is important to understand and control the process so that the variation does not increase further.

The nature of the increase can be better appreciated by looking at the relative strength as a function of current for a limited number of magnets, as shown in Figure 4. Here we see that the strength deviation depends on current, a strong indication that we are seeing a magnetic property of the steel, as opposed to a geometrical effect.

Analyzing the composition of the magnets, we determined that the strength deviation of the magnet was closely correlated with the mix of laminations in the magnet stamped from different processing runs of steel. A detailed examination of the magnetic data on the sample strips from steel coils shows statistically significant differences among the runs of steel. Two-dimensional modeling of the magnetic field using the different B-H curves reproduces the differing magnet excitation curves.

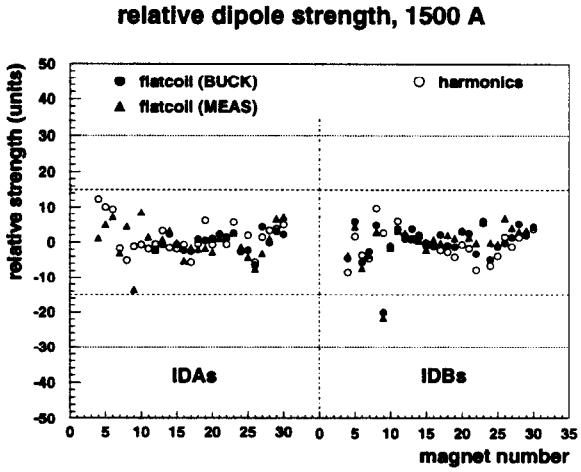

Figure. 2. Relative strength of all dipoles at 1500 A

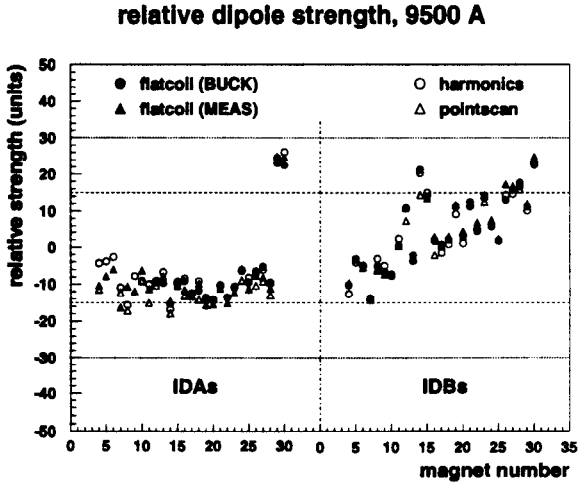

Figure. 3. Relative strength of all dipoles at 9500 A

MAGNETIC FIELD MEASUREMENTS OF THE INITIAL FERMILAB MAIN INJECTOR PRODUCTION DIPOLES

D.J. Harding, R. Baiod, B.C. Brown, J.A. Carson, N.S. Chester, E. Desavouret, J. DiMarco, J.D. Garvey, H.D. Glass, P.J. Hall, P.S. Martin, P.O. Mazur, C.S. Mishra, A. Mokhtarani, J.M. Nogiec, D.F. Orris, J.E. Pachnik, A.D. Russell, S.A. Sharonov, J.W. Sim, J.C. Tompkins, K. Trombly-Freytag, D.G.C. Walbridge, and V.A. Yarba, Fermi National Accelerator Laboratory*, P.O. Box 500, Batavia, IL 60510 USA

Abstract

A large sample of the 6-meter dipoles for the Fermilab Main Injector have been fabricated and measured. The resulting properties are reported and compared to the accelerator requirements.

I. Magnet requirements

The Fermilab Main Injector is a new proton and antiproton accelerator currently under construction at Fermi National Accelerator Laboratory [1]. It will replace the existing Main Ring in all functions. While many of the Main Ring quadrupoles will be reused in the Main Injector, the dipoles are a new design. The performance requirements of the dipoles have been studied extensively [2]. The two significant areas of magnetic performance are the magnet-to-magnet variation in the integrated magnetic field ("strength") and the variation of the strength as a function of transverse position ("shape"). We discuss these topics separately here.

A. Strength

We define the strength to be $\int_{-\infty}^{\infty} B_y dz$. The integral is taken at the center of the aperture and follows the path of the central orbit, curving with the magnet. We quote relative strengths in "units" of parts in 10^4.

Based on experience, we expected to be able to limit the variation in strength to 10 units (10×10^{-4}). The majority of our tracking studies have used the more generous assumption of a root mean square deviation of 10 units and have found that with that distribution no selection of magnets for placement in the ring is necessary. We have also tried a broader Gaussian distribution with σ=15 units and a bimodal distribution with two narrow peaks separated by 30 units [3]. In the former case, we can expect the planned trim dipoles to correct the closed orbit even with random assignment of the dipoles. In the latter case, a simple magnet placement plan is needed.

B. Shape

We define the shape to be the variation in the strength as a function of transverse position. We characterize the shape by the horizontal variation $\int_{-\infty}^{\infty} B_y(x)dz$ of the field integral and by the harmonic decomposition of the integral. We can link the two by writing

$$B_y(x) = B_0(1 + b_2(\frac{x}{r_0})^1 + b_3(\frac{x}{r_0})^2 + b_4(\frac{x}{r_0})^3 + \cdots),$$

where $B_y(x)$ is the integral, B_0 is the strength, and b_n are the normal harmonic components. We quote the components at $r_0 = 25.4$ mm and in "units" of parts in 10^4.

From the symmetry of the magnet design we expect the field to be both left-right and up-down symmetrical. For our tracking studies we have assumed distributions of the forbidden components that are consistent with the measured spread in values without questioning whether these values are real or primarily measurement error, either random or systematic. The measured values are small. We concentrate here on the allowed components.

The chromaticity sextupole system [4] is designed to compensate for the average size of the sextupole component of the dipoles. The accelerator is not very sensitive to variations in the sextupole around the ring. The decapole component is clearly measurable, but not large enough to pose a problem for the accelerator.

II. Measurement systems

The equipment and software used in measuring the magnets is described with more detail in other papers at this conference and elsewhere [5]. The request from the Main Injector project was that every magnet be measured and that in production the strength and shape be determined by at least two independent methods. A third strength measurement is used on a sample of magnets for further redundancy.

The flatcoil system uses a long, narrow, multi-turn coil that extends through the length of the magnet, performing the integral over z. The coil form is rigid and curved to match the central orbit of a particle through the curved magnet. The magnet strength, exclusive of the remanent field, is determined by measuring the change in flux through the coil as the magnet is excited with the probe held in the center of the magnet. The horizontal variation in the field is determined by measuring the change in flux as the probe is moved laterally with the current held fixed. A polynomial fit to the shape data yields coefficients proportional to the normal coefficients of a harmonic decomposition of the magnetic field. The flatcoil measurements are performed at multiple currents on every magnet.

*Work supported by the United States Department of Energy under contract No. DE-AC02-76CH03000

THE FERMILAB MAIN INJECTOR DIPOLE AND QUADRUPOLE COOLING DESIGN AND BUS CONNECTIONS

J. A. Satti
Fermi National Accelerator Laboratory*
P. O. Box 500, Batavia, IL 60510

ABSTRACT

The proposed system for connecting the low conductivity water (LCW) and the electrical power to the magnets is explained. This system requires minimum maintenance. Stainless steel headers supply LCW to local, secondary manifolds which regulate the flow to the dipole and to the copper bus which conduct both power and cooling water to the quadrupole. A combination of ceramic feedthroughs and thermoplastic hoses insulate the piping electrically from the copper bus system. The utilities for the Main Injector are grouped together at the outside wall of the tunnel leaving most of the enclosure space for servicing. Space above the headers is available for future accelerator expansion. The new dipoles have bolted electrical connections with flexible copper jumpers. Separate compression fittings are used for the water connections. Each dipole magnet has two water circuits in parallel designed to minimize thermal stresses and the number of insulators. Two electrical insulators are used in series because this design has been shown to minimize electrolyses problems and copper ion deposits inside the insulators. The design value of the temperature gradient of the LCW is 8°C.

I. INTRODUCTION

The Fermilab Main Injector (FMI) is a new 150 GeV synchrotron now under construction at the Fermi National Accelerator Laboratory .[1] The FMI will replace the existing Main Ring. New conventional dipole magnets, with water cooled conductors, will provide the primary bending for this accelerator. The proposed system for connecting the power and the water to the FMI is similar to the existing Main Ring. Where possible, the power bus is used to carry both power and water to the magnets.

II. LOW CONDUCTIVITY WATER SYSTEM

Figure 1 shows the FMI and the 8 GeV Line LCW System. There will be six utility buildings uniformly spaced around the FMI ring. These are labeled MI-10, MI-20, MI-30, MI-40, MI-50, MI-60. Each utility building will supply power and cooling water to about 1,815 feet of circumference in the FMI. The closed loop system will receive makeup water from the Central Utility Building (CUB).

A total of 18 pumps will be installed around the ring with 3 pumps per service building. Each pump has a 100 hp motor and delivers 550 GPM of LCW with a pressure head of 164 psi (380 TDH). Six inch stainless steel pipe headers will be installed above the magnets along the 10,891- foot circumference of the FMI. Eight inch headers will be used to connect the pumps from the service buildings to the manifolds in the accelerator enclosure.

All components are connected in parallel and, with the proper hydraulic resistance across each secondary manifold, the local water distribution will be balanced between service buildings. The centrifugal pumps, also connected in parallel with the magnets, will share the flow and will balance the pressure head to match the resistance across the LCW manifolds. A similar LCW system has worked well in the existing Main Ring where the hydronics have been operational for twenty-three (23) years.[2]

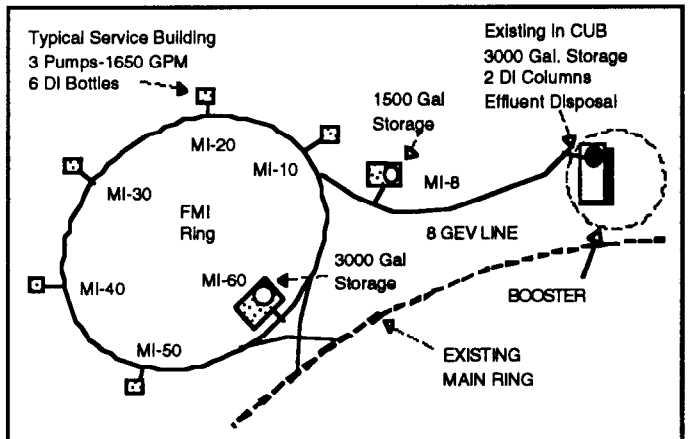

Figure 1. Main Injector & 8 GeV Line 95°F LCW System

At the pipe penetrations leading to the enclosure, valves will be installed to isolate each sector of the ring. At each utility entrance, as well as at locations half-way in-between, the enclosure has a ceiling that is one foot higher than the standard tunnel. The purpose of this extra space is to provide space for the stainless steel expansion joints. At these locations, the enlarged enclosure allows the pipes to cross over the cable trays without obstructing the normal tunnel clearance for the magnet moving vehicle.

One heat exchanger per service building is required to transfer the LCW heat load to the pond water. The normal heat load removal capacity per building will be about 2.7 MW. Approximately 8,000 GPM of LCW will be required to cool the magnets, bus, and power supplies in the FMI enclosure and the service buildings. The centrifugal pumps are capable of delivering approximately 9,900 GPM at the

*Operated by the Universities Research Association, Inc., under contract with the U.S. Department of Energy

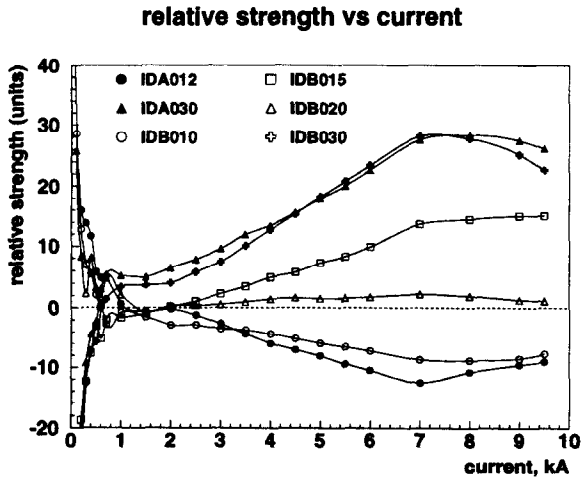

Figure. 4. Relative strength of representative dipoles as a function of current

B. Shape

The complementary measurement techniques, flatcoil and harmonics, give consistent results. Figure 5 shows the average b_3 as a function of current. This is consistent with calculations and with the performance of the prototype dipoles, upon which the chromaticity sextupole design was based.

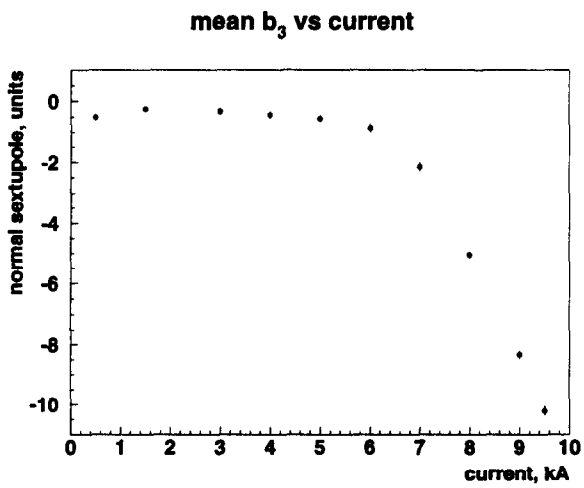

Figure. 5. Average sextupole component vs current

The sextupole components at 9500 A are histogrammed in Figure ??. All magnets fall well within the expected range of values. The distribution of the decapole component at 9500 A is shown in Figure 7. All magnets are within the established limits.

IV. Conclusions

The Fermilab Main Injector project is well into production of dipoles for the ring. By the end of March 1995 54 6-m dipoles, out of 216 required for the ring, had been completed and measured. Magnet performance is within the acceptable range established through tracking studies.

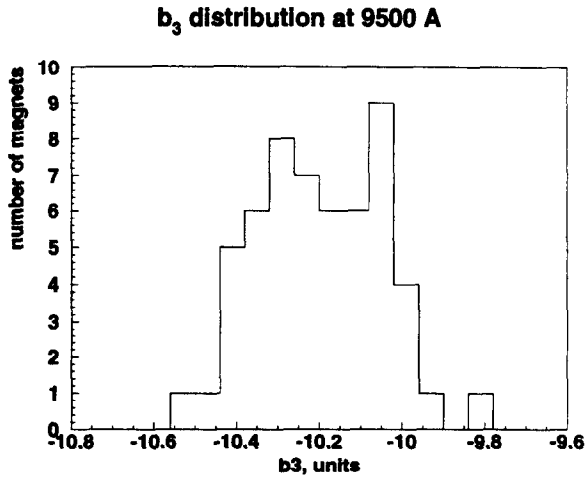

Figure. 6. Distribution of sextupole strengths at 9500 A

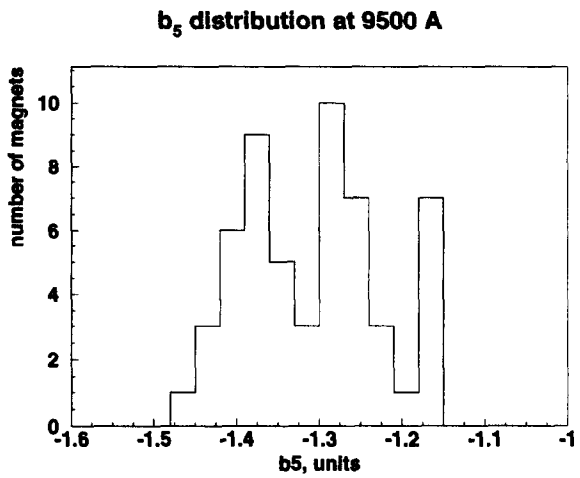

Figure. 7. Distribution of decapole strengths at 9500 A

References

[1] D. Bogert. The Fermilab Injector Complex. In *Proceedings this conference*, 1995.

[2] C.S. Mishra P.S. Martin D.J. Harding H.D. Glass and B.C.Brown. Fermilab Main Injector Magnet Acceptance Criteria. In *Proceedings this conference*, 1995.

[3] C.S. Mishra. Simulation of the Fermilab Main Injector with Production Magnet Data. In *Proceedings this conference*, 1995.

[4] C.M. Bhat et al. The Main Injector Chromaticity Correction Sextupole Magnets: Measurements and Operating Schemes. In *Proceedings this conference*, 1995.

[5] J.W. Sim et al. Software for a Database-Controlled Measurement System at the Fermilab Magnet Test Facility. In *Proceedings this conference*, 1995.